Advances in Urban Flood Management:

Addressing Data Uncertainty, Data Gaps and Adaptation Planning

by

Ashish Shrestha

A Dissertation Presented in Partial Fulfillment
of the Requirements for the Degree
Doctor of Philosophy

Approved April 2022 by the
Graduate Supervisory Committee:

Margaret Garcia, Chair
Giuseppe Mascaro
Mikhail Chester
Sarah Fletcher

ARIZONA STATE UNIVERSITY

May 2022

ABSTRACT

Cities are facing complex problems in urban water management due to unprecedented changes in climate, natural and built environment. The shift in urban hydrology from pre-development to post-development continues to accelerate the challenges of managing excess stormwater runoff, mitigating urban flood hazards and flood damages. Physically based hydrologic-hydraulic stormwater models are a useful tool for broad subset of urban flood management including risk and hazard assessment, flood forecasting, and infrastructure adaptation decision making and planning. The existing limitations in data availability, gaps in data, and uncertainty in data preclude reliable model construction, testing, deployment, knowledge generation, effective communication of flood risks, and adaptation decision making. These challenges that affect both the science and practice motivate three chapters of this dissertation. The first study conducts diagnostic analysis of the effects of stormwater infrastructure data completeness on model's ability to simulate flood duration, flooding flow rate; and assesses the combined effects of data gaps and model resolution to simulate flood depth, extent and volume (chapter 2). The analysis showed the significance of complete stormwater infrastructure data and high model resolution to reduce error, bias and uncertainty; this study also presented an approach for filling infrastructure data gaps using available data and design standards. The second study addresses the lack of long-term hydrological observation in urban catchment by investigating the process and benefits of leveraging novel data sources in urban flood model construction and testing (chapter 3). A proof-of-concept demonstrated the application and benefits of leveraging

novel data sources for urban flood monitoring and modeling. Furthermore, it highlights the need for developing and streamlining novel data collection infrastructure. The third study applies the hydrologic-hydraulic model as an adaptation planning tool and assess the effects of uncertainty in design precipitation estimates and land use change on the optimal configuration of green infrastructure (chapter 4). Several uncertainties affect infrastructure decision making as showed by variation in optimal green infrastructure configuration under precipitation estimates and land use change. Thus, the study further highlights the need of flexible planning process in infrastructure decision making.

DEDICATION

To my parents and spouse, for their constant support and encouragement.

ACKNOWLEDGMENTS

I am extremely grateful to my Professors for all the invaluable support and guidance that I have received throughout my PhD journey.

First of all, I would like to extend my sincere gratitude to my advisor, Prof. Margaret Garcia for her guidance, encouragement, kindness and continued support throughout my study. It was a great privilege and honor to be a part of Prof. Garcia's Water Systems Analysis and Policy lab, and I am very grateful for all the learning opportunities that I have received here. Thank you, Prof. Garcia, for inspiring me to explore and pursue my interests while teaching me how to find important research questions. The knowledge that I have received from Prof. Garcia during the course of my study will be valuable throughout my career in the future. I hope to continue learning from her beyond my PhD and continue contributing to solving the challenges in water and environment systems.

I would like to extend my sincere gratitude to my PhD committee members – Prof. Giuseppe Mascaro, Prof. Mikhail Chester, and Prof. Sarah Fletcher for all their guidance and feedback. I am grateful to Prof. Mascaro for his guidance and valuable suggestions on my research and writing. I am grateful to Prof. Chester for his support and inspiring questions, which helped to improve my work. I am grateful to Prof. Fletcher for her valuable suggestions that helped me to improve my research and communication.

I would like to remember some of the most interesting topics that I have learned while taking courses on uncertainty analysis for infrastructure and socio-hydrological system analysis from Prof. Garcia; environmental data analysis and watershed hydrology

from Prof. Mascaro; and urban infrastructure anatomy from Prof. Chester. They have greatly inspired me in pursuing some of the important challenges in water, environment and infrastructure systems. I am also grateful to Prof. Rebecca Muenich, who taught me key lessons on geographic information systems, which helped me a lot in framing my research work.

I am very lucky to have found myself among my great colleagues namely Behshad, Samuel, Alysha, Rui, Sara, Burcu, Krista, Annika and Sangeet with whom working together, and learning have always been memorable and fun.

I would also like to acknowledge the ASU research computing, particularly Gil Speyer and Rebecca Belshe for their support in utilizing parallel computing resources in my research. I also acknowledge the Computational Hydraulic International (CHI) for providing educational license to use PCSWMM modeling tool for this research.

TABLE OF CONTENTS

Page

LIST OF TABLES x

LIST OF FIGURES xii

CHAPTER

1 INTRODUCTION 1

1.1 Background 1

1.2 Problem Statements and Research Questions 4

2 EFFECTS OF STORMWATER INFRASTRUCTURE DATA COMPLETENESS AND MODEL RESOLUTION ON URBAN FLOOD MODELING 10

2.1 Introduction 11

2.2 Study Area, Data Collection and Processing 18

2.3 Methodology 24

2.3.1 Hydrologic-Hydraulic Model 25

2.3.2 Random Sampling of Infrastructure Data 29

2.3.3 Selective Sampling 35

2.4 Results and Discussion 37

2.4.1 Evaluation of Random Sampling 37

2.4.1.1 Effect of Roughness 40

2.4.1.2 Effect of Diameter 42

2.4.1.3 Effect of Depth 44

CHAPTER Page

2.4.1.4 Effect of Location of Missing Data 45

2.4.2 Evaluation of Selective Sampling 48

2.4.3 Research Implications and Limitations 57

2.5 Conclusions 61

3 LEVERAGING CATCHMENT SCALE AUTOMATED NOVEL DATA COLLECTION INFRASTRUCTURE TO ADVANCE URBAN HYDROLOGIC-HYDRAULIC MODELING 64

3.1 Introduction 65

3.2 Study Area 73

3.3 Materials and Methods 75

3.3.1 Hydrologic-Hydraulic Model 75

3.3.1.1 Data Requirements and Processing 76

3.3.1.2 Model Setup 78

3.3.2 Novel Data Infrastructure and Data Collection 79

3.3.2.1 Flood Camera Images 81

3.3.2.2 Citizen Science Observations 82

3.3.3 Sensitivity Analysis and Parameter Grouping 83

3.3.4 Auto-Calibration using Genetic Algorithm 85

3.3.4.1 Integrating Continuous Time Series Data 87

3.3.4.2 Integrating Continuous Single Point Data 88

3.4 Results 91

CHAPTER Page

3.4.1 Sensitivity Analysis and Parameter Grouping 91

3.4.2 Manual Validation of Model Inputs and Model Configuration ..95

3.4.3 Auto-Calibration using Genetic Algorithm 96

3.5 Discussion 99

3.5.1 Novel Data Supports Validation of Model Inputs and Configuration 99

3.5.2 Novel Data Supports Calibration 101

3.6 Conclusions 103

4 EFFECTS OF PRECIPITATION UNCERTAINTY AND LAND USE CHANGE IN THE OPTIMAL CATCHMENT SCALE GREEN INFRASTRUCTURE CONFIGURATION 106

4.1 Introduction 107

4.2 Material and Methods 113

4.2.1 Catchments Selection 114

4.2.2 Hydrologic-Hydraulic Model 119

4.2.3 GI Optimization 121

4.2.3.1 GI Configuration 121

4.2.3.2 Optimization Framework 123

4.3 Results 125

4.3.1 Effects of Uncertainty in Design Precipitation Estimates 128

4.3.2 Effects of Changes in Urban Imperviousness 132

CHAPTER Page

4.3.3 Effects of Increasing Precipitation Estimates 135

4.4 Discussion 136

4.4.1 GI Design for Pluvial Flood Risk Management 136

4.4.2 GI Adaptation Under Uncertainty.....138

4.4.3 Reflections to Other U.S. Cities.....139

4.5 Conclusions 141

5 CONCLUSION.....144

5.1 Research Summary 144

5.2 Future Research.....151

REFERENCES 155

APPENDIX

A GROUND TRUTH MODEL PARAMETERS 175

B SENSITIVITY ANALYSIS FOR PARAMETER SELECTION.....178

C INCOMPLETE INFRASTRUCTURE DATA.....181

D HYPOTHETICAL CONDUIT DISTRIBUTION FOR SAMPLING ROUGHNESS.....183

E FLAGSTAFF MODEL PARAMETERS.....189

F GREEN INFRASTRUCTURE DESIGN CONSIDERATION 196

G R-CODES.....198

LIST OF TABLES

Table Page

2.1. Data Used in This Study 21

2.2. Sensitivity Analysis of Infrastructure Related Parameters. 30

2.3. Four Selective Sampling Models. Note That HD/LD the First Two Letters Refers to Stormwater Data (i.e., HD = High Data or Complete Data, LD = Low Data or Incomplete Data) and HM/LM Refers to Model Resolution (i.e., HM = High Model Resolution, LM = Low Model Resolution). 36

2.4. System Flooding Metrics of Average of MAE and PBIAS (from Ensemble Simulations Vs. Ground Truth) and RIQR of Peak System Flooding; And Flood Duration Metrics of MAE and PBIAS (from the Maximum and Mean Duration of Flooding in Ensemble Simulations Vs. Ground Truth) and RIQR of Maximum and Mean Duration of Nodes Flooded for Random Sampling with Different Percentages of Missing Attribute-values..... 40

2.5. System Flooding Metrics of the Average MAE and PBIAS (from Ensemble Simulations Vs. Ground Truth) and RIQR of Peak System Flooding; And Flood Duration Metrics of MAE and PBIAS (from the Mean and Maximum Durations of Flooding in Ensemble Simulations Vs. Ground Truth) and RIQR of Mean and Maximum Durations of Nodes Flooded for Random Sampling of Missing Locations of Attribute-values. 48

3.1. Summary of Data Used to Build Hydrologic-hydraulic Model..... 78

3.2. Flooding Events Observed from Novel Data Sources 88

Table Page

3.3. Twelve Subgroups of Sub-catchments Identified 93

3.4. Eight Subgroups of Conduits Identified 93

4.1. Change in Imperviousness from 2001 to 2019, and 90% Confidence Interval for NOAA Atlas 14 Precipitation Estimates in 20 Most Populated (U.S. Census Bureau, n.d.) U.S. Cities 115

5.1. Key Features and Limitations of Different Novel Data Sources in Urban Flood Model Development..... 149

LIST OF FIGURES

Figure Page

1.1. Three Aspects of Advancing Urban Stormwater Modeling 4

2.1. (a) Location of the City of Phoenix and (b) Study Catchment with Complete Catchment Infrastructure Data (Referred to as the Ground Truth Data Set) 20

2.2. Spatial Data Sets Used to Develop the SWMM 1D-2D Model, (a) Stormwater Infrastructure Data, (b) Ground-based DEM, (c) 2D Mesh Grid, (d) Building Layer, (e) Soil Types, and (f) Imperviousness..... 24

2.3. Overview of the Random Sampling Process 35

2.4. Monte Carlo Sampling Results Showing Distribution of Flood Duration at All Nodes with Observed Flooding While Sampling (a-d) Roughness, (e-h) Diameter and (i-l) Depth at Different Levels of Missing Attribute-values. One Hundred Iterations (Grey) Are Compared with the Ground Truth Model (Red). Note: Density Plots (Wickham, 2009) Are Smoothed Version of Frequency Polygon Based on Kernel Smoothers Useful to Compare Shape of the Distributions; Here, Default Bandwidth Adjustment of 1 and Gaussian Kernel Was Selected..... 38

2.5. Monte Carlo Sampling Results Showing (a-c) Maximum System Flooding, (d-f) Maximum Duration of Nodes Flooding, and (g-i) Average Duration of Nodes Flooding with Different Percentages of Missing Sampling Roughness, Diameter or Depth Data. Boxes Represent the 25^{th}, 50^{th} and 75^{th} Percentiles and Whiskers

Represent ±1.5×IQR of the 25th and 75th Percentiles. Horizontal Red Dash Lines Represent the Values Simulated by the Ground Truth Model. 39

2.6. Monte Carlo Sampling Results Showing, (a-c) Maximum System Flooding, (d-f) Maximum Duration of Nodes Flooding, and (g-i) Average Duration of Nodes Flooding While Sampling Roughness, Diameter and Depth at 50% PMD from *Upstream* Versus *Downstream* Locations. Boxes Represent the 25th, 50th and 75th Percentiles and Whiskers Represent ±1.5×IQR of the 25th and 75th Percentiles. Horizontal Red Dash Lines Represent the Ground Truth Model… 47

2.7. Slope Distributions of (a) High-resolution (0.3-m) DEM, (b) Low-resolution (9.7-m) DEM and (c) Sub-catchments in High- and Low-resolution Models… 50

2.8. Boxplots for Distributions of Maximum Flooded Depth in 2D Grid Cells. Note: Boxes Represent the 25th, 50th and 75th Percentiles and Whiskers Represent ±1.5×IQR of the 25th and 75th Percentiles. 51

2.9. Hyetograph and Flooding (Flux) Hydrograph in the Four Selective Sampling Models. Negative Flooding Flux Indicates Net Flow Back into the Drainage System. 52

2.10. Flooded Extent and Depth in Four Selective Sampling Models, (a) HDHM, (b) HDLM, (c) LDLM and (d) LDHM. Note: i). Peak Flood Depths Are 0.45 m, 0.28 m, 0.3 m and 0.48 m for HDHM, HDLM, LDLM and LDHM, Respectively, ii). Boxes [I - IV] Are Pointing to the Differences in Estimating Depth and Extent..... 53

Figure Page

2.11. Significance of Data Completeness and Model Resolution in Terms of Modeling Hydrologic and Hydraulic Processes 56

3.1. Study Area 74

3.2. Overview of Experimental Novel Data Infrastructure. Solid Lines Show Flow of Information from Automated Flood Cameras; Dashed Lines Show Flow of Information from Citizen Scientist Contributors. 80

3.3. Pictures Showing Installed (a) a Typical Automated Flood Camera Installation, (b) Flood Gauge (Automatically Read by Flood Cameras) Installed at a Hotspot Location, and (c) an Example of Street Flooding Event..... 80

3.4. Methodological Framework for (a) Parameter Grouping and (b) Optimization Algorithm for Parameterization 85

3.5. Schematic of Flooding (SWMM 1D) and Flooding Depth (SWMM 1D-2D) Occurring at the Same Location. Using Rising Limb, Time Integration of Flooding or the Area under the Curve of Flooding Flow Rate, and Flooding Depth Are Linearly Fit to Extract Surface Flooding Depth Using Flooding Flow Rate. 91

3.6. One-at-a-time Sensitivity Analysis Results 92

3.7. Layers of Surface Properties Data, Particularly (a) Soil Types and (b) LULC for Grouping Parameters Related to Sub-catchment, and (c) Built Material and (d) Building Age as a Proxy for As-built Stormwater Infrastructure Age for Grouping Parameters Related to Conduits..... 94

Figure Page

3.8. Stormwater Network Showing (a) Incomplete Disconnected Network with Missing Conduits Where Flooding Could Not Be Simulated and (b) Corrected Stormwater Network 96

3.9. Calibration and Validation Results Showing (a) Fitness Using a Genetic Algorithm, (b) Simulated and Observed Flood Water Level Using Remotely Sensed Flood Camera Observations for Event A, and Validation Using Single Point Observations for (c) Event B and (d) Event C 98

3.10. Coefficient of Determination (R^2) for Fitted Linear Relationship Between Floodwater Depth in SWMM 1D-2D Model Time Integration of Flooding Flow Rate in SWMM 1D at the given Location of Coupled 1D-2D Model 99

4.1. (a) Location of the City of Phoenix, (b) Change in Urban Imperviousness (%) from 2001 to 2019 and Locations of Two Catchments, Stormwater Components in (c) Study Cat. 1 or Downtown Phoenix (DTP) and (d) Study Cat. 2 or South Mountain Phoenix (SMP) 118

4.2. Change in Urban Imperviousness (%) from 2001 to 2019 Using Data from NLCD (MRLC, n.d.) in (a) Cat. 1 and (b) Cat. 2 119

4.3. Example of Flooding (a) in Cat. 1, Occurred on September 23rd, 2019 and (b) in Cat. 2, Occurred on August 12th, 2014 (Source: *FloodAware* (ASU/NAU, 2021) and *Report a Flood, Flood Control District of Maricopa County* (FCDMC, n.d.)) 119

Figure Page

4.4. Available Space for GI in Each Discretized Sub-catchment Is Estimated by Extracting Area Occupied by Buildings and Streets For (a) Cat. 1 and (b) Cat. 2 123

4.5. Pre-green Infrastructure Condition in Two Catchments as Simulated by SWMM Showing the Maximum Flood Rate from Flooded Junctions, Peak Runoff from Sub-catchments, and the Duration of Exceedance of Conduits' Capacity. The Year in Parentheses for Cat. 1 Refer to Imperviousness Conditions in 2019 (as well as for 2001) and for Cat. 2 Refer to 2001 or 2019. 127

4.6. Pareto Optimal Solution for GI Installations to Reduce the Peak System Flooding in Two Catchments (at the Imperviousness Level of 2001 and 2019) Using Mean and Confidence Intervals (i.e. Lower and Upper Values) of the Atlas 14 Estimates. The Year in Parentheses for Cat. 1 Refer to Imperviousness Conditions in 2019 (as well as for 2001) and for Cat. 2 Refer to 2001 or 2019. 130

4.7. Optimal Configuration of GI (Bio-retentions and Green Roofs) at Least Possible Cost in Cat. 1 for Mitigating Peak Flooding. Panels Are Showing the Number of GI Required. NGI_T, NGI_M and AGI_T Refers to the Total Number, Maximum Number in Any of the Sub-catchments and Total Area of GI Required. 131

4.8. Optimal Configuration of GI (Bio-retentions) at Least Possible Cost in Cat. 1 for Reducing Peak Flooding to 2 m^3/s. Note: The Maximum Flood Reduction Possible is up-to 2 m^3/s given the Constraint and GI Configuration Options.

Figure Page

Panels Are Showing the Number of GI Required. NGI_T, NGI_M and AGI_T Refers to the Total Number, Maximum Number in Any of the Sub-catchments and Total Area of GI Required. 134

4.9. Pareto Optimal Solution for GI Installations to Reduce the Peak System Flooding under Four Stages of 5-year Return Period Rainfall Estimate Change (a) +5%, (b) +10%, (c) +25%, (d) +50% 136

4.10. Dynamics of Change Occurring Across Cities That Will Potentially Influence GI Planning 141

CHAPTER 1

INTRODUCTION

1.1 Background

A growing number of cities face complex problems in urban water management due to unprecedented change in climate, land use change and aging infrastructure. The shift in urban hydrology with land development increases peak runoff and runoff volume, intensifying the challenges of managing excess stormwater runoff, mitigating urban flood hazards and preventing flood damages (University of Maryland & Texas A&M University, 2018; Walsh, Fletcher, & Burns, 2012; W. Zhang, Villarini, Vecchi, & Smith, 2018). The intensifying extreme precipitation, increasing urban densification and sprawl, and inadequate stormwater infrastructure are causing functional failure of existing stormwater infrastructure, increasing flood prone areas and urban flood risks in cities. Pluvial flooding, or rainfall induced urban flooding, in particular is of growing concern. Pluvial flooding has historically received less attention in flood assessments, modeling efforts, and even within private or government insurance programs, compared to the fluvial and coastal flooding mechanisms (First Street Foundation, 2020; Bernice R. Rosenzweig et al., 2018; The National Academy Press, 2019). The Federal Emergency Management Agency's (FEMA's) flood hazard analysis and mapping focus only on riverine and coastal flooding (The National Academy Press, 2019), but the risks from pluvial flooding are significant (First Street Foundation, 2020). In the U.K., it has been estimated that damages from urban pluvial flooding in 2008 exceeded $0.36 billion, which is a lower cost than the $0.8–$2.8 billion estimated for fluvial and coastal flooding;

however, future projections indicate that losses due to pluvial flooding will become similar to or higher than those of other flooding types by 2080 (Dawson et al., 2008; Hall, Sayers, & Dawson, 2005). Furthermore, the exact numbers of pluvial floods and flood damages are not well recorded and disseminated in the U.S. and the limited information available on urban flooding damages are mostly from flood damage insurance claims, both national and commercial (University of Maryland & Texas A&M University, 2018). Pluvial flooding contributes to major urban flooding episodes, e.g., *in the U.S.* – several urban flooding in Cook County, Illinois between 2007 to 2011 (Festing et al., 2014), a 1000-year rainfall event in Ellicott City, Maryland in May 2018, and heavy rainfall and flooding in the metropolitan Detroit area in August 2014 (University of Maryland & Texas A&M University, 2018), *and globally* – urban flooding in Copenhagen, Denmark in July 2011; Catania, Italy in October 2018 (Prokić, Savić, & Pavić, 2019); Chennai, India in November and December 2015 (Nithila Devi, Sridharan, & Kuiry, 2019); Ho Chi Minh, Vietnam in November 2018 (Leitold, Garschagen, Tran, & Revilla Diez, 2021); Beijing, China in July 2012 (Jiang, Zevenbergen, & Ma, 2018); and Nagoya City, Japan in Autumn 2020 (Tanaka, Kiyohara, & Tachikawa, 2020).

The broad subset of urban flood risk management encompasses flood assessments, insurance programs, impact assessments, flood forecasting and prediction, and strategic flood adaptation planning (Jha, Bloch, & Lamond, 2012). Physically based hydrological models have been an invaluable tool in improving our understanding of urban hydrological and hydraulic processes by simulating urban water quantity, quality, and interactions among external environmental variables in flood assessment, emergency

operations, designing urban stormwater infrastructure and resilience planning in cities (Y. Guo, 2001; B. R. Rosenzweig et al., 2021; Zoppou, 2001). Application of such models in the urban watershed (e.g. flood forecasting) is becoming more important due to ongoing urbanization and climate change (Sikorska, Scheidegger, Banasik, & Rieckermann, 2012). Advances in computational resources and data acquisition technologies such as advent of airborne laser scanning LiDAR coupled with high accuracy global positioning system improved the capability to efficiently generate high resolution Digital elevation models (DEMs) over large spatial scale, alongside resources and tools for pre-processing of LiDAR data (Soininen, 2004; K. Zhang & Cui, 2007), have led to improvement in process representation and output accuracy of hydrological models. Such high-resolution terrestrial data at cheaper costs has enabled building hyper resolution urban flood models incorporating fine street details, such as street curbs and buildings (Bates, Marks, & Horritt, 2003; Bermúdez & Zischg, 2018; Timothy J. Fewtrell, Duncan, Sampson, Neal, & Bates, 2011; Noh, Lee, Lee, Kawaike, & Seo, 2018).

Despite the available resources and tools, uneven availability of terrain properties data, gaps in or inaccessibility of stormwater infrastructure data, lack of in-situ hydrological observation in urban channels, other uncertainties in model inputs (e.g., precipitation estimates), hinder effective urban stormwater model development and testing. The infrastructure data gaps affect accurate process representation in model causing output uncertainty, error and bias. The gaps in hydrological observation affect model construction, parameterization and its reliable use. To inform decision making, models must provide information at the scale of the decision and clearly communicate

assumptions and uncertainties. Current gaps include a lack of data to assess and improve model accuracy in urban areas and no assessment of the impact of common data gaps (e.g., drainage infrastructure data) on model uncertainty. The key to advancing hydrological modeling is improving the hydrological data availability for forcing and evaluating hydrological models; and addressing epistemic uncertainties (i.e., lack of knowledge rather than random variability) (Beven, 2019). This dissertation focused on the three aspects of advancing stormwater modeling, addressing data gaps and data uncertainty, model construction and testing, and model-based applications for infrastructure planning (Figure 1.1).

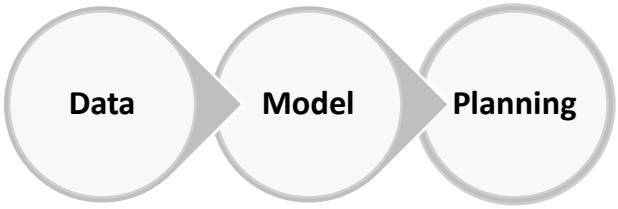

Figure 1.1. Three Aspects of Advancing Urban Stormwater Modeling

1.2 Problem Statements and Research Questions

Urban flooding is a natural hazard which cannot be prevented (Rahmati, Darabi, Panahi, Kalantari, & Naghibi, 2020) but that can be managed with adequate flood mitigation interventions and informed decision making. The risk of urban flooding will likely increase globally due to more intense and frequent extreme precipitation due to climate change, and urban sprawl (Wehner, Arnold, Knutson, Kunkel, & LeGrande,

2017). The addition of infrastructure and land development results in highly heterogenous catchments with complicated runoff flow paths and increased impervious urban surfaces. Where there is inadequate stormwater storage and conveyance, these changes result in localized pluvial flooding. Localized impacts in this heterogenous environment are consequential as six inches of moving floodwater can knock down a pedestrian, twelve inches can cause vehicles to loose traction (National Weather Service [NWS], n.d.) and a few inches of water overtopping the street curb can result in basement flooding, damages to underground infrastructures like train stations. Hydrologic-hydraulic models are a critical tool for flood prediction, infrastructure design, and adaptation planning (Pathak et al., 2015). A reliable model should produce an accurate and precise simulation of flood flow rate, volume, duration, and extent. Thus, it is crucial to identifying possible sources of model error and uncertainty. The key requirement for improving the accuracy of physically based pluvial flood models is integration of stormwater infrastructure data and high-resolution terrain data into hydrologic-hydraulic model (Association of State Floodplain Managers [ASFPM], 2020). Unfortunately, complete stormwater infrastructure data are often not available due to data sharing restrictions or data gaps (Veregin, 1999) occurring from errors of omission (i.e., infrastructure components not being recorded) and error of commission (i.e., assignment of incorrect data). The limited availability of high-resolution spatial data (e.g., 1-m DEM) to adequately capture surface heterogeneity also challenge the accurate simulation of flood depth, extent and volume. Moreover, a consistent framework to deal with stormwater infrastructure data gaps is non-existent. Thus, it is important to understand

how different nature (i.e., by amount and spatial distribution) of stormwater infrastructure data gaps affect model performance; and how such gaps interact with the model resolution limited by availability of high-resolution terrain data.

Achieving higher accuracy and precision of stormwater model is an iterative process. The different layers of data involved in model construction – stormwater infrastructure components, surface channels and topography, imperviousness, slope, soil types – must all be accurate and up-to-date. In the dynamic urban environment where change in land surface could change the hydraulics of flow routing, continuous observation of flood occurrence, flow and depth is critical to parameterize the model through single step auto-calibration or continuous auto-calibration framework. Unfortunately, a pervasive lack of long-term hydrological observations in urban environment, particularly at the scale of streets and urban streams impede accurate parameterization and delays the application of such models for real-time flood forecasting, flood assessment or model-based decision making (University of Maryland & Texas A&M University, 2018). There is urgency to efficiently fill this data gap such as observations of flood related variables (e.g., flood water depth) at the frequently flooded locations across entire catchment. The application of novel data such as image based proxy water level measurement and reports based on citizen science contribution techniques (João P. Leitão, Peña-Haro, Lüthi, Scheidegger, & Moy de Vitry, 2018; Moy De Vitry, Dicht, & Leitão, 2017; Moy de Vitry & Leitão, 2020) proven to be useful in ungauged river basins (Etter, Strobl, van Meerveld, & Seibert, 2020; Lowry, Fienen, Hall, & Stepenuck, 2019; Nardi et al., 2021) and in pilot scale urban stormwater facility

(Moy De Vitry et al., 2017) should be extended to urban catchment for advancing pluvial flood models.

Adaptation decision making for pluvial flood mitigation in urban catchments is challenged by the technical and financial obstacles to retrofit or replace stormwater conduits and other detention facilities due to spatial interdependencies (Chester & Allenby, 2019) with transportation and other infrastructure systems, resulting in lock-in (Gilrein et al., 2019). This challenge is exacerbated in networked infrastructure, such as transmission, distribution or conveyance systems, which are less adaptable as upgrading capacity in a given location requires the replacement of several sections of conduits both upstream and downstream. To overcome this rigidity in stormwater infrastructure and minimize its risk of functional failure, catchment scale green infrastructure (GI) can be deployed to supplement the hydraulic capacity of the grey infrastructure network by retaining the surface runoff and minimizing peak flow in the system. Catchment scale adaptation to urban flooding requires tools to aid the identification of the optimal amount, spatial distribution and type of green infrastructure at the least cost.

However, any adaptations to the stormwater system must consider that key driving variables of precipitation and impervious cover are uncertain and change with time. The standard rainfall design documents for stormwater infrastructure have significantly improved from the U.S. Weather Bureau Technical Paper 40 (TP40) released in 1961 and HYDRO 35 released in 1977 (V. Te Chow, Maidment, & Mays, 1998; Lopez-Cantu & Samaras, 2018) till the newest document as National Oceanic and Atmospheric Administration (NOAA) Atlas 14 released in 2014. Atlas 14 superseded all

other standards for its wider spatial and temporal coverage (NOAA/NWS, n.d.; Perica et al., 2018). However, the uncertainty in Atlas 14 estimates given as a 90% confidence interval, particularly for shorter duration rainfall (i.e., sub-daily to sub-hourly) present the risk of over or under building stormwater infrastructure such as green infrastructure. In addition, the ongoing urban densification and sprawl could affect the performance and adoption of green infrastructure. Identifying and quantifying such uncertainties is the crucial step in overcoming risks of planning failure and developing appropriate adaptation frameworks.

The overarching research goal for this study is to understand the current knowledge gaps in science and management of urban stormwater systems and to advance urban flood management through improved knowledge in modeling practice and infrastructure planning. Specifically, this dissertation addresses the following research questions in three chapters [2-4].

- Chapter 2: *Effects of stormwater infrastructure data completeness and model resolution on urban flood modeling*
    - How do the proportion and spatial distribution of infrastructure data gaps impact model performance?
    - How does the spatial resolution of the terrain data interact with infrastructure data gaps to impact the model performance?
- Chapter 3: *Leveraging catchment scale automated novel data collection infrastructure to advance urban hydrologic-hydraulic modeling*

- Can novel data sources compensate for the general lack of real-world hydrological observations in urban environment and help to refine and calibrate urban hydrologic-hydraulic models?

- Chapter 4: *Effects of precipitation uncertainty and land use change in the optimal catchment scale green infrastructure configuration.*
  - How to optimally configure GI for ideal type, amount and spatial distribution for catchment scale planning to mitigate urban flood while minimizing cost of implementation?
  - How does the uncertainty in precipitation design standards affect the optimal design configuration of GI?
  - How does the change in urban imperviousness over time affect the optimal GI configuration?

CHAPTER 2

EFFECTS OF STORMWATER INFRASTRUCTURE DATA COMPLETENESS AND MODEL RESOLUTION ON URBAN FLOOD MODELING

This chapter has been adapted from a published article: Shrestha, A., Mascaro, G., & Garcia, M. (2022). Effects of stormwater infrastructure data completeness and model resolution on urban flood modeling. *Journal of Hydrology*, *607*(July 2021), 127498. https://doi.org/10.1016/j.jhydrol.2022.127498

Abstract: The accuracy of hydrologic and hydrodynamic models, used to study urban hydrology and predict urban flooding, depends on the availability of high-resolution terrain and infrastructure data. Unfortunately, cities often do not have or cannot release complete infrastructure data, and high-resolution terrain data products are not available everywhere. In this study, we quantify how the accuracy and precision of urban hydrologic-hydrodynamic models vary as a function of data completeness and model resolution. For this aim, we apply the one-dimensional (1D) and coupled one- and two-dimensional (1D-2D) versions of the U.S. Environmental Protection Agency's Storm Water Management Model (SWMM) in an urban catchment in the city of Phoenix, Arizona. Here, we have collected detailed infrastructure data, a high-resolution 0.3-m LiDAR-based digital elevation model, and catchment properties data. We tested several model configurations assuming different levels of (i) availability of stormwater infrastructure data (ranging from 5% to 75% of attribute-values missing) and (ii) terrain

aggregation (i.e., 4.6 m and 9.7 m). These configurations were generated through random Monte Carlo sampling for SWMM 1D and selective sampling with four cases for SWMM 1D-2D. We ran simulations under the 50-year return period design storm and compared simulated flood metrics assuming the highest-resolution and complete data model configuration as a reference. The study found that the model may over or underestimate flood volume and duration with different levels of missing data depending on the parameters — roughness, diameter or depth, and that model performance is more sensitive to missing data that is downstream and closer to the outfall as opposed to missing data upstream. Errors in flood depth, area and volume estimation are functions of both the data completeness and model resolution. Missing feature data leads to overestimation of flood depth, while lower model resolution results in underestimating flood depth and overestimating flood extent and volume.

2.1 Introduction

Urban flooding is a natural hazard impacting public health, environmental quality and the economy (Rahmati et al., 2020). Although the national-level economic and social costs of urban flooding in the U.S. are not routinely recorded, past flood events have resulted in significant property damage and casualties (The National Academy Press, 2019; University of Maryland & Texas A&M University, 2018). For example, urban flooding in Cook County, Illinois resulted in flood losses at a cost of $660 million between 2007 to 2011 (Festing et al., 2014). Additionally, a 1000-year rainfall event in Ellicott City, Maryland in May 2018 caused over one billion dollars in damages, and

heavy rainfall in the metropolitan Detroit area in August 2014 resulted in over $1.8 billion in damages (University of Maryland & Texas A&M University, 2018). Damages of urban flooding have been also documented outside of U.S., including in Copenhagen, Denmark in July 2011; Catania, Italy in October 2018 (Prokić et al., 2019); Chennai, India in November and December 2015 (Nithila Devi et al., 2019); Ho Chi Minh, Vietnam in November 2018 (Leitold et al., 2021); Beijing, China in July 2012 (Jiang et al., 2018); and Nagoya City, Japan in Autumn 2020 (Tanaka et al., 2020).

Unfortunately, the risk of urban flooding will likely increase worldwide because of intense urbanization and climate change. Urban growth results in a conversion of natural land into impervious areas, which in turn increases runoff and reduces infiltration if proper drainage systems are not put in place. Global warming will likely lead to more intense and frequent extreme precipitation (Farris, Deidda, Viola, & Mascaro, 2021; Jung, Chang, & Moradkhani, 2011; Moftakhari et al., 2015; Wehner et al., 2017; W. Zhang et al., 2018). Climate projections for the U.S. estimate that the intensity of the heaviest 1% of precipitation events will likely rise across most regions under both intermediate and worst-case climate change scenarios of Representative Concentration Pathway (RCP) 4.5 and RCP 8.5, with the highest projected increase of 40% by 2100 (compared to 1986 - 2015) under RCP 8.5 in Midwest and Northeast (The National Academy Press, 2019).

One of the major flood-generating mechanisms in cities is pluvial flooding, which occurs when the precipitation intensity exceeds infiltration rate and drainage capacity (Bernice R. Rosenzweig et al., 2018). Pluvial flooding is particularly impactful in urban areas because of the lower threshold for runoff generation and the shorter time of

concentration. This flood mechanism has received less attention compared to fluvial or coastal flooding (Bernice R. Rosenzweig et al., 2018). For example, the Federal Emergency Management Agency's (FEMA's) flood hazard analysis and mapping focus only on riverine and coastal flooding (The National Academy Press, 2019). In a study by the First Street Foundation (2020), which included pluvial flooding among other flooding mechanisms, the number of properties across the U.S. with substantial flood risk (defined as inundation greater than 1 cm during 1 in 100 year flood) was found to be 1.7 times FEMA's estimate, confirming the importance of pluvial flooding. In the U.K., it has been estimated that damages from urban pluvial flooding in 2008 exceeded $0.36 billion, which is a lower cost than the $0.8–$2.8 billion calculated for fluvial and coastal flooding; however, future projections indicate that losses due to urban flooding will become similar to or higher than those of other flooding types by 2080 (Dawson et al., 2008; Hall et al., 2005).

The simulation of pluvial flooding requires capturing a range of hydrologic and hydraulic processes, including rainfall-runoff transformation, overland flow routing, and pipe flows. For this aim, hydrologic models with different levels of sophistication have been coupled to hydraulic models simulating water flow in the drainage networks and on the land surface (Guo et al., 2020; Leandro et al., 2009; Noh et al., 2018; Seyoum et al., 2012; Vojinovic and Tutulic, 2009). A key requirement to increase the predictive skill of these coupled hydrologic-hydraulic models is to incorporate small-scale heterogeneities of terrain and stormwater infrastructure into the simulations (T. J. Fewtrell, Bates, Horritt, & Hunter, 2008; Gallegos, Schubert, & Sanders, 2009). This is because the

impacts of pluvial flooding vary significantly at small spatial scales. For example, six inches of moving floodwater can knock down a pedestrian and cause vehicles to loose traction (National Weather Service [NWS], n.d.); in urban areas, where topography is highly heterogeneous, such changes in elevation can happen over short distances. While recent advances have been made towards model improvement and coupling (Cantone & Schmidt, 2011; Chang, Wang, & Chen, 2015; Henonin, Russo, Mark, & Gourbesville, 2013; Jorge Leandro & Martins, 2016; Nanía, León, & García, 2015; Wu, Wang, Guo, Lai, & Chen, 2018), the sources of errors in simulations of urban flooding have not yet been fully explored because of uncertainty and limited availability of geospatial data (terrain, soil, land cover, and infrastructure) and high-resolution precipitation forcing required to setup and run the simulations.

Of particular importance to increase accuracy of pluvial flooding prediction is the integration of infrastructure and high-resolution terrain data (Association of State Floodplain Managers [ASFPM], 2020). Infrastructure data includes all components of built stormwater systems, such as catch basins, manholes, conduits, detention and storage basins, drywells and outfalls, whereas terrain data includes urban features such as buildings, street curbs, overpasses and bridges. Unfortunately, these datasets are often incomplete or of poor quality and data collection efforts are resource intensive. Important characteristics of such spatial data quality are completeness, accuracy, consistency and current-ness (Fox, Levitin, & Redman, 1994; Veregin, 1999). Data completeness as defined by Fox et al. (1994) is the degree to which a data collection has values for all the attributes of all the features. Guptill and Morrison (1995) and Veregin (1999) further

characterize data completeness as feature completeness, attribute completeness and value completeness. For example, in a stormwater database, features include components like conduits, catch basins, and manholes; each feature has attributes, such as material or diameter for conduits; and attributes have numerical or categorical values. In a complete stormwater database, all the system components as features; and its attributes and values are present.

Model development is also challenged by the limited availability of high-resolution spatial data (e.g., 1-m digital elevation models or DEMs), and the need to balance computational cost with accuracy requirements. The resolutions of commonly available DEMs (e.g., 10 m in U.S. (United States Geological Survey [USGS], n.d.)) do not sufficiently capture fine details of urban infrastructure features such as walls, curbs, steps and storm drains, thus preventing the simulation of overland flow in complex urban environments (Fewtrell et al., 2008; Krebs et al., 2014; Leitão et al., 2016; Sampson et al., 2012). Past studies have cautioned that the ideal spatial resolution is between 2 and 5 m for the effective representation of urban features (Arrighi & Campo, 2019; Dottori, Di Baldassarre, & Todini, 2013). The advent of airborne Light Detection and Ranging (LiDAR) has increased the availability of high-resolution (less than 1 m) topographic data that would allow incorporating small-scale heterogeneities found in urban basins into hydrologic models (Bates et al., 2003; Bermúdez and Zischg, 2018; Fewtrell et al., 2011; Noh et al., 2018; Sampson et al., 2012). Despite this promising capability, LiDAR products are available at limited sites, are expensive to acquire, and require significant computational resources to be processed and used in numerical models. More insight is

then needed to weigh costs and benefits of investment in LiDAR for urban flood modeling.

Previous studies have evaluated the impacts of simplifying the model representation of certain elements (Krebs et al., 2014), and prior research demonstrates that select aggregation may have limited impacts on model results. For example, Elliot et al. (2009) assessed different aggregations of detention tanks and bioretention, as well as their associated catchment areas, finding that there is little effect on predictions of mean flow, baseflow and water quality at the outlet. However, while aggregation of stormwater control features allows modeling water balance or outflow hydrograph at a lower computational cost, this approach provides limited information on location, duration, and extent of the flood, which is crucial when modeling the impacts of pluvial flooding. Thus, additional research is needed to assess the feasibility of aggregation for spatially distributed street flooding estimation.

As hydrologic-hydraulic models for urban flood modeling are critical to flood prediction, infrastructure design, and adaptation planning, it is crucial to also understand the impact of different sources of error and uncertainty (Pathak et al., 2015). For engineers and planners developing asset management plans (Harvey et al., 2017), designing flood mitigation infrastructure (Kabisch, Korn, Stadler, & Bonn, 2017; Kuriqi & Hysa, 2021) or rehabilitating drainage structures (Martínez, Sanchez, Toloh, & Vojinovic, 2018), accurate hydraulic information of the drainage system as well as communication of output uncertainty is vital. Several past studies on different catchment scales focused on, (1) quantifying the rainfall error uncertainty on hydrologic model

outputs arising from temporal resolution (Lyu, Ni, Cao, Ma, & Tian, 2018), data products such as satellite rainfall (Bitew & Gebremichael, 2011) or radar rainfall error propagation (Hjelmstad, Shrestha, Garcia, & Mascaro, 2021; Sharif, Ogden, Krajewski, & Xue, 2002); (2) quantifying effect of DEM resolution on urban flood modeling (J. P. Leitão, Boonya-aroonnet, Prodanović, & Maksimović, 2009; J. P. Leitão & de Sousa, 2018). However, little is known about modeling errors arising from missing infrastructure data (e.g., missing features or components) or properties of these features (e.g., missing attributes), and standard approaches on how to deal with data gaps are nonexistent. Further, the effect of DEM and model resolution in conjugation with completeness of infrastructure features in coupled 1D-2D model is not fully understood or quantified.

This study aims at addressing two research questions motivated by the challenges in pluvial urban flood modeling described above, including: (1) How do the proportion and spatial distribution of infrastructure data gaps impact model performance? and (2) How does the spatial resolution of the terrain data interact with infrastructure data gaps to impact the model performance? Model performance is defined as accuracy and precision in modeling flood flow rate, volume, duration, and extent. To examine these research questions, we simulated pluvial flooding in an urban catchment in the city of Phoenix, Arizona using a semi-distributed, coupled hydrological-hydraulic model based on the U.S. Environmental Protection Agency's (EPA) Storm Water Management Model. We first explored the effect of missing data (i.e., attribute-value of parameters) using the one-dimensional rainfall-runoff and pipe flow model (SWMM 1D). We then examined the combined effect of model resolution (i.e., high and low model resolution) and data

completeness (i.e., missing stormwater features) using the coupled 1D-2D model (SWMM 1D-2D). In sum, our objectives are to assess model error, bias and uncertainty arising from missing infrastructure attribute data; and to investigate the combined effect of infrastructure feature data gaps and coarsening model resolution.

2.2 Study Area, Data Collection and Processing

To answer our research questions, we focus on an urban catchment in the city of Phoenix, Arizona, since the city faces periodic pluvial floods and the required infrastructure data are complete and accessible (Figure 2.1a). Phoenix is the capital of the state and the main city of one of the largest metropolitan regions in the U.S., with a population of approximately 4.5 million people. It is in central Arizona and the northeastern Sonoran Desert, downstream of the confluence between the Salt and Verde Rivers. According to the Köppen classification, the climate is hot desert or arid (BWh) with extreme hot summers and mild short winters. The average yearly precipitation is 204 mm, while mean temperature is 24 °C (Mascaro, 2017). Climate is characterized by two main seasons that influence the rainfall regime. The first includes a summer period from July to September that is dominated by the North American Monsoon, when convective activity leads to diurnally modulated, localized thunderstorms with short durations (less than 1 h) and high rain intensity (Balling & Brazel, 1986). The second season, which ranges from late October through March, is dry and occasionally interrupted by cold fronts, causing widespread storm systems with low-to-moderate rainfall intensity and relatively longer durations of up to a few days (Sheppard, Comrie, Packin, Angersbach,

& Hughes, 2002). Monsoonal thunderstorms cause severe flash flood events in the region, though other storm types can also trigger flooding. For example, in September 2014 the remnants of Hurricane Norbert triggered pluvial flooding, inundating major roadways throughout the valley (NWS, 2014).

In central Arizona, the spatial variability of annual, seasonal and extreme rainfall is moderately to significantly controlled by terrain, which varies from 220 to 2,325 m above mean sea level (MSL) (Mascaro, 2017, 2018, 2020). The topography of Phoenix is generally flat. The urban form is characterized by a street pattern running in precise grids, and such is the stormwater infrastructure layout. Our study catchment has a total area of 2.4 km^2. The catchment runoff drains to the south of the main outfall into the Salt River (Figure 2.1b). The soil type distribution in the study catchment is presented in Appendix A. The weighted average imperviousness relative to the discretized sub-catchments' area is 71.24% while maximum is 99% (Appendix A).

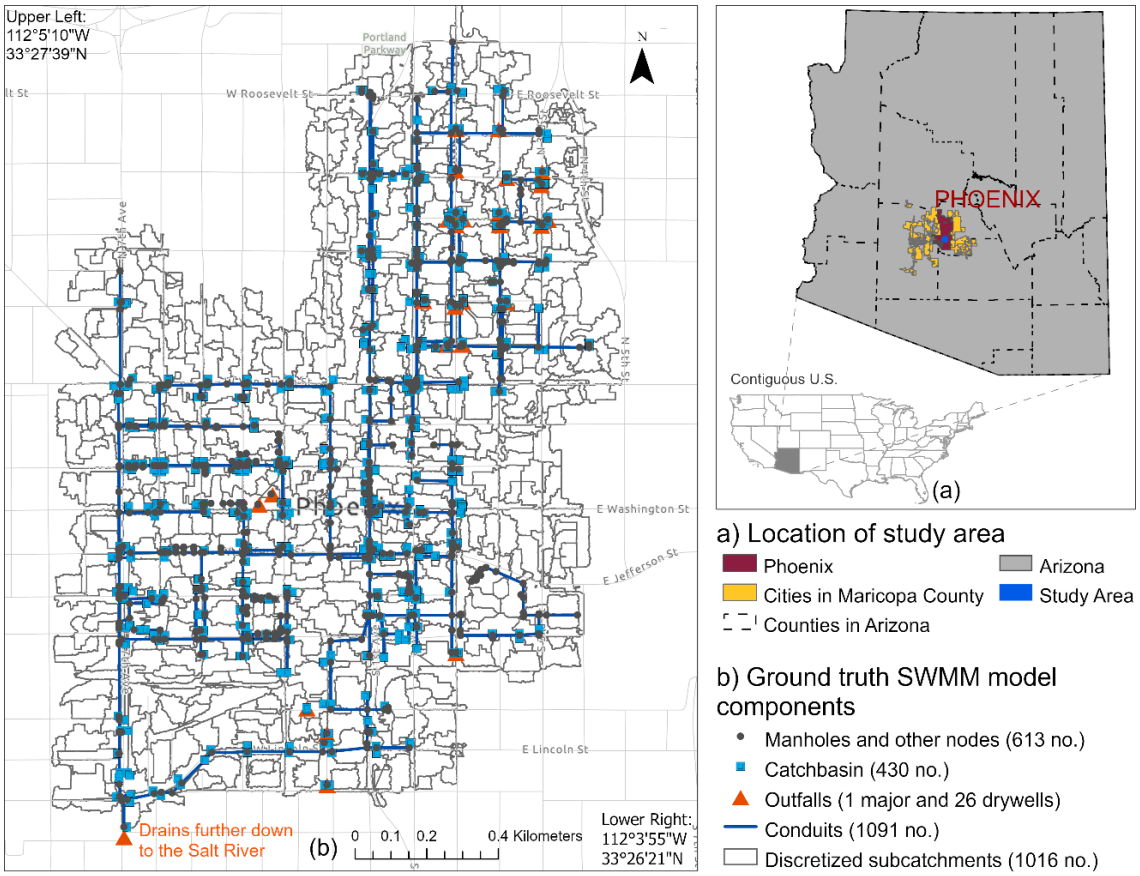

Figure 2.1. (a) Location of the City of Phoenix and (b) Study Catchment with Complete Catchment Infrastructure Data (Referred to as the Ground Truth Data Set)

The summary of data used in this study is shown in Table 2.1 and Figure 2.2. Table 2.1 classifies data as vector, raster, or point cloud data. These data are either raw, processed by the authors for this study or secondary data obtained from the noted source. Figure 2.2 shows the layers of spatial data required to build SWMM 1D-2D models. SWMM 1D model also utilizes the same layers without terrain data layers, namely building and mesh grids.

Table 2.1. Data Used in This Study

Data	Data type	Source
Stormwater infrastructure data	Vector (Secondary data)	Phoenix Public Works Department and Flood Control District of Maricopa County
LiDAR point cloud data	Point cloud (Raw data)	USGS 3D Elevation Program (USGS, n.d.) and Arizona State University (ASU) Geo Spatial hub database
Digital Elevation Model (DEM)	Raster (Processed data)	LiDAR point cloud dataset (ASU, 2018)
Digital Surface Model (DSM)	Raster (Processed data)	LiDAR point cloud data (ASU, 2018)
Soil types and parameters	Vector (Secondary data)	United States Department of Agriculture – Natural Resources Conservation Service, Web Soil Survey database (USDA-NRCS, n.d.); Arizona Department of Transportation, Highway Drainage Design Manual (ADOT, 2014)
Urban imperviousness data	Raster (Secondary data)	National Land Cover Database, Multi-Resolution Land Characteristics Consortium (MRLC, n.d.)

Stormwater infrastructure data with complete features and attribute-values is critical to build the hydrologic-hydraulic model and simulate catchment behavior. The geodatabase for the infrastructure components in Phoenix is stored and updated at irregular intervals by the Phoenix Public Works Department. We obtained the infrastructure data, which is not publicly available, from the Public Works Department in 2019. To ensure that there are no missing data or inconsistencies in the GIS database, we verified through field visits that surface infrastructure features were properly located. The stormwater infrastructure data for the study catchment includes 430 catch basins to collect stormwater runoff; 613 manholes and other nodes which connect upstream and downstream conduits; 1,091 conduits with attributes of material, year built, depth, slope, shape and size; 26 drywells which infiltrate stormwater and are usually present in flat topography; and 1 major outfall where stormwater drains to the Salt River. The details of stormwater components in our study catchment are shown in Figures 2.1b and 2.2a.

Following the definition of data completeness by Guptill and Morrison (1995) and Veregin (1999), in this study we characterize data completeness as *feature completeness*, which refers to the known presence and location of all stormwater infrastructure components, and *attribute-value completeness*, which refers to known attributes and values of each component. Accuracy can also be assessed for both features and attribute-values. *Feature accuracy* refers to whether the feature type and location are correct, while *attribute-value accuracy* refers to whether infrastructure attributes (e.g., diameter) are correct. This study uses the single most current (and thus consistent) infrastructure dataset; therefore, this analysis does not focus on data consistency nor current-ness. Here, we assume that our field-verified infrastructure data set is both complete and accurate. We then refer to this infrastructure dataset as the ground truth and the corresponding model built as the ground truth model.

Point cloud LiDAR data were available as a terrain data with 0.3 m spacing for the City of Phoenix (ASU, 2018). Only the point cloud data with return points excluding buildings and vegetations were selected (using the LAS filter and create LAS dataset geoprocessing tool in ArcGIS Pro) to create a ground-based DEM (Figure 2.2b) that includes the details of street level and curbs. Since the use of the 0.3-m resolution DEM is computationally too intensive for 2D overland flow computations, a 4.6-m resolution DEM was also generated to create the 2D model (Figure 2.2c). In addition to the DEMs, we created a 0.3-m Digital Surface Model (DSM) that includes buildings (Figure 2.2d) but not trees (as trees do not impede water flow throughout their full canopy area) in

order to delineate the watershed. The buildings act as an impermeable obstruction layer in SWMM 1D-2D model.

Data on the catchment soil types and properties (e.g., suction head, saturated hydraulic conductivity; Figure 2.2e) were obtained from the Arizona Department of Transportation (ADOT, 2014). Urban imperviousness data from 2016 with a resolution of 30 m was used as seen in Figure 2.2f (MRLC, n.d.). The time series of design storm for a 1/50 annual exceedance probability with 45-min duration and 5-min intervals was created from National Oceanic and Atmospheric Administration (NOAA) Atlas 14 point precipitation frequency estimates (NOAA/NWS, n.d.) using an alternating block method (V. Te Chow et al., 1998). This study primarily focuses on extreme flood estimation rather than infrastructure design; thus, a higher return period was chosen. This design storm was used as the input for all simulations. We selected a storm duration of 45 min equivalent to the time of concentration for the catchment.

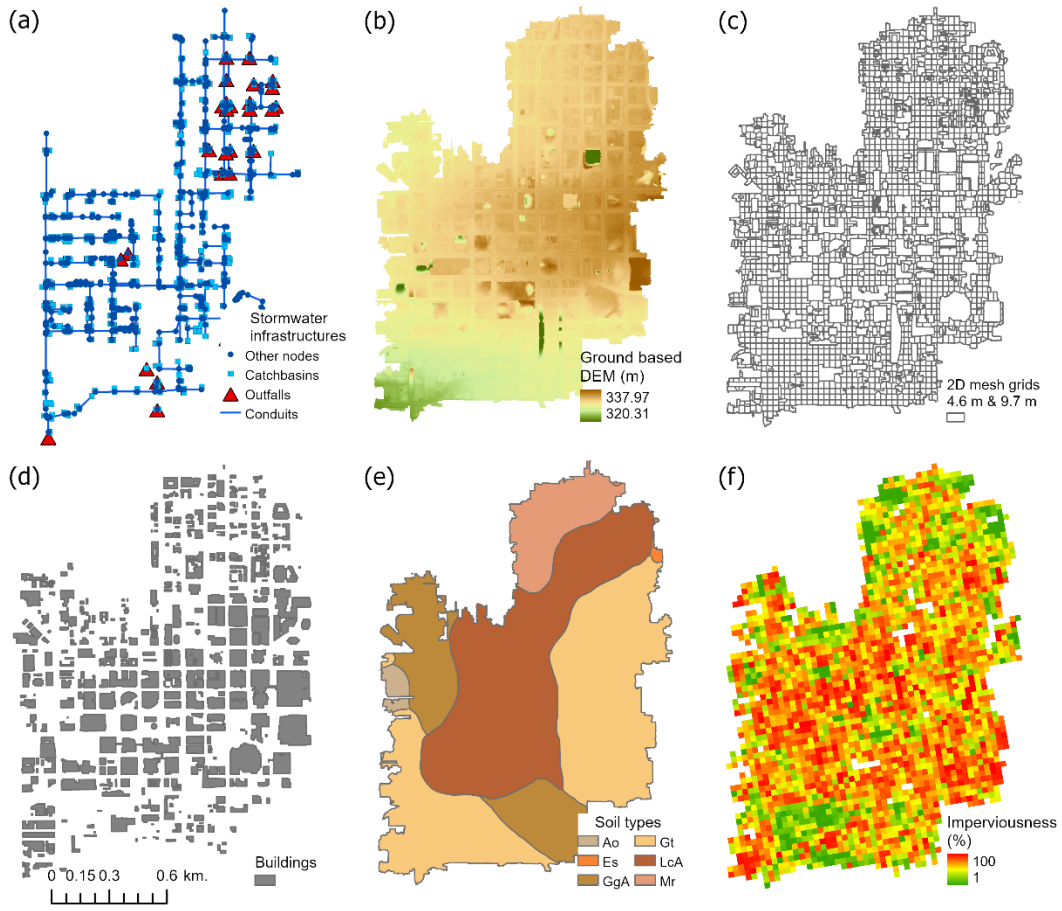

Figure 2.2. Spatial Data Sets Used to Develop the SWMM 1D-2D Model, (a) Stormwater Infrastructure Data, (b) Ground-based DEM, (c) 2D Mesh Grid, (d) Building Layer, (e) Soil Types, and (f) Imperviousness

2.3 Methodology

In the following sections we describe the development of the semi-distributed hydrologic-hydraulic model using 1D and coupled 1D-2D approaches. We then present the algorithm to fill attribute-value data gaps and the Monte Carlo sampling approach for attribute-value completeness. Lastly, we describe the selective sampling approach to assess the combined effect of feature completeness and model resolution.

2.3.1 Hydrologic-Hydraulic Model

We used the U.S. EPA's SWMM version 5.1 (1D model) and Computational Hydraulics International (CHI's) PCSWMM version 7.3.3095 (coupled 1D-2D model). To execute the model and facilitate Monte Carlo sampling, we used the R package 'swmmr' version 0.9.1 (Leutnant, Döring, & Uhl, 2019). SWMM is a hydrologic-hydraulic modeling tool that simulates rainfall-runoff and routing processes for single precipitation events or in a continuous fashion in urban or rural catchments. It estimates two main processes: i) runoff, which is computed on a collection of discretized sub-catchments that generate runoff and pollutants due to precipitation; and ii) routing, which is the transport of runoff across an underground network of conduits, overland channels and other components. SWMM is a semi-distributed model, and it accounts for various hydrologic processes such as time-varying rainfall, evaporation from standing water, rainfall interception in depression storage, infiltration into unsaturated soil layers, percolation into groundwater layers, interflow between groundwater and the drainage system, non-linear reservoir routing of overland flow and stormwater capture by low impact development. The details about theoretical background, equations, variables, features and capabilities of SWMM can be found in Rossman (2017) and James et al. (2010).

In this study, we apply two implementations of SWMM: 1) a one-dimensional drainage model (SWMM 1D) and 2) a coupled 1D-2D model (SWMM 1D-2D) that adds two-dimensional routing of overland flow of floodwaters. We used SWMM 1D to test the

effect of infrastructure data attribute-value completeness. The 1D model was chosen for its faster computation time compared to the coupled 1D-2D model and the ability to execute the model from the source code, which enables Monte Carlo sampling. SWMM 1D-2D was used to assess the combined effects of data feature completeness and model resolution. In practice, a large spatial infrastructure data set is rarely 100 percent complete due to manual data entry error, compilation error and antiquated data as new construction or rehabilitation takes place. However, for this study we assume that the data we acquired from the Phoenix Public Works Department and verified by walk-through surveys are 100 percent complete and accurate. We define this data as the ground truth, where all the required features and attribute-values are complete and accurate. The ground truth model, built from this data and the highest feasible resolution of DEM, serves as the basis for comparing simulations described in the next section.

The hydrologic component of SWMM simulates the rainfall-runoff transformation, after accounting for losses, through a non-linear reservoir model, where the reservoir capacity is maximum depression storage. In this model, the study area catchment is discretized into sub-catchments to reflect the spatial heterogeneity in topography, drainage pathway, land cover and soil characteristics that impact rainfall-runoff. We utilized the 0.3-m DSM, consisting of street profiles, buildings and general topography, to delineate the watershed and discretize it into smaller sub-catchments with an average area of 2,428 m^2 using the watershed delineation tools of PCSWMM. The hydrologic model input is precipitation, and the output from each sub-catchment are surface runoff and losses due to infiltration and evaporation. Surface runoff is defined as

the excess volume above the depression storage, which considers the initial abstraction such as surface ponding, interception by flat roofs, vegetation and surface wetting, which eventually evaporates or infiltrates following the storm. Depression storages of 1.25 mm for impervious surfaces and 2.5 mm for pervious surfaces, as suggested by the American Society of Civil Engineers (1992), were assigned for each sub-catchment. To calculate losses due to infiltration, we selected the Green-Ampt infiltration model implemented in SWMM with parameters derived from soil types (ADOT, 2014) which are presented in Appendix A. Here, discrete event simulation for the 50-year return period, 45-min design storm for downtown Phoenix (NOAA/NWS, n.d.) is applied to force all of the models. We assumed a constant evaporation rate of 0.76 cm/day (Western Regional Climate Center [WRCC], n.d.) corresponding to the average during monsoon season. The parameters used for the stormwater system are summarized in Appendix A. The governing equations and additional details for the hydrologic processes as employed in the SWMM can be found in Rossman (2017) and James et al. (2010).

The hydraulic component of SWMM uses the dynamic wave routine that solves unsteady flow through the network of conduits and nodes, using the conservation of mass and momentum equations. Dynamic wave routing solves the complete one-dimensional Saint-Venant flow equations, whose details can be found in Rossman (2006), which account for channel storage, backwater effects, entrance/exit losses and pressurized flow. Flooding in the system occurs when the hydraulic grade line at a node exceeds the threshold of available depth (i.e., rim elevation). The flooded water in SWMM 1D is accounted as flooding losses which will not re-enter the drainage network unless ponding

is allowed. The surcharge depth for manholes was assigned as 0.4 m which is equivalent to the resistance of manhole lid cover weight. The parameters for the sub-catchments and infrastructure are extracted directly from the attribute-values in the infrastructure database, soil data or DEM. These parameters include rim elevation, invert elevation and depth for catch basin and manholes junctions or nodes; roughness, length, diameter, cross-section and slope for conduits; invert elevation for outfalls and drywells nodes; and area, slope, imperviousness and Green-Ampt parameters for sub-catchments. The relevant outputs from the hydraulic component include: (1) time series of flooding and flow at all nodes and conduits respectively, (2) flood loss time series (i.e., flow exiting the drainage system when the hydraulic grade line reaches the surface) at all nodes and in aggregate (hereafter, referred to as system flooding), and (3) duration of flooding and surcharge at all nodes. The duration of node flooding is the length of time when the hydraulic grade line is above the rim elevation for a particular node. To maintain numerical stability and remove continuity error, a time step of 1 second was selected for both SWMM 1D and 1D-2D models.

For 1D-2D coupled modeling we used PCSWMM due to its additional capability to simulate overland flood routing and associated flood extent, depth, and duration in two dimensions. This model extends the fully dynamic 1D approach in EPA's SWMM5 to 2D free surface flow using a non-uniform mesh that captures the topography, geometry and built structures. SWMM 2D domain solves SWMM5 dynamic wave routing with or without inertial terms; ignoring inertial terms creates diffusive wave routing, which is virtually indistinguishable from full-term dynamic wave solution (Finney et al., 2012;

James et al., 2013). In the 2D domain, the overland surface is discretized into a square mesh and represents each 2D cell with a 2D node or a junction, where invert elevation for these nodes is assigned the ground surface elevation or rim elevation of adjacent coupled 1D nodes (Finney et al., 2012; James et al., 2013). In the 2D domain of 1D-2D coupled model, grid cells require slope and roughness parameters. SWMM 1D-2D uses the same sub-catchment delineation and catchment properties, as well as hydraulic network and hydrologic properties, as described above for SWMM 1D. The catch basin nodes are coupled with 2D mesh cells using orifices in 1D-2D model, such that the volume of water exiting an orifice, when flooding occurs, is routed over the 2D mesh cells. This excess flow can pond on the overland grid cells and re-enter the drainage network when the hydraulic grade subsides below ground elevation.

2.3.2 Random Sampling of Infrastructure Data

First, we tested the significance of infrastructure data completeness on the model. A one-at-a-time sensitivity analysis was conducted to identify the important infrastructure parameters using a built-in tool available in PCSWMM (Karen Finney & Gharabaghi, 2011). Sensitivity analysis assesses the rate of change in response of the model with respect to changes in the model input parameter and the relative importance of parameters to have more accurate values, as measured by the sensitivity gradients (W. James, 2003). Details of sensitivity analysis are presented in Appendix B. We selected five infrastructure-related parameters from stormwater components: conduit diameter, node depth (i.e., maximum distance from invert elevation to rim elevation), conduit

roughness, inlet offset (i.e., the distance from a conduit's inlet end to the connected node invert elevation), and outlet offset (i.e., the distance from a conduit's outlet end to the connected node invert elevation). All parameters are sampled uniformly within lower to higher parameter values given by an uncertainty level of 50% as described in Appendix B. Out of the five parameters tested, we found that the three most sensitive parameters are conduit roughness, conduit diameter and node depth (hereafter, referred to as roughness, diameter and depth), as shown in Table 2.2 where larger absolute values of the sensitivity gradient indicates more sensitive parameters.

Table 2.2. Sensitivity Analysis of Infrastructure Related Parameters.

Parameter	Initial parameter value	Mean sensitivity gradient
Diameter	ground truth	-0.270
Depth	ground truth	-0.197
Roughness	ground truth	0.109
Outlet offset	5 cm	-0.001
Inlet offset	5 cm	0.000

To test the impact of missing attribute-value data on the model, we developed an algorithm to randomly sample conduits and nodes, remove values of roughness, diameter and depth in these selected features, and estimate these missing attribute-values using the remaining data and design standards. The algorithm enables us to test many combinations of missing attribute-values using Monte Carlo sampling. The replacement component of the algorithm is essential as a SWMM model cannot be run without specifying all parameter values. The replacement criteria for missing attribute-value is implemented in accordance with the available design standards and modeling practice. The detailed process algorithm is described below, and the overall method for random sampling is illustrated in Figure 2.3.

The algorithm to sample roughness, diameter and depth, illustrated in Figure 2.3, develops and runs a new SWMM 1D model for each iteration $N = 100$ times by randomly removing a specified percentage of each of the three parameters identified above, then filling these gaps based on the remaining information available. The process can be summarized into three main steps:

1. Randomly select the number of conduits and nodes corresponding with the percent of missing attribute-values specified (i.e., *m* number of features to be sampled per parameter). For the selected sample, delete existing roughness, diameter, or depth.
2. Replace deleted attribute-values with an informed estimate. The estimation algorithm is specific to the parameter:
    a. Roughness: identify the upstream pipe and apply its roughness. If the upstream roughness attribute is missing, then use the downstream roughness. If both upstream and downstream roughness are missing, randomly sample an empirical distribution function (EDF) of roughness from available information (i.e., conduits with known roughness). The empirical distribution of roughness in the ground truth model is presented in Appendix D.
    b. Diameter: identify the upstream pipe and apply its diameter. If the upstream diameter attribute is missing, then use the downstream diameter. If both upstream and downstream diameters are missing, then use the mean diameter of all conduits in the dataset with known diameters.

c. Depth: identify the upstream node and apply its depth. If upstream depth is missing, then use the depth of downstream feature. If both upstream and downstream depths are missing, assume a minimum cover of ~0.91 m as per the Arizona drainage design manual (ADOT, 2014). The node depth information is shared by both connected node (or junction) and conduits. Note that there are a few conduits with ~0% slope in the ground truth and randomly sampled models, particularly for shorter length conduits, but the overall slope is positive. In addition, elevation of the street surface and the rim elevations gradually slope downward from upstream to downstream nodes, thus in this particular catchment the negative slopes are avoided when sampling depth.

3. Run SWMM 1D and extract the time series of system flooding and duration of flooding (if present) at each node.

Model accuracy is defined relative to the ground truth model output and is quantified by the mean absolute error (MAE) and percent bias (PBIAS). The MAE and PBIAS for system flooding (SF in subscript) are defined as:

$$MAE_{SF} = \frac{1}{N}\sum_{j=1}^{N}\left(\frac{1}{T}\sum_{t=1}^{T}\left|y_{t,j} - x_t\right|\right) \quad (1)$$

$$PBIAS_{SF} = \frac{1}{N}\sum_{j=1}^{N}\left[\frac{\sum_{t=1}^{T}\left(y_{t,j} - x_t\right)}{\sum_{t=1}^{T} x_t}\right] \quad (2)$$

where, $y_{t,j}$ is the simulated flow at each time steps t (t = 1, …, T) for the j-th (j = 1, …, N) iterations (where N = 100), and x_t is the value simulated by the ground truth model. Both MAE_{SF} and $PBIAS_{SF}$ were first computed as the comparison of hydrographs obtained from sampled and ground truth models, and then averaged across all 100 iterations.

For the duration of node flooding, MAE and PBIAS (FD in subscript) were computed from the mean and maximum durations of node flooding in 100 iterations compared to the ground truth, which is defined as:

$$MAE_{FD} = \frac{\sum_{j=1}^{N} |y_j - x_j|}{N} \tag{3}$$

$$PBIAS_{FD} = \frac{\sum_{j=1}^{N} (y_j - x_j)}{\sum_{j=1}^{N} x_j} \times 100 \tag{4}$$

where, y_j is mean (or maximum) duration of node flooding for each j = *1 to* N^{th} iteration (where N = 100), x_j is the mean (or maximum) duration of node flooding in the ground truth model.

Model uncertainty describes the degree of variation in model output across sampled simulations and is quantified by the relative interquartile range (RIQR), which is defined as:

$$RIQR = \frac{q_{0.75} - q_{0.25}}{q_{0.5}} \times 100 \tag{5}$$

where, $q_{0.75}$, $q_{0.25}$, and $q_{0.5}$ represent upper quartile, lower quartile, and median, respectively, for the empirical distributions of either maximum system flooding (i.e., peak flow) or duration of flooding averaged (or maximum) across all nodes. Precision is referred to as the inverse of uncertainty.

The significance of missing data was tested in terms of the level and location of missing data. For different levels of missing data (5%, 25%, 50% and 75%), the number of features sampled, *m*, is the corresponding percentage of missing data multiplied by the total number of relevant features (i.e., conduits or nodes). Then, to assess the impact of the location of missing data, we assumed that 50% of data is missing and divided the catchment into two regions, the upstream and downstream. The 50% missing data level was selected because, as shown later in the results, model error increased consistently across parameters with increasing missing data until 50% when sampling the full catchment; beyond 50% the pattern was mixed. The upstream and downstream features were identified by conditional selection of features that are above or below the median distance from the main outfall for the upstream or downstream region, respectively. To test the influence of the location of missing data, the random sampling method described above with the same $N = 100$ iterations was repeated with the removed attribute-values limited to the upstream and then downstream regions of the network. For random sampling, only the SWMM 1D model was used since the computation time of SWMM 1D-2D is too long to perform many runs. The SWMM 1D-2D model was reserved for selective sampling, as described next.

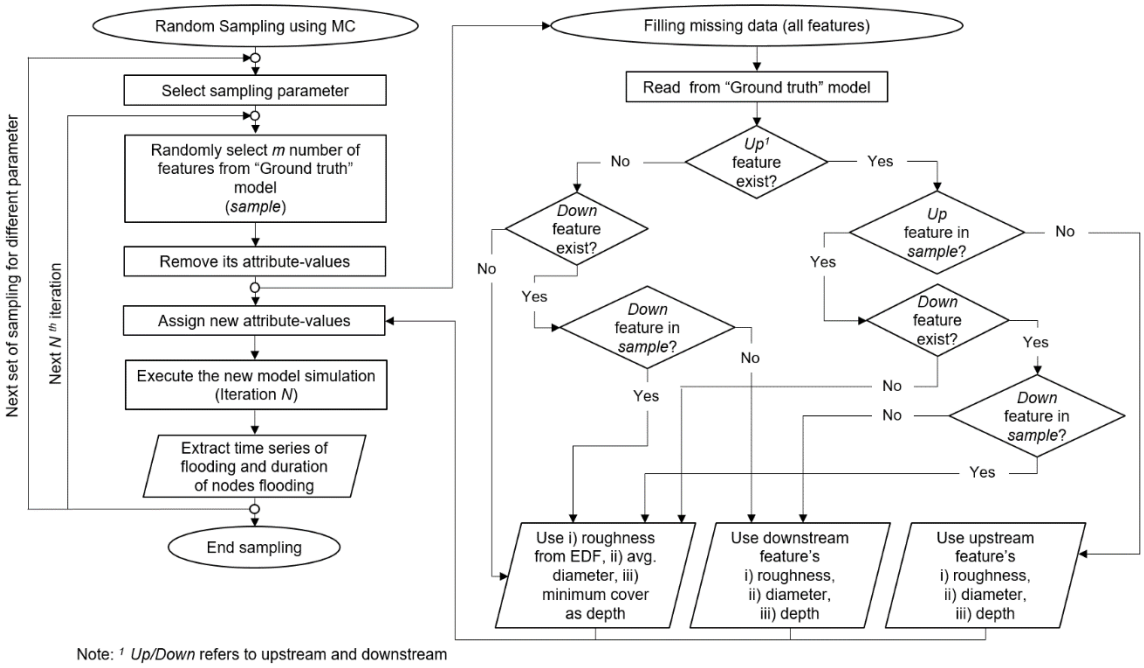

Figure 2.3. Overview of the Random Sampling Process

2.3.3 Selective Sampling

We applied selective sampling of SWMM 1D-2D models to assess the impact of different combinations of feature data completeness and model resolution on model performance. Model resolution for the semi-distributed model is defined in terms of the resolutions of the 2D mesh grid and the DEM utilized to create such a grid. Four selective sampling models were created (Table 2.3).

Table 2.3. Four Selective Sampling Models. Note That HD/LD the First Two Letters Refers to Stormwater Data (i.e., HD = High Data or Complete Data, LD = Low Data or Incomplete Data) and HM/LM Refers to Model Resolution (i.e., HM = High Model Resolution, LM = Low Model Resolution).

Sampling model	Details on infrastructure	DEM resolution (m)	2D mesh cell resolution (m)
High infrastructure data completeness and high model resolution (HDHM)	ground truth	0.3	4.6
High infrastructure data completeness and low model resolution (HDLM)	ground truth	9.7	9.7
Low infrastructure data completeness and low model resolution (LDLM)	Incomplete infrastructure model where ~50% of the upstream components (features) were missing from the ground truth model (Appendix C)	9.7	9.7
Low infrastructure data completeness and high model resolution (LDHM)	Incomplete infrastructure model where ~50% of the upstream components (features) were missing from the ground truth model (Appendix C)	0.3	4.6

In the low-resolution models (HDLM and LDLM), slopes for the discretized sub-catchments were assigned from the coarser-resolution, 9.7-m DEM to account for the fact that high-resolution terrain could not be available in all places and that the most commonly available DEM resolution from USGS is 1/3rd arc second (~10 m). Although two of the selective sampling models (LDLM and LDHM) have missing features or incomplete infrastructure data, the attribute-values for all remaining features are the same as the ground truth. The selective sampling results were compared in terms of flood depth, volume and extent. Flood depth refers to the maximum water level observed in the 2D mesh cells at the time of peak flooding. Flood volume refers to the sum of all flooding fluxes from 1D nodes to 2D grid cells through orifices integrated over the whole flood

period. Flood extent refers to the sum of the areas of 2D mesh cells with flood water >0 mm at the time of peak flooding.

2.4 Results and Discussion

This section first presents simulation results from Monte Carlo sampling of SWMM 1D model recounting the effects of different levels and locations of incomplete data on modeled peak flood flow and duration. Then, we present SWMM 1D-2D modeling results for four selective sampling models characterized by combinations of complete or incomplete infrastructure data and high or low model resolution, particularly focusing on flood depth, extent and volume.

2.4.1 Evaluation of Random Sampling

The impacts of missing attribute-values for the three selected model parameters on the simulated flooding conditions and metrics are summarized in Figures 4 and 5. Specifically, Figure 2.4 shows the distribution of simulated flood duration at all nodes for the three sampled parameters in 100 Monte Carlo sampling and the ground truth model at different percentages of missing attribute-values. Figure 2.5 presents boxplots of 100 Monte Carlo sampling for maximum system flooding (Figures 2.5a-c), maximum flooding duration (Figures 2.5d-f), and average flooding duration (Figures 2.5g-i) as a function of percent of missing data (hereafter, PMD). Table 2.4 reports error and uncertainty metrics as defined in Section 2.3.2. For the clarity of exposition, these figures and table are discussed in the following three sub-sections focusing separately on

sampling roughness, diameter, and depth. Finally, in the last subsection, we illustrate the effect of missing attribute-values at upstream and downstream portions of the basin for PMD = 50% for the three parameters.

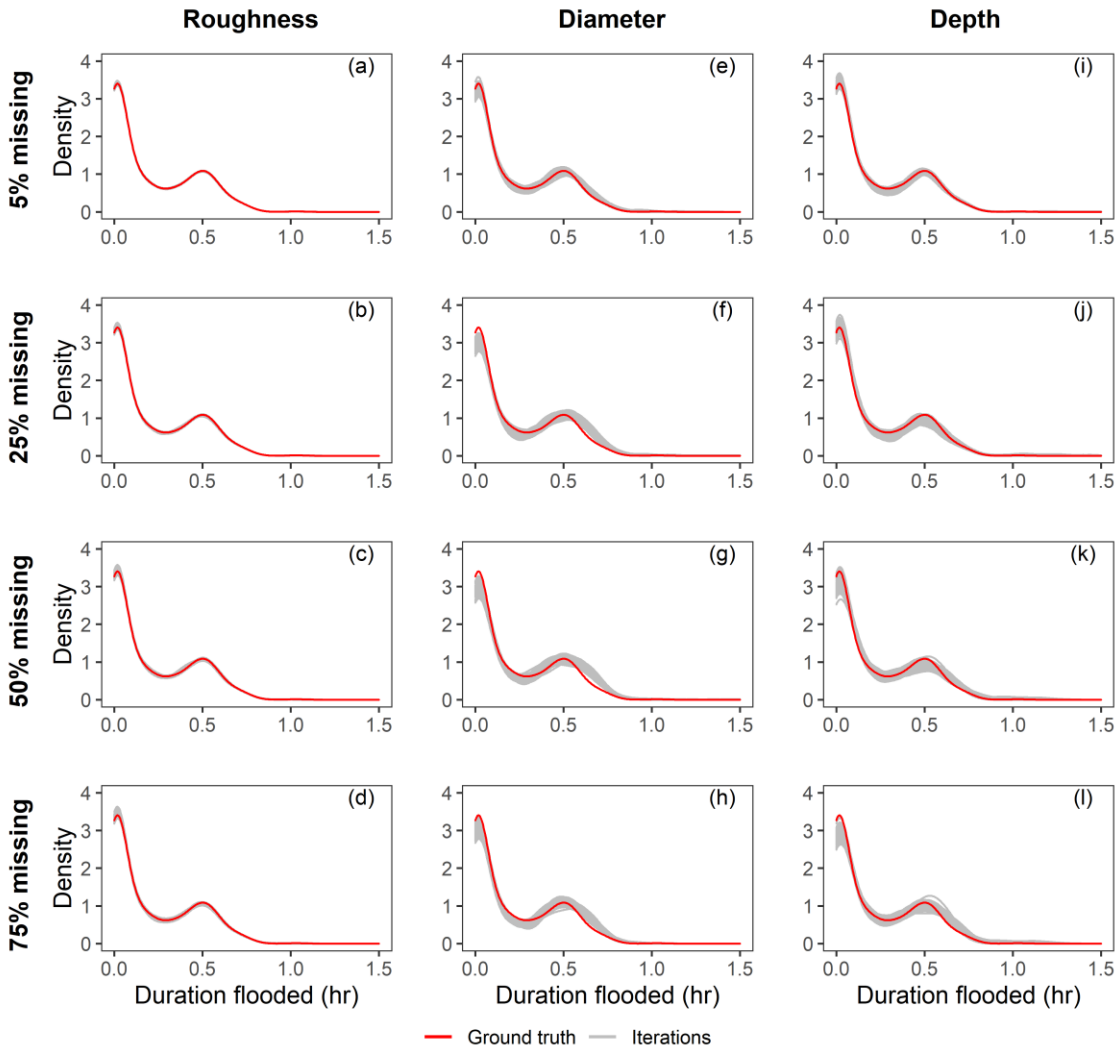

Figure 2.4. Monte Carlo Sampling Results Showing Distribution of Flood Duration at All Nodes with Observed Flooding While Sampling (a-d) Roughness, (e-h) Diameter and (i-l) Depth at Different Levels of Missing Attribute-values. One Hundred Iterations (Grey) Are Compared with the Ground Truth Model (Red). Note: Density Plots (Wickham, 2009) Are Smoothed Version of Frequency Polygon Based on Kernel Smoothers Useful

to Compare Shape of the Distributions; Here, Default Bandwidth Adjustment of 1 and Gaussian Kernel Was Selected

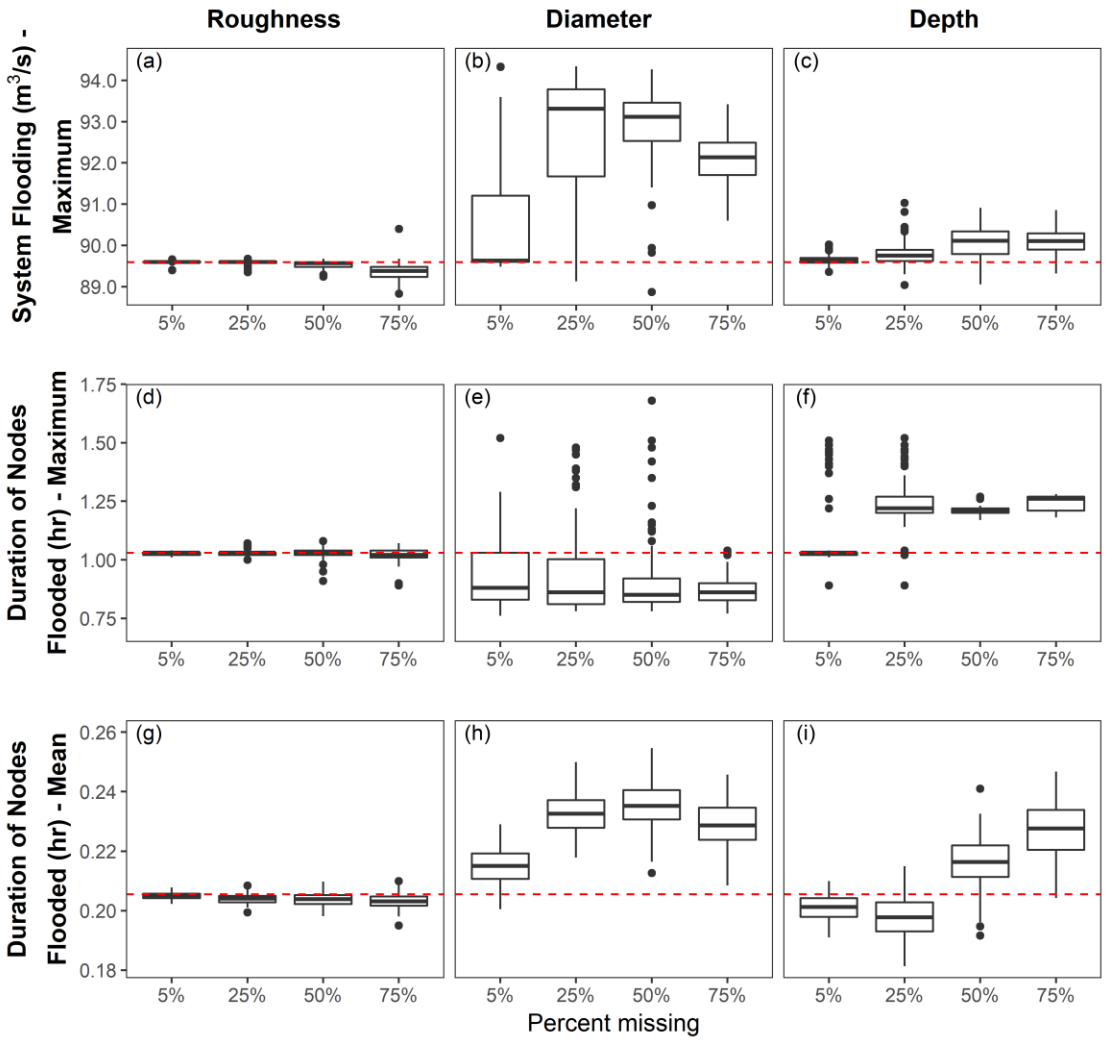

Figure 2.5. Monte Carlo Sampling Results Showing (a-c) Maximum System Flooding, (d-f) Maximum Duration of Nodes Flooding, and (g-i) Average Duration of Nodes Flooding with Different Percentages of Missing Sampling Roughness, Diameter or Depth Data. Boxes Represent the 25th, 50th and 75th Percentiles and Whiskers Represent ±1.5×IQR of the 25th and 75th Percentiles. Horizontal Red Dash Lines Represent the Values Simulated by the Ground Truth Model.

Table 2.4. System Flooding Metrics of Average of MAE and PBIAS (from Ensemble Simulations Vs. Ground Truth) and RIQR of Peak System Flooding; And Flood Duration Metrics of MAE and PBIAS (from the Maximum and Mean Duration of Flooding in Ensemble Simulations Vs. Ground Truth) and RIQR of Maximum and Mean Duration of Nodes Flooded for Random Sampling with Different Percentages of Missing Attribute-values

Sampling		**System flooding**			**Flood duration (Maximum)**			**Flood duration (Mean)**		
Attri-bute	**PMD (%)**	**MAE (m^3/s)**	**PBIAS (%)**	**RIQR (%)**	**MAE (hr)**	**PBIAS (%)**	**RIQR (%)**	**MAE (hr)**	**PBIAS (%)**	**RIQR (%)**
Roug-hness	5	0.34	-0.00	0.01	0.00	-0.40	0.97	0.00	-0.30	0.74
	25	0.85	-0.04	0.03	0.01	-0.10	0.97	0.00	-0.70	1.08
	50	1.69	-0.15	0.13	0.01	-0.30	1.94	0.00	-0.90	1.50
	75	3.62	-0.45	0.27	0.02	-1.00	2.94	0.00	-1.20	1.53
Dia-meter	5	20.48	3.00	1.79	0.15	-9.10	22.73	0.01	4.60	4.00
	25	55.28	9.00	2.26	0.17	-8.80	22.38	0.03	13.20	4.11
	50	62.06	10.14	1.00	0.18	-11.70	11.76	0.03	14.60	4.16
	75	60.84	9.82	0.85	0.16	-15.80	8.43	0.02	11.30	4.46
Depth	5	1.93	0.24	0.13	0.05	4.00	0.97	0.00	-2.00	3.11
	25	9.76	1.54	0.30	0.21	20.60	5.74	0.01	-3.60	4.93
	50	18.76	2.92	0.61	0.18	18.00	1.65	0.01	5.10	4.89
	75	20.79	3.26	0.44	0.21	20.70	4.76	0.02	10.80	5.87

2.4.1.1 Effect of Roughness

We begin by discussing Figure 2.4, where the distribution of flood duration simulated by the ground truth model is displayed by a red curve, whereas the ensemble simulations of 100 iterations for different levels of missing data are shown by grey curves. The ground truth model predicts that 564 nodes will be flooded for a varied duration from 0.01 to 1.03 hr, or an overall average duration of 0.21 hr. The density plot for ground truth (Figure 2.4) shows the number of flooded nodes decreases rapidly for durations up to 0.2 hr, rises slightly until 0.5 hr, and then decreases at a lower rate up to about 1 hr. When only 5% of the roughness data are missing, the ground truth

distribution is well captured across the simulations (Figure 2.4a). However, as PMD increases (Figures 2.4b-d.), the Monte Carlo runs simulate slightly higher number of nodes that are flooded for 0.01 hr, and slight increase in uncertainty observed between 0.1 and 0.5 hr.

Figures. 5a,d,g and Table 2.4 show that errors, bias and uncertainty of the simulated flood metrics increase only slightly as PMD of roughness increases. Bias and uncertainty are low but increase for higher PMD, as seen in the peak flooding flow rate (maximum PBIAS of -0.45%, max RIQR of 0.27%), maximum duration (maximum PBIAS of -1%, max RIQR of 2.94%) and average duration (maximum PBIAS of -1.2%, max RIQR of 1.53%). In other words, when the data available on pipe roughness decreases, our algorithm designed to replace missing data results in low error, bias and uncertainty. This is explained in part by algorithm skill and in part by the fact that in the ground truth data the majority (90%) of the conduits are concrete (including reinforced concrete and rubber gasket reinforced concrete pipe, all of which have an average roughness of 0.015 $sec/m^{1/3}$ as presented in the Appendix D). Given the shape of this empirical distribution the probability of sampling the incorrect roughness is low. Acknowledging that other locations will present a greater challenge for sampling roughness, we investigated how the PMD for roughness would affect the model outputs if the distribution was not dominated by a single conduit material. For this we created a hypothetical set of conduits (using the same model and holding other parameters constant) where distribution of materials is 12% concrete, 51% corrugated metal pipe, and 37% smooth plastic (HDPE or PVC). This distribution is valid per the drainage

design standards (City of Phoenix, 2013) (see Appendix D for details). In this hypothetical conduit distribution, we found that error, bias and uncertainty are higher but remain moderate at 50% PMD or lower (PBIAS less than 5%, RIQR less than 10%, as presented in Appendix D). The error associated with different PMD of roughness could be reduced with information on the relationship between pipe age, size, and material, if available.

2.4.1.2 Effect of Diameter

The effect of increasing the diameter PMD on the simulated distribution of flood duration is (Figures 2.4e-h): (1) lower (higher) number of nodes for durations between 0.01 and 0.3 hr (0.6 and 0.9 hr), (2) equal likelihood of simulating higher or lower number of nodes flooded between 0.3 and 0.5 hr. However, the uncertainty does not increase consistently with PMD. The boxplots of the three flood metrics related to missing diameter data exhibit a nonlinear behavior (Figures 2.5b,e,h). The peak system flooding and mean flood duration are overestimated, while maximum flood duration is underestimated. This is because the maximum flood duration tends to occur at the peripheral nodes (connected to 0.3-m diameter pipes) in the network where sub-catchment runoff drains into the network, whose downstream conduit's diameter are usually > 0.3 m. Thus, the current sampling algorithm underestimates peripheral node surcharge and flooding, and the majority of Monte Carlo simulations underestimate maximum flood duration. For all metrics, the largest MAE is obtained for PMD = 50%. The largest PBIAS for peak system flooding and mean flood duration is also obtained for

PMD = 50%. The largest uncertainty for peak system flooding is obtained for PMD = 25%, for maximum flood duration is obtained for PMD = 5%, but for mean flood duration is obtained for PMD = 75% while uncertainty range is similar for PMD = 5% to 25% (Table 2.4). When sampling from PMD = 5% to 50%, error increased for all metrics, but uncertainty decreased for peak system flooding and maximum flood duration or remained stable for mean flood duration. At PMD = 75%, sampling results showed slight improvement in accuracy as shown by MAE and observed in Figures 2.5b,e,h. These outcomes are a consequence of the algorithm adopted to replace missing diameter data. As PMD rises, there are more chances that missing diameters are assigned the average diameter of the stormwater system (see Figure 2.3), so that several peripheral pipes (trunk pipes) in the network are oversized (undersized). In the ground truth model, 68.7% of conduits are circular 0.3-m pipes, but the average is 0.46 m. The average and median diameter are similar in this case, and both result in the selection of the same standard conduit size (0.46 m or 18 inches). Overestimating small pipes reduces the risk of stormwater capacity constraints and surcharge in the periphery of the network, which explains decrease in maximum system flooding and duration of flooding. In contrast, underestimating large pipes leads to increased probability of surcharge along the main conduit, which can also lead to surcharge in upstream peripheral conduits. It is also important to note that maximum flooding duration does not signify maximum flood flow rate or volume, just the longest duration.

2.4.1.3 Effect of Depth

The effect of missing depth on the simulated distribution of flood duration is that when PMD = 5%, the model simulated more flooded nodes between 0.01 and 0.1 hr but lower between 0.2 and 0.5 hr (Figure 2.4i). While at PMD = 25%, the model is equally likely to simulate higher or lower number of nodes that will be flooding between 0.01 and 0.1 hr, while it mostly simulates lower number of nodes flooded between 0.2 and 0.7 hr (Figure 2.4j). When PMD = 50% or 75%, the model simulates lower number of nodes flooded between 0.01 and 0.1 hr, it is equally likely to simulate higher or lower number of nodes flooded between 0.1 and 0.5 hr, but more likely the model simulates higher number of nodes flooded between 0.5 and 0.9 hr (Figures 2.4k-l). Error in estimating peak system flooding and average duration of nodes flooding (as shown by MAE and PBIAS) increases monotonically with increasing PMD, with the largest error occurring at PMD = 75% (Figure 2.5c,i). Lowest precision (or highest uncertainty) occurs at different PMD for different metrics (Table 2.4). There was an increase in precision for estimating peak system flooding when PMD increased to 75% from 50%, and for estimating maximum flood duration when PMD increased to 50% from 25% (Table 2.4 and Figure 2.5 c,f). At PMD = 5%, the model response does not significantly change in terms of peak system flooding (Figure 2.5c) or maximum duration of nodes flooded (Figure 2.5f), except the outliers for highest duration of nodes flooded are from few significant nodes being assigned average depth whose upstream and downstream depth are missing. As PMD increased from 50% to 75% for the peak system flooding and from 25% to 75% for maximum duration of node flooding, the model accuracy didn't change much as shown

by MAE and PBIAS (Table 2.4). The model simulates lower mean duration of nodes flooded when PMD is 5% or 25%, and higher when PMD is 50% or 75% (Figure 2.5i). This is because when PMD is 5% or 25% it is more likely that upstream or downstream depth is present which either increases the depth or creates uniform slopes, thus improving the capacity of the network causing less surcharge. In contrast when PMD is 50% or 75% it is more likely that both the upstream and downstream depth are missing, thus minimum depths are assigned creating non-homogenous depth. Thus, modelers should be cautious in estimating missing depth.

In sum, this analysis demonstrates how the missing infrastructure attribute-values affects estimation of pluvial flooding under reasonable assumptions for filling missing roughness, diameter and depth based on available information and design standards (as shown in Figure 2.3). While estimation could be improved by carefully examining each instance of missing data individually, this is often not feasible due to resource constraints. This estimation method can quickly estimate many missing attribute-values and the specific algorithms can be adjusted to fit local design standards and available information.

2.4.1.4 Effect of Location of Missing Data

We also examined how model performance is affected by the location of missing data, by assuming PMD = 50% either in the upstream or downstream portion of the network, as described in the methodology. Figure 2.6 shows boxplots of flood metrics derived from N = 100 Monte Carlo sampling, while metrics values are reported in Table

2.5. Appendix D presents the effect of missing roughness in hypothetical conduit distribution. It is apparent that lack of information in the downstream section leads to higher error, bias, and uncertainty. This means that when missing data is in the downstream region of the catchment, the approximation to fill missing data that works for upstream attributes may be insufficient. It also establishes the relative importance of a feature's distance from the outfall, indicating that distance from the outfall might be an important input into a more sophisticated estimation algorithm.

Monte Carlo sampling for the three parameters showed varied degrees of relative importance. Out of the three attributes, missing diameter had the most effect in downstream sampling, as it could lead to the highest error in system flooding and average duration of nodes flooding. Missing diameter in the downstream section led to the lowest model precision, as indicated by a RIQR of 0.8% for system flooding and a RIQR of 14% (and 4%) for maximum (and mean) duration of nodes flooding (Figure 2.6 and Table 2.5).

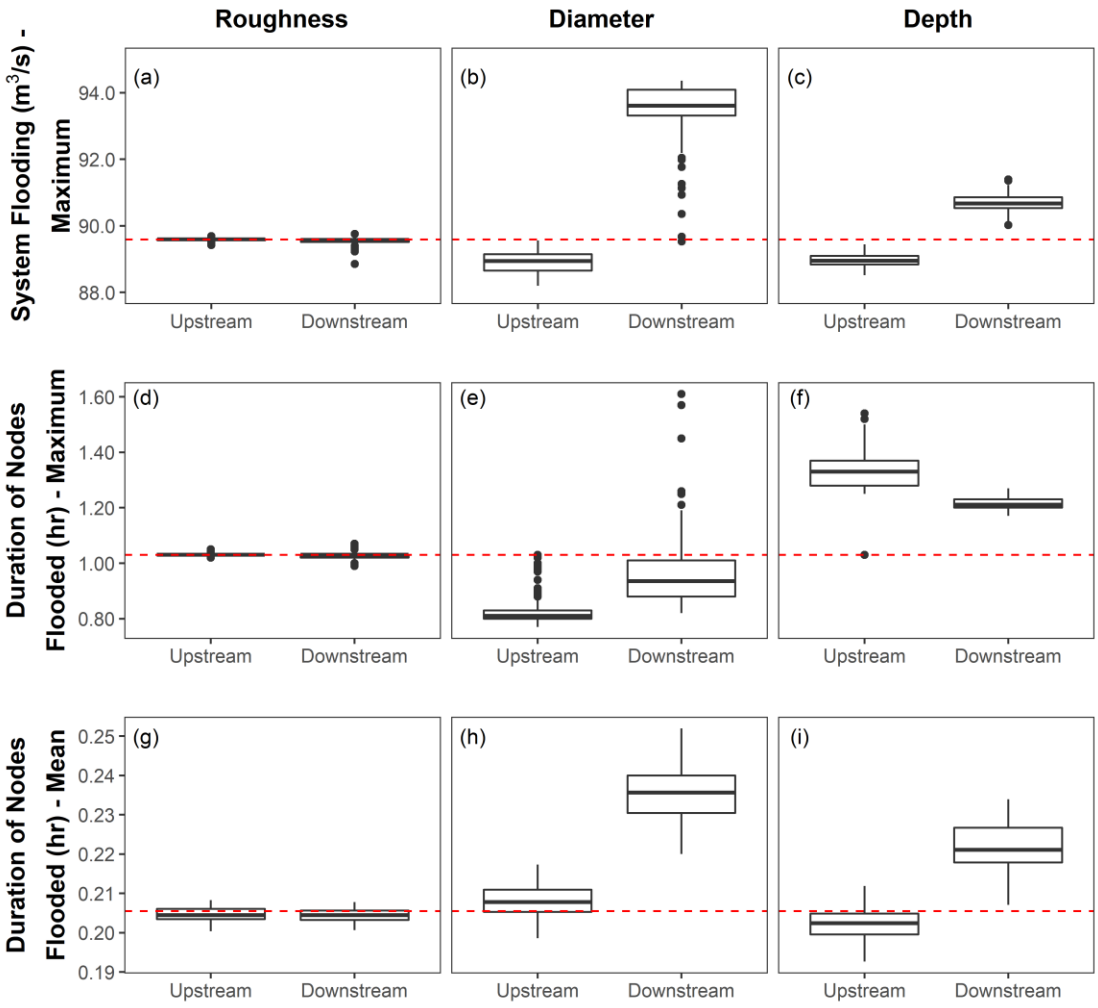

Figure 2.6. Monte Carlo Sampling Results Showing, (a-c) Maximum System Flooding, (d-f) Maximum Duration of Nodes Flooding, and (g-i) Average Duration of Nodes Flooding While Sampling Roughness, Diameter and Depth at 50% PMD from *Upstream* Versus *Downstream* Locations. Boxes Represent the 25th, 50th and 75th Percentiles and Whiskers Represent ±1.5×IQR of the 25th and 75th Percentiles. Horizontal Red Dash Lines Represent the Ground Truth Model.

Table 2.5. System Flooding Metrics of the Average MAE and PBIAS (from Ensemble Simulations Vs. Ground Truth) and RIQR of Peak System Flooding; And Flood Duration Metrics of MAE and PBIAS (from the Mean and Maximum Durations of Flooding in Ensemble Simulations Vs. Ground Truth) and RIQR of Mean and Maximum Durations of Nodes Flooded for Random Sampling of Missing Locations of Attribute-values.

Sampling		System flooding			Flood duration (Maximum)			Flood duration (Mean)		
Attri-bute	**Location of missing data**	**MAE (m^3/s)**	**PBIAS (%)**	**RIQR (%)**	**MAE (hr)**	**PBIAS (%)**	**RIQR (%)**	**MAE (hr)**	**PBIAS (%)**	**RIQR (%)**
Rough-ness	Upstream	0.87	0.00	0.00	0.00	0.00	0.00	0.00	-0.40	1.20
	Downstream	1.73	-0.10	0.10	0.01	-0.40	1.00	0.00	-0.50	1.10
Dia-meter	Upstream	7.73	-0.60	0.60	0.2	-19.50	3.70	0.00	1.20	2.70
	Downstream	83.95	10.40	0.80	0.1	-5.50	14.00	0.03	14.50	4.00
Depth	Upstream	5.23	-0.40	0.30	0.3	29.70	6.70	0.00	-1.60	2.60
	Downstream	24.21	2.80	0.40	0.2	18.40	2.50	0.02	8.10	4.00

2.4.2 Evaluation of Selective Sampling

The following section describes the impact of model resolution and infrastructure feature completeness on modeled flood depth, volume and extent. Four cases were modeled, each containing either high (0.3-m DEM and 4.6-m 2D mesh, HM) or low (9.7-m DEM and 9.7-m 2D mesh, LM) resolution and either high (complete information, HD) or low (50% of upstream features missing, LD) infrastructure data (see Table 2.3). To visualize differences across the domains, changes in DEM resolution resulted in changes in the slope of discretized catchments, as shown in Figure 2.7. It is notable that the slopes of low-resolution models (LDLM and HDLM) are much flatter than high-resolution models (LDHM and HDHM), which include details of street profile and curbs (Figure 2.7c). This means that the heterogeneity of surface topography is well-captured by high-

resolution models, whereas low-resolution models suffer a loss of terrain information (Figures 2.7a,b).

Figure 2.8 illustrates boxplots of maximum flood depth at each cell in the four sampling domains. HDLM has a narrower distribution, while LDHM has a wider distribution. The distributions for all four models are positively skewed. All interquartile ranges including maxima showed the similar pattern. LDHM resulted in the highest maximum flood depth (0.48 m), which is closest to the ground truth (i.e., HDHM) value of 0.45 m. Low-resolution models LDLM and HDLM underestimated maximum flood depth compared to the ground truth at 0.3 m and 0.28 m, respectively. Underestimation was most profound when the infrastructure data is complete, but model resolution is coarse (HDLM).

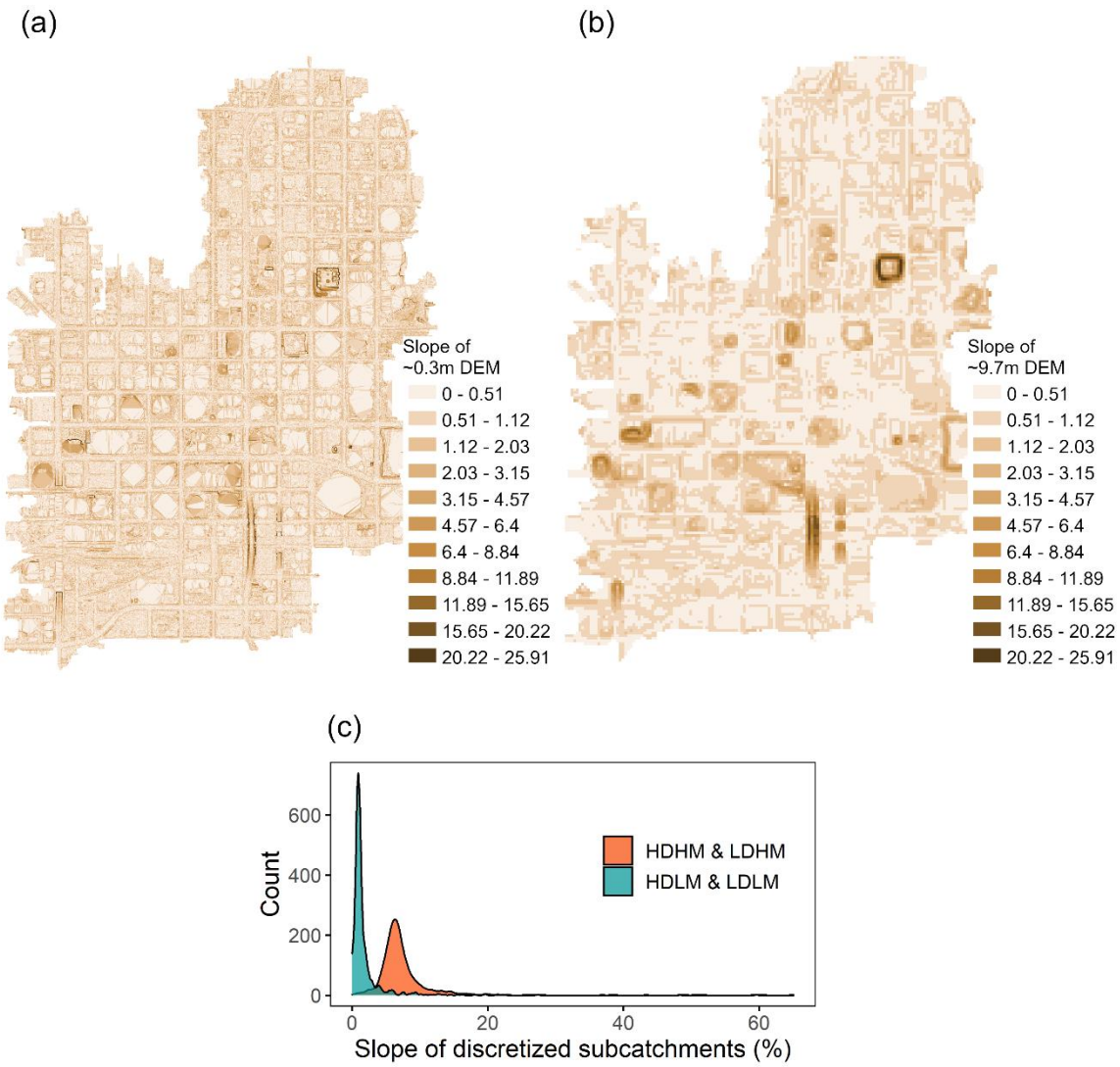

Figure 2.7. Slope Distributions of (a) High-resolution (0.3-m) DEM, (b) Low-resolution (9.7-m) DEM and (c) Sub-catchments in High- and Low-resolution Models.

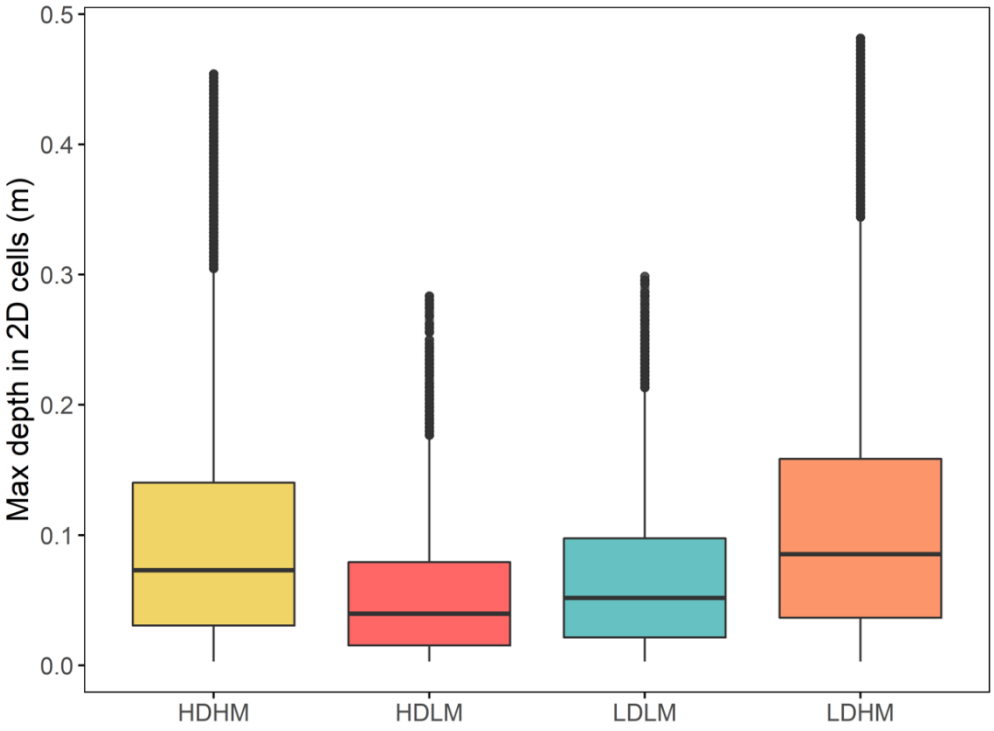

Figure 2.8. Boxplots for Distributions of Maximum Flooded Depth in 2D Grid Cells. Note: Boxes Represent the 25th, 50th and 75th Percentiles and Whiskers Represent ±1.5×IQR of the 25th and 75th Percentiles.

Figure 2.9 illustrates the pluvial flooding fluxes in the four selective sampling models for all orifices that connect the coupled SWMM 1D's node with SWMM 2D's mesh grid cells. The flooding flux is the aggregate of all spatially distributed flood fluxes occurring at each timestep. All three tested model configurations overestimated the total flooding volume compared to the ground truth (HDHM). The overestimation of peak flooding flux was observed when there is incomplete data (LDHM and LDLM). This makes sense, as features such as inlets and conduits that would otherwise collect and

convey stormwater are absent from these models. However, in the high-resolution model LDHM, the exchange of flood water between overland flow and underground drainage was more efficient compared to LDLM. Thus, compared with HDHM, LDHM may have incomplete data, but its higher resolution results in lower error than with LDLM in term of total flood volume.

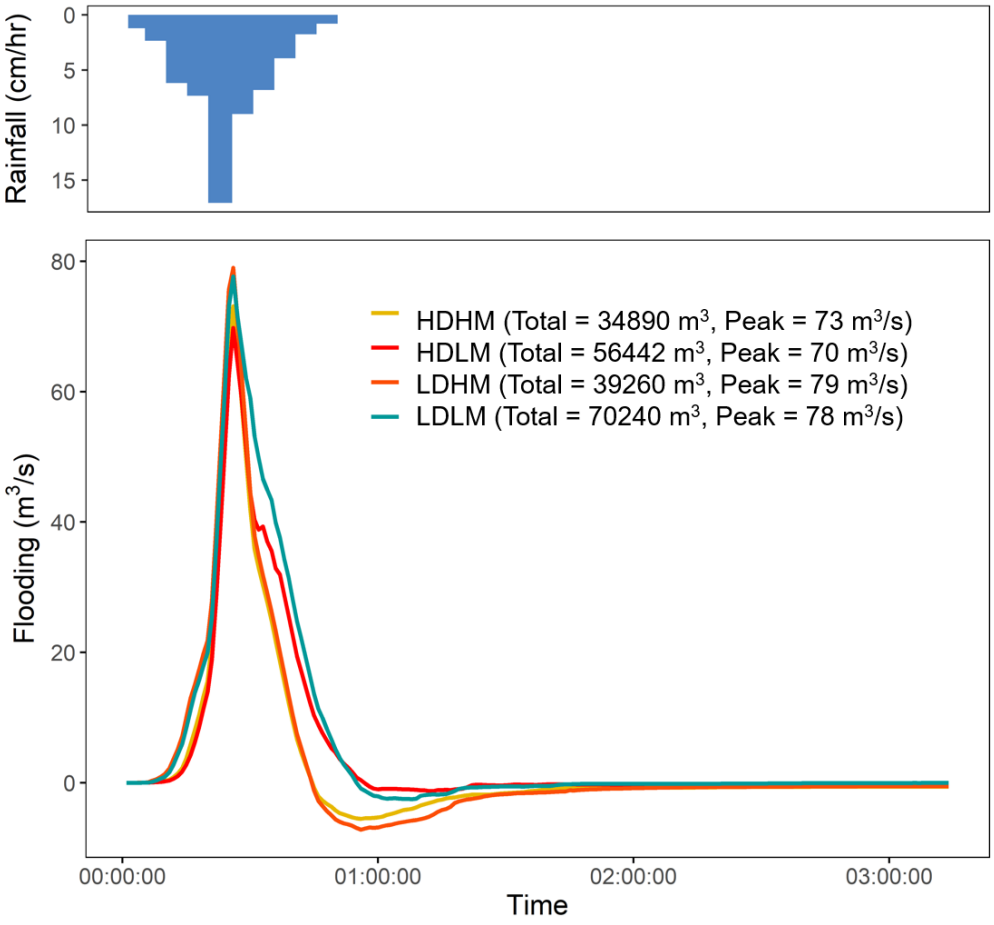

Figure 2.9. Hyetograph and Flooding (Flux) Hydrograph in the Four Selective Sampling Models. Negative Flooding Flux Indicates Net Flow Back into the Drainage System.

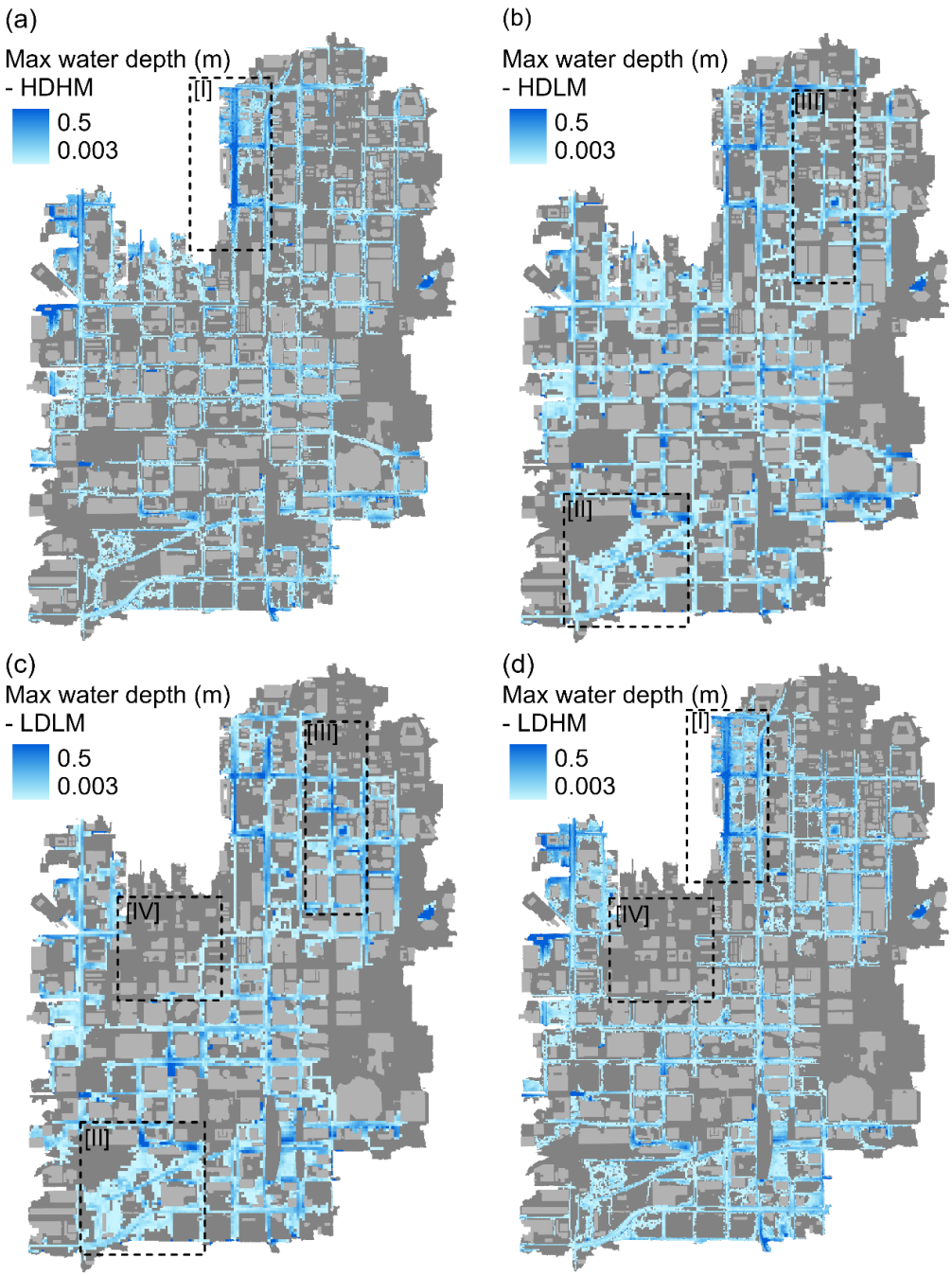

Figure 2.10. Flooded Extent and Depth in Four Selective Sampling Models, (a) HDHM, (b) HDLM, (c) LDLM and (d) LDHM. Note: i). Peak Flood Depths Are 0.45 m, 0.28 m, 0.3 m and 0.48 m for HDHM, HDLM, LDLM and LDHM, Respectively, ii). Boxes [I - IV] Are Pointing to the Differences in Estimating Depth and Extent.

The spatial flooding pattern of maximum grid cell flood depth for the four selective sampling models is shown in Figure 2.10. The high flood depths occurred in HM models as highlighted in Box [I] (Figure 2.10a,d), with the maximum occurring in LDHM (Figure 2.10d), and the minimum occurred in HDLM (Figure 2.10b). However, large flood extent occurred in LM models as highlighted in Box [II] (Figure 2.10b,c), with the maximum occurring in HDLM, as compared to other two HM models. In the case of incomplete stormwater infrastructure data, missing features, particularly catch basins, preclude a realistic estimate of localized flooding and result in overestimates of flood volume, depth and extent. For example, as highlighted with Box [III] some of the areas flooded when infrastructure data is incomplete (LDLM and LDHM; Figure10c-d), remain dry when complete data is available (HDHM and HDLM; Figure10a-b). This is because in SWMM 1D-2D, overland flow drains to the underground drainage system through catch basins and can re-enter the drainage system after surcharge condition recedes. Note that this is a key distinction between SWMM 1D and SWMM 1D-2D. In SWMM 1D-2D, the exchange of flood water takes place between the surface and subsurface as the flux in flood volume changes, whereas in SWMM 1D, the water leaving the catch basins is counted as flooding and cannot reenter the drainage system. For this reason, the maximum system flooding simulated in the ground truth SWMM 1D model (89.6 m^3/s) is higher than in the two-dimensional HDHM model (73 m^3/s). Also due to the limitations of the general 1D-2D modeling approach as employed in this study, where a larger portion of infrastructure data is missing such as an area highlighted in Box [IV],

LD models will not estimate surface flooding, as all catchment areas must be linked to a catch basin.

Model resolution also plays a role, as overland flood water is more effective at re-entering the drainage system in higher-resolution models. The maximum depth out of the four selective sampling models was observed in the high-resolution models. However, the maximum flooded area and flood volume were observed in the low-resolution models, as local depressions are smoothed in the coarser DEM and the flood water spreads more readily to surrounding grid cells (Figure 2.10). The error in flood depth, area and volume is the function of both the data completeness and model resolution. All surcharged flow spills onto the overland surface, represented by the mesh grid, and flows both on the surface in 2D and in through the pipe network in 1D. In the high-resolution models, higher heterogeneity in elevation allows depressions to be better represented, so that there are chances for the surface flow to re-enter into the 1D components. This results in lower pluvial flood volume compared to the low-resolution models. It is crucial for mesh grids in SWMM 1D-2D to represent true topographic features at the scale of flooding hazards in order to model the physical process accurately. The use of 9.7 m DEM and 9.7 m mesh grids underestimates heterogeneity in surface elevation and topographic features relevant to pedestrian and vehicle flood hazards.

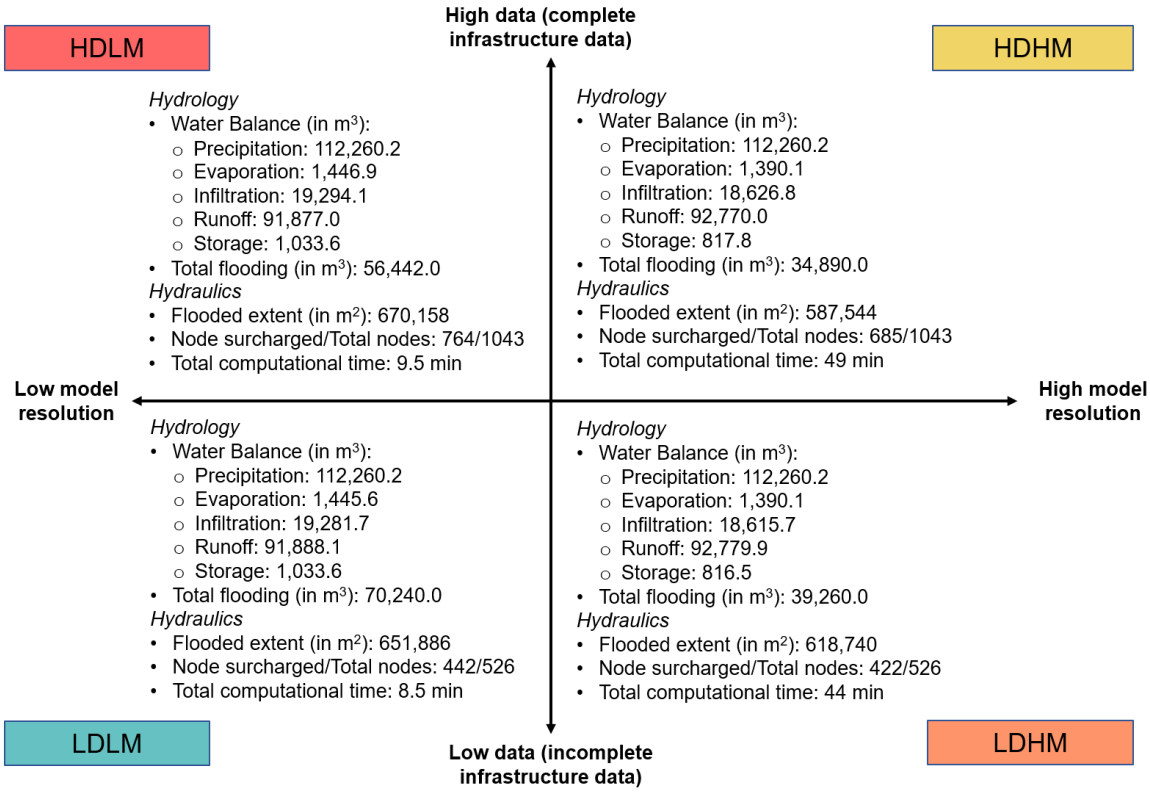

Figure 2.11. Significance of Data Completeness and Model Resolution in Terms of Modeling Hydrologic and Hydraulic Processes

Figure 2.11 summarizes the hydrological and hydraulic output for each scenario. In terms of hydrology, when the model resolution was coarse, infiltration and evaporation were slightly overestimated, and runoff was underestimated due to the flatter slopes and loss of terrain detail (Figure 2.11). In term of hydraulics, in the 1D component of SWMM 1D-2D, the relative comparison of the total surcharged nodes showed higher number of nodes are surcharged in lower resolution model, this is because the rim elevation for nodes in HM and LM models are extracted from 0.3-m DEM with heterogeneous slope and 9.7-m DEM with flatter slope.

Our results agree with prior work by Ozdemir et al. (2013), which found an increase in maximum water depth and decrease in inundation extent with increasing DEM resolution. Prior work on DEM properties and flood inundation in natural stream reaches by Saksena and Merwade (2015) also found that coarser DEM resolution overpredicts the flood extent. Further, Hossain Anni et al (2020) used the 1D-2D coupled MIKE FLOOD model and found that the absence of detailed stormwater infrastructure data significantly overestimated flood water volume. Our work aligns with these results but extends this area of research to investigate how DEM resolution and data gaps interact (Figure 2.11).

2.4.3 Research Implications and Limitations

Spatial data quality as defined by accuracy, current-ness, completeness, consistency (Fox et al., 1994), has been widely recognized to be of significant value in research and practice. This is especially true when electronic databases are produced, integrated and updated by multiple private and public sectors, and the reliance on secondary data sources increases for decision-support tools. As the effect of data completeness on urban flood modeling has not been fully understood, this study aimed to understand the effect of stormwater infrastructure data completeness on urban flood modeling. For the producers of these datasets, it is necessary to understand how incomplete data and errors propagate to model performance. As per Veregin (1999) data incompleteness occurs due to the errors of omission (i.e., infrastructure components not being recorded) and error of commission (i.e., assignment of incorrect data). For consumers of these datasets, this study cautions careful evaluation of data quality before

analysis and decision making. The study also highlights the absence of a consistent approach to filling missing stormwater infrastructure data for modeling applications.

The first experiment of this study assessed the impact of stormwater infrastructure attribute-value completeness on hydrologic and hydrodynamic model performance by auto-filling data gaps using an algorithm based on available data and design standards. Note that there is no established way to fill missing data at scale, thus we have utilized design standards and available data that are readily available in practice and could be automated (as done here to facilitate Monte Carlo sampling) or executed manually (without the need for coding expertise). Therefore, the algorithm is appropriate to address a set of research questions closely linked to practice. Design standards vary locally, and the algorithms could be customized. For example, the minimum cover required for conduits differs regionally due to winter temperatures and risk of freezing. One limitation of this study is that the findings are specific to the city of Phoenix. The relationship between PMD, error and uncertainty might vary with the characteristics of the network and catchment. However, the method and algorithm could be readily adapted to other catchments to understand the effects of these characteristics. The error and precision resulting from missing data was in part a product of the algorithm used to estimate missing attribute-values. Further refinements to this algorithm could improve performance and reduce the error and uncertainty associated with attribute-value gaps. Additionally, a limitation in random sampling was that the features were complete in all the models and only attribute-values get removed and replaced in sampling. The random sampling algorithm does not consider missing features, since it would require auto model

building or network generating programming. This is out of scope of the current analysis but assessing the combined impact of missing feature and attribute-values is an important line of future work.

In addition to assessing the impact of missing attribute-values, the first experiment helps to prioritize data collection efforts. Results showed that missing attribute-values pertaining to the downstream region of the drainage network lead to higher model error and uncertainty when compared to upstream data gaps (Figure 2.6). This suggests that, if resources for field surveys are limited, prioritizing the downstream section of the network would yield greater improvements in accuracy. Results also show that model performance is particularly sensitive to missing diameter values as shown by MAE and PBIAS (Tables 2.4 and 2.5). This suggests that efforts to improve attribute-value estimation algorithms should focus on diameter. However, the results presented here are for one catchment; testing the impact of the location of missing data in other catchments with different network geometry and topography should be explored further. Although the Monte Carlo based sampling algorithm was developed to investigate the effect of PMD and location of missing data on model performance, this experiment confirms the utility of the approach to filling missing attribute data. For example, the results demonstrate that missing roughness data could be effectively estimated using an empirical distribution of available roughness information, in conjunction with information from adjacent conduits. Further improvements in estimating minimum depth and diameter when upstream or downstream attributes are missing, can improve the accuracy and precision of the model.

The second experiment of this study tested the effects of infrastructure data completeness and model resolution on model performance. Model resolution is usually selected based on the desired level of simulation accuracy, time availability and resource availability. Further analysis is needed to compare the value of incremental changes in model resolution to the effort and resources required. However, even when data and computational resources are readily available, the appropriate model resolution critically depends on the core purpose of the model. For example, within urban flood modeling, the core purpose of estimating total flood volume, versus the location or duration of flood impacts, might suggest a different model resolution. Low-resolution models have the benefit of lower computation time, which may be critical for applications such as real time pluvial flood forecasting or quick flood estimation. In this study, the low-resolution model simulation took 9.5 min while the high-resolution model took 49 min (note, these computation times were based on the computer specification of 64-bit i7 CPD @ 3.6 GHz processor used in this experiment). However, for infrastructure planning, including adaptation of existing stormwater infrastructure, model accuracy is more important than computation time. In pluvial flood estimation, the difference of a few inches of water could mean basement flooding, disruption of traffic and safety hazards. Further, the uncertainty from incomplete data and coarser model resolution selection is too high to optimize flood control measures such as green infrastructure, which have localized flood mitigation potential. We used 50 % missing features in the low data (incomplete infrastructure data) models and further analysis using different levels of missing stormwater infrastructure features, in combination with different model resolutions on

different types of catchments would be beneficial. While the key effects quantified here are specific to the study area some results are generalizable as there will be similar but varied degree of error, bias and uncertainty in simulating hydrologic-hydraulic variables due to missing attribute-value and features of stormwater infrastructure, and selection of model resolution.

2.5 Conclusions

This study consists of a two-part experiment to investigate the effect of data completeness and model resolution on urban flood model performance by random sampling and selective sampling. An algorithm was built to randomly remove and replace attribute-values for the hydrologic-hydraulic stormwater model built using the EPA's SWMM. Random sampling was done for attribute-values using the 1D model; then, selective sampling was applied to feature data completeness and model resolution using the computationally demanding 1D-2D model. Results demonstrated that the relationship between model uncertainty and PMD is dependent on the attribute or parameter in question. In contrast, accuracy consistently decreases with an increasing PMD, except for diameter. We also found that missing data in the downstream section of the catchment leads to greater uncertainty and lower accuracy compared to missing data upstream. This finding can inform the prioritization of data collection and verification efforts where resources are limited. The total flood duration and extent may be over or underestimated due to incomplete infrastructure data, depending on model resolution. In the SWMM 1D-2D selective sampling, the highest flood depth was simulated by the high-resolution

models. In contrast, the highest flood extent and volume were simulated by the low-resolution models. In sum, both data completeness and model resolution determine the accuracy of flood depth, extent and volume estimates. This emphasizes the importance of high-resolution modeling and complete data for urban flood estimation at the scale of pedestrian and vehicle flood hazards where accurate flood extent, volume and depth are critical.

The risks of pluvial flooding are projected to grow in many cities as they experience more intense precipitation due to climate change and as urbanization decreases permeable area. Modeling can be an effective tool to understand pluvial flooding and make projections that enable effective adaptation and response. Understanding, quantifying and communicating error and uncertainties arising from various sources are essential for decision making. However, infrastructure data gaps are a common obstacle and prior research has not addressed the impact of these gaps on model performance. In addition, access to high-resolution LiDAR is limited globally. In this study we focused on infrastructure data gap and model resolution, which are key pieces to an accurate and precise model. This study shows that the error and uncertainty in simulating hydrologic-hydraulic variables due to prevalence of missing stormwater infrastructure and selection of improper model resolution could be significant and might affect the quality of the model application. Hydrologic-hydraulic models are increasingly being used in stormwater design, real time modeling of pluvial flooding, and impact or damage assessment. With the growing focus on the importance of pluvial flooding as well as increasing use of physically based models we need a cost-effective approach to

overcome data gaps. This problem can be dissected into two sub parts: assessment and application. The Monte Carlo based sampling algorithm was developed as an assessment approach to quantify the effect of missing attribute-value. As presented here, the algorithm can also be used to fill missing attribute-values in large stormwater infrastructure datasets. It can be further developed to improve its accuracy and precision and to adapt it to different contexts. In sum, this work takes a first step to address an understudied challenge in urban stormwater modeling, developing tools and insights useful in both research and practice.

CHAPTER 3

LEVERAGING CATCHMENT SCALE AUTOMATED NOVEL DATA COLLECTION INFRASTRUCTURE TO ADVANCE URBAN HYDROLOGIC-HYDRAULIC MODELING

This chapter has been adapted from the working paper Shrestha, A., Garcia, M. Doerry, E. (2022). Leveraging catchment scale automated novel data collection infrastructure to advance urban hydrologic-hydraulic modeling.

Abstract: The lack of long-term hydrological observations in urban catchments presents a significant obstacle to construction and testing of urban flood models for flood forecasting and risk mapping. In the limited number of cases where appropriate sensor infrastructure exists, calibration is performed with flow, velocity or depth data from sensors installed in underground sewers or natural channels. However, such sensor infrastructure monitoring the stormwater drainage networks is rarely present in cities. Data on pluvial flooding *at the surface* is even more rarely available, particularly over longer timeframes, leading to limited (or no) model calibration, and unknown prediction uncertainty. Unfortunately, installation and maintenance of a dense network of conventional automated underground and surface level sensors, particularly in urban areas, is cost-prohibitive and hampered by a range of organizational and technical obstacles. Commonly available networked technologies such as traffic cameras and cell phones, if properly leveraged, could provide a high-quality, cost-effective source of urban

hydrological observations that could significantly improve the urban flood models. In this proof-of-concept study, we examine the applicability of surface flood stage data collected from street-level cameras and cell phone-based observations contributed by citizens, which are collectively referred to as novel data, to calibrate and parameterize an urban hydrologic-hydraulic model developed using the U.S. EPA Stormwater Management Model for the City of Flagstaff, Arizona. We use continuous time series of water level data extracted from street level camera imagery, along with single point flood observations from citizens, automatically collected by a novel large-scale flood monitoring infrastructure for major rainfall events. The parameter set for calibration was selected using one-at-a-time sensitivity analysis and parameter grouping for features sharing similar physical properties to ensure the parameters represent spatial heterogeneity. To optimize the model parameters, we use a single-objective genetic algorithm, a class of evolutionary algorithm, to minimize the root mean square error observation standard deviation ratio (RSR). The results demonstrate a proof-of-concept showing benefits of surface water level measurements using novel data sources for model construction and calibration, advancing pluvial flood modeling in challenging urban contexts.

3.1 Introduction

Rainfall induced urban flooding, most commonly known as *pluvial flooding*, is a common phenomenon in growing number of cities (Abebe, Kabir, & Tesfamariam, 2018; Acosta-Coll, Ballester-Merelo, Martinez-Peiró, & De la Hoz-Franco, 2018; Jiang et al.,

2018; Nicklin, Leicher, Dieperink, & Van Leeuwen, 2019; Bernice R. Rosenzweig et al., 2018; Schmitt & Scheid, 2020). Rapid expansion of metropolitan areas, both densification and sprawl, compounded by aging and inadequate wastewater and stormwater infrastructure and, in some regions, climate change driven increases in extreme rainfall are raising urban flood risk (Moftakhari, AghaKouchak, Sanders, Allaire, & Matthew, 2018; Bernice R. Rosenzweig et al., 2018; Johanna Sörensen & Mobini, 2017). Urban flooding can cause loss of life, damage to property and infrastructure, disruption to the social environment, vehicular and pedestrian traffic delays, and soil and water pollution. Increasing urban flooding across the U.S. is a growing source of economic loss, social disruption and housing inequality (University of Maryland & Texas A&M University, 2018). Although damages from urban flooding are often reported as an aggregate figure for a whole city or region, the actual disruption and damage affects citizens personally at the scale of individual streets; thus, an aim of future modeling efforts must be to provide analysis and predictions at this street scale.

Strategic urban flood risk management typically weaves together elements including flood assessments, insurance programs, impact assessments, flood forecasting and prediction, and soft and hard flood adaptation planning to mitigate or prevent flooding impacts (Jha et al., 2012). Importantly, accurate and robust physically based or data driven numerical models are the cornerstone for successful implementation of any urban flood risk management strategy. Such hydrological and hydraulic models are powerful tools for modeling rainfall-runoff and flood routing processes in support of urban flood forecasting, adaptation and planning (Henonin, Russo, Mark, &

Gourbesville, 2013; Miguez & Veról, 2017; Price & Vojinovic, 2008; B. R. Rosenzweig et al., 2021). The ability of hydrologic-hydraulic models to simulate, and predict accurate flood depth, extent and duration at such high spatial resolution depends on a number of factors, including completeness of stormwater infrastructure data, model resolution (Shrestha, Mascaro, & Garcia, 2022), and importantly, on the parameterization process and the feedback from observational data into the model development process.

Model calibration is an integral part of improving the predictive ability and reliability of numerical hydrologic-hydraulic models. The most widely accepted calibration approach is automatic calibration by algorithmic search for a pareto optimal solution using single or multi-objective optimization functions (Shahed Behrouz, Zhu, Matott, & Rabideau, 2020). Common optimization algorithms include evolutionary algorithms such as genetic algorithms (Krebs, Kokkonen, Valtanen, Koivusalo, & Setälä, 2013; Wang, 1991; Yang, 2014), including the non-dominated sorting genetic algorithms (Shinma & Reis, 2011), and differential evolution (Yazdi, Yoo, & Kim, 2017). In the absence of adequate (in coverage, density or quality) observational data or sufficiently powerful computational resources, manual “trial and error” techniques can also be used to calibrate such models (Boyle, Gupta, & Sorooshian, 2000). Some studies have also explored Bayesian calibration approaches to account for input and model uncertainty (Gao, Yang, Han, Huang, & Zhu, 2020). All these approaches are proven methods for urban hydrologic-hydraulic model calibration, but all depend critically on or can be substantially improved by access to high-quality observational data at high temporal and spatial resolutions.

Unfortunately, a pervasive lack of long-term hydrological observations in urban environment, particularly at the scale of streets and urban streams, commonly presents a major obstacle to efficient model construction, calibration and validation (University of Maryland & Texas A&M University, 2018). This is one of the key reasons that pluvial flooding has historically received disproportionately less attention in flood assessments, modeling, flood forecasting, and even in private or government insurance programs, compared to the fluvial and coastal flooding mechanisms (First Street Foundation, 2020; Bernice R. Rosenzweig et al., 2018; The National Academy Press, 2019). This further precludes urban flood risk mapping in cities, and model based stormwater infrastructure planning and design (J. Leandro, Djordjević, Chen, Savić, & Stanić, 2011; Spekkers, Veldhuis, & Clemens, 2011; Tscheikner-Gratl et al., 2016). In particular, model accuracy depends on adequate calibration of model parameters to ensure that it accurately reflect dynamic catchment characteristics; incomplete or incorrect parameterization can rapidly degrade model accuracy to a point where the model is useless for communicating flood risk, infrastructure decision making or planning (Horritt, 2006; Moy de Vitry & Leitão, 2020; Pathak et al., 2015). More broadly, the lack of observation data has made it difficult to develop adequate guidelines, best practices, and formal requirements for testing and validating large scale urban hydrological models, and for parameter selection and calibration; developing such standards will be a key requirement for effective real-world urban stormwater model development and deployment. In sum, the pervasive lack of observational data in urban areas impacted by pluvial flooding represents a major obstacle to developing, validating, and properly calibrating urban stormwater models.

What is urgently needed is an efficient approach to gathering such observations, i.e., by monitoring and recording flood occurrence and flood characteristics at the resolution of impacts during flooding events. Ideally, such datasets would uniformly cover the entire catchment being modeled and provide simultaneous and continuous hydrologic observations at the street, city block, and catchment scale throughout each storm event.

Efforts to instrument stormwater systems to provide such observations have been limited, and have typically relied on sensors that measure water flow or depth at the cross section of stream or inside built drainage structures (Moy De Vitry et al., 2017). Installation of such sensor networks presents enormous logistical and financial challenges related to installation and maintenance (Davids, van de Giesen, & Rutten, 2017), but also raises a number of specific practical concerns: (1) the density of sensors required to effectively parameterize a large or heterogeneous catchment is prohibitive in both cost and installation effort; (2) parameters do not remain static as the physical terrain properties and underground drainage condition changes over time; and (3) observations in the channels do not sufficiently connect to or characterize actual flooding conditions on the streets.

At the same time, ongoing developments in urban infrastructure and networked technologies have created a vast new set of potential data sources to inform stormwater management efforts. This is where effective leveraging alternate data sources could allow for substantial improvements in model testing and refinement. Specifically, information extracted from a rapidly growing pool of networked traffic and surveillance camera imagery, harvested from social network posts, flood reports, or collected by citizen

scientists can potentially yield quantitative or qualitative hydrological information at wide variety of spatial (i.e., density) and time (i.e., time intervals, past, real or near time) scales (Helmrich et al., 2021). We collectively refer to these sources as novel data sources and their observations as novel data. Several studies have examined the potential use of novel data to generate qualitative and quantitative measurements in ungauged basins such as to monitor flood occurrence, measure stream water depth or identify timing for peak flooding (Assumpção, Popescu, Jonoski, & Solomatine, 2018; Etter et al., 2020; Le Coz et al., 2016; Lowry et al., 2019; Nardi et al., 2021; Starkey et al., 2017); others have utilized it to quantify hydraulic flow properties such as depth, discharge and velocity using data processing tools and techniques (João P. Leitão et al., 2018; Moy De Vitry et al., 2017; Moy de Vitry & Leitão, 2020).

However, development of practical frameworks, methods, and best practices for leveraging novel data sources for hydrological model construction, model parameterization, or model-based decision making are still at an early experimental phase (Nardi et al., 2021). Two crucial challenges raised by integration of novel data into urban flood model calibration algorithms are: (1) prioritization and grouping of parameters to calibrate model reflecting heterogenous catchments efficiently, and (2) reliably and automatically converting observations to hydrological variables comparable with model outputs. Physical surface properties like soil type, land use / land cover (LULC), as well as nature and condition of stormwater infrastructure can vary greatly within the area of interest. Moreover, novel data utilize existing data sources (i.e. installed cameras, citizen cell phones, network sources) without the need for substantial investment for separate

infrastructure, as opposed to traditional in situ sensors, which incur high installation and maintenance costs. Such data collection infrastructure using novel data sources can generate high amount of data distributed over the catchment at the fraction of the cost required by traditional in situ sensors required to generate same coverage of data. Leveraging novel data sources has the potential to improve the parameterization of model as more observations of local scale catchment responses helps to detect local scale variation of true parameter values. Especially in the high resolution, fully or semi-distributed hydrologic-hydraulic model, the number of model elements or components such as discretized sub-catchments, number of conduits and catch basins or manholes are significantly higher compared to the lumped models. Thus, proof-of-concept efforts that bring together technology and users of hydrological information, and that leverage the capability and capacity of novel data sources to measure water depth or flood occurrence with substantial coverage at high spatial and temporal resolution are essential to advance urban flood studies.

For this study, we classify novel data into two distinct types: continuous time series, and continuous single point data. A key characteristic of novel data sources is that they represent observations at the ground surface, and therefore understanding of the interaction between surface and the underground stormwater drainage network is essential. This is particularly true for calibrating one dimensional (1D) hydrologic-hydraulic models, since 1D models cannot quantify overland flooding unlike two dimensional (2D) or coupled 1D-2D models, and use of 2D or 1D-2D models for calibration is less feasible due to longer computation time it takes (Jorge Leandro et al.,

2009; Mark, Weesakul, Apirumanekul, Aroonnet, & Djordjević, 2004). The continually increasing number of network-connected cameras and other sensors in urban landscapes, coupled with increased citizen engagement via mobile applications and social networks, will only increase the quality, density, and coverage of novel data. Thus, we expect that the approach to using novel data sources for calibrating hydrological model explored here to grow in relevance and efficacy over time.

In sum, the availability and quality of novel data sources is steadily increasing and leveraging these data sources can potentially provide a rich source of observational data, including hydrologically significant variables not accessible via conventional sensor systems, at a fraction of the cost of conventional sensors. The goal of this study is to understand the potential benefits offered by novel data sources in more detail. In particular, the overarching research question driving this study is: how leveraging novel data sources compensate for the general lack of consistent, high quality hydrological observations in urban contexts and, specifically, can these novel data be used to effectively refine and calibrate urban hydrological flood models? In working to adapt novel data sources to explore this question, we develop new methods: (1) parameter grouping which combines the elements of the models based on physical properties that it shares (i.e., soil types data and LULC were used to group sub-catchments, and material types and age of infrastructure were used to group conduits) to minimize parameter selection without compromising the spatial heterogeneity, and (2) statistical relationships between 1D and coupled 1D-2D models which establishes relationship between flooding flow rate in 1D model and surface water depth in 1D-2D model. We first developed a

one-dimensional SWMM model for the targeted study area, then collected a variety of novel data for that area across a suitable timeframe, and finally attempted to apply the collected data for model calibration and validation. In the following sections, we present the details of our study, present the results of our analysis, and discuss limitations and benefits of novel data with respect to hydrological model construction, testing and calibration.

3.2 Study Area

The study area chosen for our analysis is an urban catchment of the city of Flagstaff in Northern Arizona; we chose this area due to the availability of relatively complete and reliable stormwater system design and connectivity information, as well as availability of several sources of novel data collected in the context of a broader "smart city" (ASU/NAU, 2021) flood management project. The study catchment is a hydrologically separate urban subset of Rio de Flag catchment lying at the average attitude of 2130 m elevation; in a semi-arid climate with a Köppen classification as warm dry-summer Mediterranean climate. Flagstaff receives average of 510 mm of annual rainfall and experiences two distinct wet periods: summer (i.e., June 21st – September 20th) accounts for 34% of annual rainfall and winter (i.e., December 21st – March 20th) for 28% of annual rainfall (Hereford, 2015), with a summer monsoon typically extending from July to September. Buildings in Flagstaff range from a historical downtown core dating back to as early at the mid-1800s to more modern buildings built after 1999 throughout an incrementally growing municipality. This incremental urban expansion and

renewal is reflected in the stormwater infrastructure as well, with interconnected older and new sections. The city experienced recent urban flooding due to heavy monsoon rains accompanied by flash flooding in July 2021 (NWS, n.d.-a), and historic flooding in the catchment was reported in the 1970s, 1960s, 1950s, 1930s, and back to as early as 1888 (USACE, 1975). Figure 3.1 shows the location of the study area and presents details of the as-built stormwater infrastructure components in both the physical form and in our hydrologic-hydraulic model. The study catchment has the total area of 5.5 km^2, and the ground elevation ranges from 2085 m to 2153 m above mean sea level.

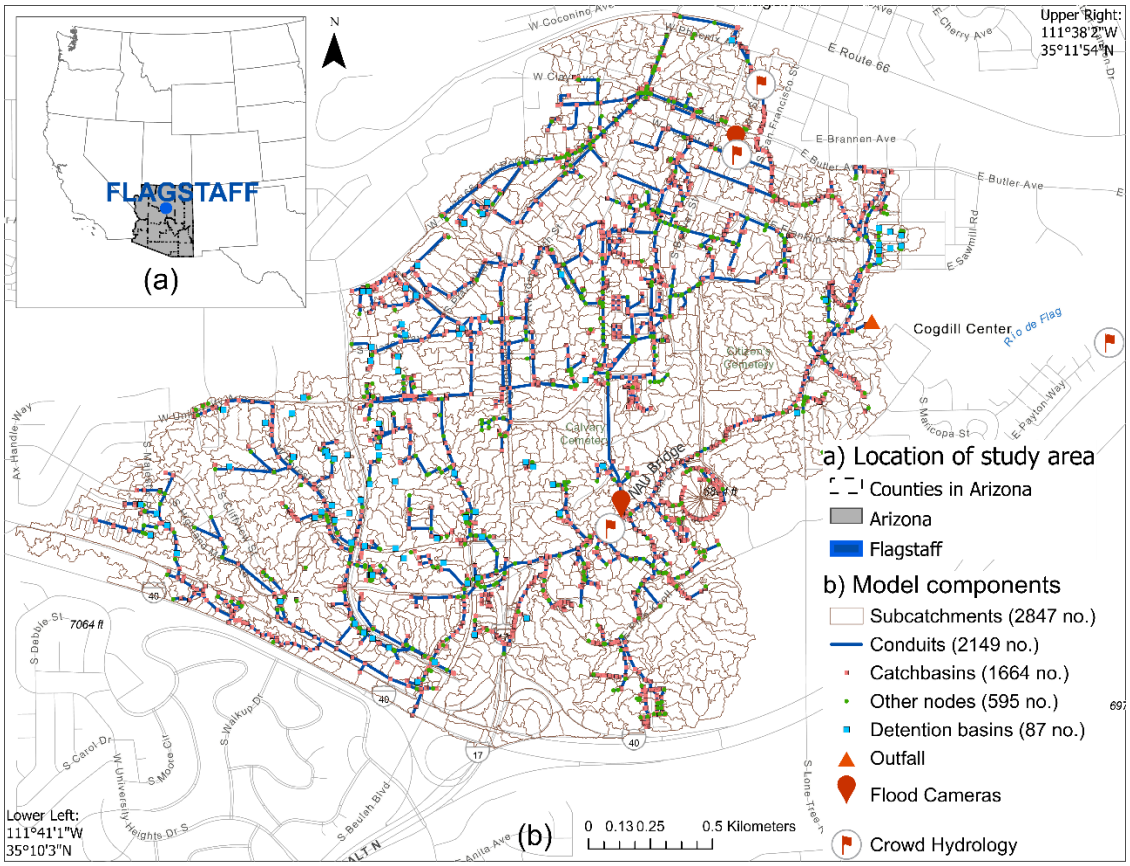

Figure 3.1. Study Area

3.3 Materials and Methods

In this section we give detailed descriptions of all key elements of our analysis: the data types driving the analysis, the construction of hydrologic-hydraulic model, the parameter selection process, and the novel data-driven model calibration framework.

3.3.1 Hydrologic-Hydraulic Model

The hydrologic-hydraulic model for the urban catchment of city of Flagstaff was built for this study using the Stormwater Management Model (SWMM, version 5.1) by the U.S. Environmental Protection Agency to simulate hydrologic and hydraulic processes in the study catchment. SWMM is a semi-distributed model which simulates rainfall-runoff and routing processes for single precipitation events or in a continuous fashion in urban or rural catchments. Runoff and routing are the two main processes the model estimates. Runoff is computed on a collection of discretized sub-catchments through the non-linear reservoir model, where the reservoir capacity refers to the maximum depression storage. Routing captures the transport of runoff via the underground network of conduits, overland channels and other components. The runoff computation also accounts for other relevant hydrological processes such as evaporation from standing water, rainfall interception in depression storage, infiltration into unsaturated soil layers, percolation into groundwater layers, interflow between groundwater and the drainage system, and stormwater capture by low impact development. Further details about theoretical background, governing equations, and features of SWMM can be found in Rossman (2017) and James et al. (2010). Other

similar hydrologic-hydraulic modeling tools for stormwater commonly used in engineering practice are SWMM based proprietary shells (K Finney et al., 2012; R. James et al., 2013; Mikelonis, Boe, Calfee, & Don Lee, 2018): PC-SWMM by CHI, XPSWMM by XP solutions, InfoSWMM by Innovyze, tools from Mike by DHI (Abbott, 1999; Mike, 2009): Mike Urban, Mike MOUSE and Mike 11, and CivilStorm by Bentley (Ramos, Pérez-Sánchez, Franco, & López-Jiménez, 2017), all of which have similar modeling process and data requirements.

3.3.1.1 Data Requirements and Processing

The boundaries of the study catchment delimit a built-up urban area of the Rio de Flag watershed. A hydrologically separate sub-basin was identified as the study catchment using the watershed delineation tool of PCSWMM, driven by a high resolution (0.3 m) LiDAR based Digital Surface Model (DSM). The DSM consisted of buildings and street curbs in addition to ground return points. Further, a LiDAR-generated Digital Elevation Model (0.3 m) was used to determine sub-catchment slopes and rim elevations for nodes in both SWMM 1D and 1D-2D models, and for generating 2D mesh cells at 5x5m resolution for the SWMM 1D-2D model. In this way, the total catchment area of 5.5 km^2 was further discretized into 2847 smaller sub-catchments with average area of 2023 m^2. Urban imperviousness data at 30 m resolution (MRLC, n.d.) was used to estimate average imperviousness in the discretized sub-catchments: among the discretized sub-catchments, the weighted average imperviousness relative to area is 62% and the maximum is 98%. The infiltration process represented by Green-Ampt equation,

the simplified Richard's equation, depends on parameters influenced by soil types and LULC. The LULC data at 30 m resolution was used to extract infiltration parameters for each sub-catchment.

The infrastructure component of the SWMM model extracts infrastructure-related parameters from the stormwater geodatabase. The stormwater geodatabase from the City of Flagstaff containing all the infrastructure components is shown in Figure 3.1b. The study catchment stormwater conveyance system consists mostly of conduits and a natural open channel (the Sin Clair Wash along the Northern Arizona University campus) which mostly remains dry between rainfall events. The cross sections for this natural open channel were extracted from the DEM. Incomplete or missing features or attributes in the geodatabase due to human error and missing or irregular updates to the database are inevitable, yet it is essential to fill these data gaps to avoid model or output uncertainty. Missing physical features are highlighted by discontinuities in the stormwater network and missing attributes appear as missing characteristics like conduit diameter, material, and Manning's roughness for various conduit segments within the network. To fill in the missing physical features, we organized targeted field surveys to identify missing components; missing attributes were deduced from nearby upstream or downstream features, if present, or via informed estimates using heuristics detailed in Shrestha et al. (2022). The details of data used in this study is summarized in Table 3.1.

Table 3.1. Summary of Data Used to Build Hydrologic-hydraulic Model

Data	Data type	Version	Source
Terrain and land surface			
LiDAR point cloud data	Point cloud (Raw data)	2020	USGS 3D Elevation Program (USGS, n.d.)
Digital Elevation Model	Raster (Processed data)	2020	LiDAR point cloud data, USGS 3D Elevation Program (USGS, n.d.)
Digital Surface Model	Raster (Processed data)	2020	LiDAR point cloud data, USGS 3D Elevation Program (USGS, n.d.)
Soil type and parameters	Vector (Secondary data)	2019	United States Department of Agriculture – Natural Resources Conservation Service, Web Soil Survey database (USDA-NRCS, n.d.); Arizona Department of Transportation, Highway Drainage Design Manual (ADOT, 2014)
Land use / land cover (LULC)	Raster (Secondary data)	2019	National Land Cover Database, Multi-Resolution Land Characteristics Consortium (MRLC, n.d.)
Urban imperviousness data	Raster (Secondary data)	2019	National Land Cover Database, Multi-Resolution Land Characteristics Consortium (MRLC, n.d.)
Building layer	Vector (Secondary data)	2018	City of Flagstaff (City of Flagstaff, n.d.)
Conveyance			
Stormwater infrastructure features data	Vector (Secondary data)	2019	City of Flagstaff, Coconico County
Stormwater infrastructure attributes data	Vector (Secondary data)	2019	City of Flagstaff, Coconico County
Additional data			
Building Age – Census tract data	Vector (Secondary data)	2018	U.S. Census Bureau's American Community Survey (ACS)(ACS, n.d.)

3.3.1.2 Model Setup

Our core model was a semi-distributed one dimensional (1D) hydrologic-hydraulic model built using the SWMM. We also built a coupled 1D-2D model to develop a statistical relationship between the flooding flow rate produced by the 1D model (as the independent variable), and the surface flooding depth (as the response

variable). To drive modeling, we used Multi-Radar/Multi-Sensor System (MRMS) gridded radar rainfall data at 2 min temporal resolution (NSSL, n.d.). Surface runoff, infiltration losses and evaporation processes were accounted in every sub-catchment, and we used a constant evaporation rate of ~0.41 cm/day (Kişi, Ali Baba, & Shiri, 2012) corresponding to the average daily values for Flagstaff. For Green-Ampt infiltration parameters, initial moisture deficit of the soil, the soil's hydraulic conductivity, and the suction head at the wetting front was derived using soil type and LULC spatial datasets (ADOT, 2014).

3.3.2 Novel Data Infrastructure and Data Collection

The experimental setup for data infrastructure within the study catchment boundary includes installation of flood gauge with flood camera at one location, and installation of flood gauges without cameras at several locations. A schematic overview of the experimental novel data collection infrastructure is shown in Figure 3.2; examples of the cameras and gauges used are shown in Figure 3.3a-c.

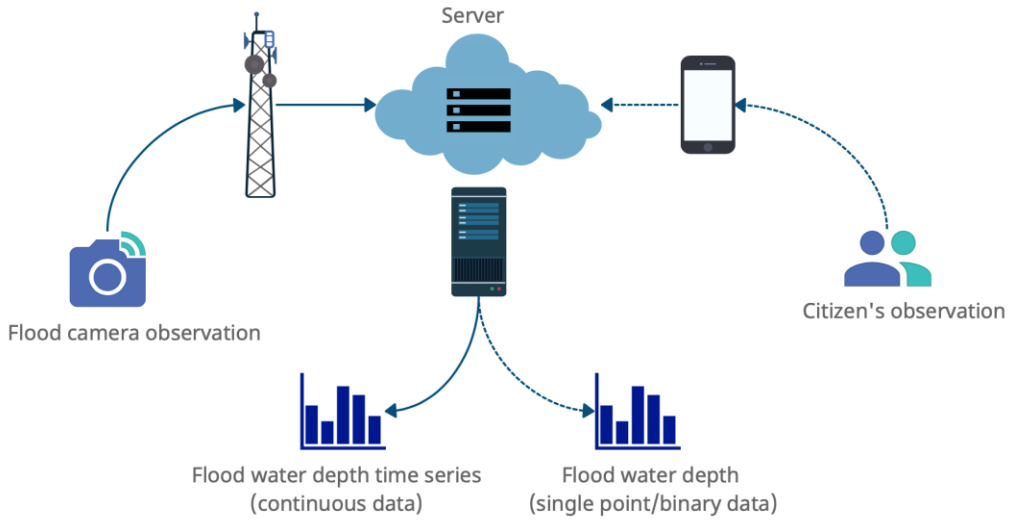

Figure 3.2. Overview of Experimental Novel Data Infrastructure. Solid Lines Show Flow of Information from Automated Flood Cameras; Dashed Lines Show Flow of Information from Citizen Scientist Contributors.

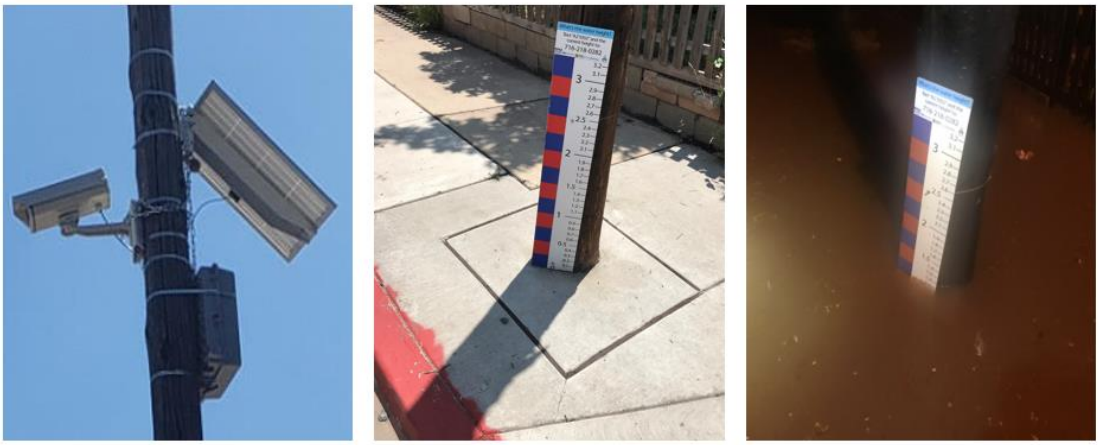

Figure 3.3. Pictures Showing Installed (a) a Typical Automated Flood Camera Installation, (b) Flood Gauge (Automatically Read by Flood Cameras) Installed at a Hotspot Location, and (c) an Example of Street Flooding Event

3.3.2.1 Flood Camera Images

In the context of broader, ongoing "smart city" project (ASU/NAU, 2021), we developed a sophisticated informatics infrastructure with the capability to automatically and continuously monitor and extract flood stage over long term from a large network of camera sources. Cameras used included municipal traffic cameras, municipal and personal web cams, and custom-designed solar-power "smart cams", all connected to a central cloud-based server infrastructure via hard-wired ethernet or cellular data modem. The cameras were configured to monitor a fixed frame view and provided high-resolution still images to the server on demand. Image collection rate was dynamically driven by evolving meteorological conditions at each specific camera location; rates varied from one image every 24 hours during (uninteresting) dry periods, automatically ramping up incrementally based on evolving high-acuity (nominally National Oceanic and Atmospheric Administration (NOAA), Global Forecast System (GFS) 0.25 degree resolution) forecasts and weather radar analysis, to provide up to one image per minute during heavy storm events. This approach efficiently provides high measurement density during times when stormwater infrastructure is active, while avoiding unnecessary data collection at other times. Incoming images were centrally processed to automatically extract stage data using a variety of custom-developed image processing techniques; for the data used here, stage was extracted from images using a custom occlusion-based image processing algorithm focusing on a calibrated staff gauge placed in the image frame. Both extracted stage value and the image were stored to support accuracy analysis; analysis (human vs. machine estimation of staff gauge reading) was reliably

high (average >90%) when binning readings into 5cm bins. Only daytime readings were taken. This automated, continuous flood stage monitoring network has been in place for nearly three years, improving over the course of the project with research advances in camera systems, image processing techniques, and coverage of camera network. Data collected can be reviewed using a secure, web-based portal that provides an integrated "floodmap" (ASU/NAU, 2021) view of the monitoring network, allows operators to specify a timeframe of interest, and displays hydrographs for each camera station. Data for any time period and subset of sensors may, of course, also be exported for further analysis, as was done for the modeling effort described here.

3.3.2.2 Citizen Science Observations

Citizens reports of flooding levels were another novel data used in our analysis, and these were generated by a citizen science infrastructure also installed in the context of a broader, ongoing "smart cities" project (ASU/NAU, 2021). The infrastructure consists of large, visible staff gauges placed in drainages adjacent to roads and other pedestrian or cycling pathways within the city; each "station" is augmented by signage inviting citizens to read the staff gauge and text the gauge name (identifier) and observed water level to a phone number (or, optionally, enter them at a website). The study area catchment targeted here includes three such citizen science stations. In addition, staff gauges installed as targets for the automated flood cameras also include citizen science signage and can be read/reported by passersby. Collection of citizen reports in a central server, methods for reading and parsing received reports, and merging of extracted flood

stage values by station into the main database is described in detail by Lowry et al. (2019). Notably, this crowdsourced data stream is intermittent and opportunistic, depending on the quantity and motivation of citizens passing by the stations; the data provided here is therefore discrete point-source data, i.e., time-stamped water depths. While there is, in principle, potential to collect a more continuous time series of flood stage data via citizen science stations like these, our general finding is that citizen participation at the stations in our study was intermittent and sparse, limited to single or few data points for each weather event.

3.3.3 Sensitivity Analysis and Parameter Grouping

The sensitivity analysis of hydrologic and hydraulic parameters, which is running model several times for different values of input parameters to measure rate of change in the model response with respect to change in input parameters (W. James, 2003), is a useful tool to identify key parameters necessary for model calibration. For the model with small catchment where surface properties are homogeneous this approach should suffice but the large heterogeneous catchment (as presented in section 3.3.1), incorporating this variability is crucial. One-at-a-time sensitivity analysis was done was done following the method by James (2003) to identify key SWMM parameters for model calibration. However, this sensitivity analysis considers the model as a single uniformly homogeneous unit, without incorporating spatial heterogeneity of parameters that tend to differ with respect to its physical or surface properties. Thus, the parameter grouping

approach to incorporate the spatial heterogeneity while minimizing parameter set is described next.

The number of parameters for our model is large (>25000), based on a semi-distributed model with 2847 sub-catchments and 2149 conduits, in which each component may have a different parameter value. Further, in this proof-of-concept study, the number of interesting weather events (i.e. storms) observed was small, increasing the computational and equifinality challenges of parameterization, given that key process-based parameters identified through one-at-a-time sensitivity analysis will not be same throughout the large catchment due to spatial heterogeneity. To reduce the search space for optimization, the sub-catchments and conduits were grouped by relevant common physical properties (Figure 3.4a), including:

- Soil type and LULC, which determine the Green-Ampt infiltration and runoff generation processes.
- The condition of conduits and its material types, which shape the hydraulic routing dynamics in drainage networks, i.e., materials, condition and age of infrastructure determines the Manning's roughness. Since built age of infrastructure was one of the missing attributes from the stormwater geodatabase, a close proxy building age from census tract data (ACS, n.d.) was utilized with the assumption that stormwater infrastructure is as old as the neighborhood.

Information on soil type and LULC layers was extracted to discretized sub-catchment polygons, and material types and proxy-built age information was extracted to

conduits layers using the Spatial Join tool of ArcGIS, in order to generate subcategories of sub-catchments and conduits.

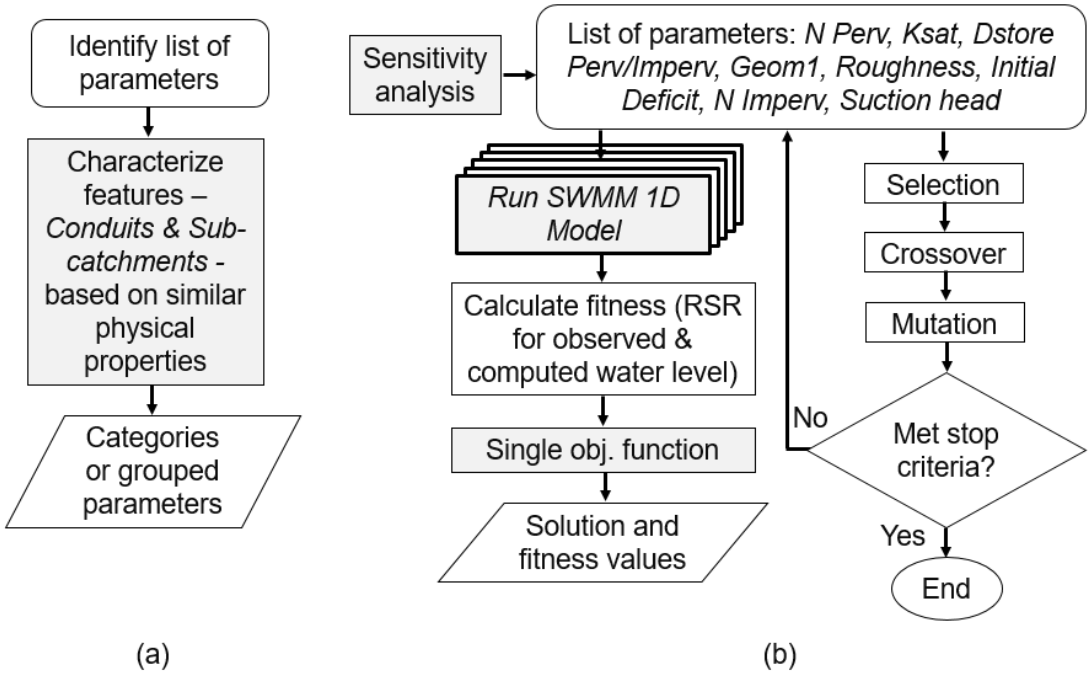

Figure 3.4. Methodological Framework for (a) Parameter Grouping and (b) Optimization Algorithm for Parameterization

3.3.4 Auto-Calibration using Genetic Algorithm

Calibration of parameters in stormwater system modeling is essential because, even in the well-informed prior knowledge of the physical stormwater system, the epistemic and aleatory uncertainties in data (e.g., outdated DEM, variations in hydraulic conductivity associated with a soil type) and model structure (e.g., incorrect tabulation of attribute-values) can lead to significant inaccuracies in model outputs. To calibrate our SWMM 1D model, we used a single objective optimization method using a genetic algorithm (Scrucca, 2021); execution of the model was performed in the R environment

(Leutnant et al., 2019). The auto-calibration of a SWMM model using a genetic algorithm (Holland, 1992) involves running the model with different sets of parameter values to create sets of individual model runs known as realizations or populations (here, population size is 280). The fitness of each individual, as determined by RSR (Eqn. 1), establishes the probability of being selected for subsequent generations. In hydrological modeling terms, individuals with distinct genetic structures, refer to a model with different parameter values. Each generation is an iteration to create a populations from which genetic operators perform crossover, mutation and selection (Yang, 2014). The crossover, mutation and selection process generates a new population of individual parameter sets from the current population probabilistically as per the fitness such that the solutions with better fitness results are passed on to the next generation (Scrucca, 2021). Here, 100 generations or iterations were used. As each of the individual model runs is independent, the execution of model runs was parallelized and distributed across the CPU cores of a computational cluster. Our choice of this approach was inspired by successes using it in similar contexts: genetic algorithms have been used in parameterization of a conceptual rainfall-runoff model by Wang (1991), for calibration of SWMM model by Dent et al. (2004), Cho & Seo (2007), Shinma & Reis (2011) and Krebs et al. (2013), and even for rehabilitation, capacity or cost optimization of drainage network by Ogidan & Giacomoni (2016), Martínez-Solano et al. (2016) and Zhou et al. (2019). More practically, this method is highly parallelizable, allowing us to efficiently run the realizations in clusters (Scrucca, 2021). The fitness function for the algorithm

aims to minimize the root mean square error observation standard deviation ratio (RSR) (D. N. Moriasi et al., 2007) between observed and simulated water levels, defined as:

$$\mathrm{RSR} = \frac{\mathrm{RMSE}}{\mathrm{STDEV_{obs}}} = \frac{\sqrt{\sum_{t=1}^{T}\left(Y_t^{obs} - Y_t^{sim}\right)^2}}{\sqrt{\sum_{t=1}^{T}\left(Y_t^{obs} - Y^{mean}\right)^2}} \quad (1)$$

where, Y_t^{obs} and Y_t^{sim} are the observed and simulated water levels at each time step or observation (t = 1, 2, .., T), respectively, and Y^{mean} is the mean of observed data.

A one-at-a-time sensitivity analysis was conducted to identify the key SWMM parameters, followed by selection of parameter set to reflect spatial heterogeneity but optimize parameterization complexity using the parameter grouping approach outlined above in section 3.3.3. The details of the optimization process are summarized in Figure 4b. As discussed earlier, surface level observations from two novel data sources were used to drive the calibration process: continuous time series flood camera stage data, and single point water level observations from citizen science contributions.

3.3.4.1 Integrating Continuous Time Series Data

The automated flood cameras generate a continuous time series of observed water depth values, at varying temporal intervals ranging from 12 hours to 1 minute (the cameras use evolving local weather forecasts to dynamically increase reading frequency as weather events arrive), as discussed in section 3.3.2.1. The flood camera and gauge installed in one of the open channels within our study catchment area provided observational data that was paired with the water depth outputs computed for the same open channel conduit within the SWMM 1D model; this paired observed-simulation

hydrograph was then directly used in the optimization algorithm. Site inspection verified that there is no baseflow and that the channel remains dry without any rainfall. A flooding event captured on February 22nd, 2020 (hereafter: Event A) in one of the open channels inside the Northern Arizona University (NAU) was utilized for calibration (Table 3.2).

Table 3.2. Flooding Events Observed from Novel Data Sources

Event	Location	Date	Source
Event A	Inside NAU campus	02/22/2020	Flood camera
Event B	Leroux St. and Dupont St.	07/24/2021	Field survey/ Crowd Hydrology
Event C	Leroux St. and Dupont St.	08/17/2021	Flood camera

3.3.4.2 Integrating Continuous Single Point Data

Crowdsourced observations of the flood water level typically take the form of a passing citizen who notices that some water is present at a citizen science station and sends in a measurement. Thus, such data are usually single data point per person per station. Although contributions from multiple citizen scientists passing a station at different times in the same event might supply additional data points, a full hydrograph is unlikely. Nonetheless, such isolated single-point observations can be used to calibrate or validate a hydrological model when no other data is available. The main challenge of integrating such observational data in an optimization routine lies in accurately converting the observed overland street water depth to the output variable of SWMM 1D model. The problem here is that the observed street water depth is a function of both the stormwater system dynamics (which are modeled by the SWMM 1D) model, and the surface and overland flow dynamics given by the terrain (which are not captured by a SWMM 1D model). To address this challenge, we developed a method leveraging an

auxiliary SWWM 1D-2D (built using PCSWMM version 7.3.3095) model to bridge this gap. In this way, we can benefit from the speed and computational efficiency of the SWMM 1D model, while also connecting its outputs to observed surface water levels to perform calibration. The following paragraphs explain our method in more detail.

Flooding in SWMM 1D occurs when the hydraulic grade line at nodes exceeds rim elevation of the catch basin or manhole; this overflow volume is known as *flooding loss*. Flooding loss in SWMM 1D model is the water exiting the stormwater network from nodes which do not re-enter the underground drainage unless ponding option is allowed. Each of the flooded nodes generates a certain flooding loss (e.g. a hydrograph). The SWMM 1D-2D model has the additional capability to simulate overland flood routing and dynamic exchange of flood water between overland and underground drainage systems, as well as the capability to simulate flood depth and velocity overland. The 1D components of the SWMM 1D-2D model (i.e., all 1664 catch basins) are coupled with the 2D components (i.e., mesh grid cells) using orifices where the overland flooding occurs in the system; the flooding occurs from the same catch basin nodes as in the SWMM 1D model. In this way, we perform a one-time simulation/computation to establish a fixed statistical relationship between 1D flooding loss and surface water depth (from the 2D model) for each node; this then becomes the basis for linking observed surface water levels to 1D model output to drive model calibration.

To further clarify this method, Figure 3.5 shows a flooding hydrograph for nodes in our SWMM 1D model, as well as flooding depth occurring in coupled mesh grids cell in our SWMM 1D-2D model. The flooding loss (shown as flooding flow rate in Figure

3.5) in SWMM 1D and surface flooding in the SWMM 1D-2D occurs at the same time and water depth continues to increase until the flooding loss from catch basin stops. The time segment from when water accumulation starts until it peaks is known as the *rising limb* for the flood water depth; the segment after the peak is the *recession limb*. The time integration of flooding loss (flow rate) (i.e., the beginning of flooding loss till it becomes constant) as independent variable is fitted with rising limb of water depth as response variable using linear regression. The recession limb of the flood water depth is fitted using an exponential decay function independent of flooding loss because recession happens after flooding loss ends, which was determined by inspecting the shape of the recession curves in both flooding time series in SWMM 1D and flooding depth time series in SWMM 1D-2D. This statistical relationship is established for all the catch basins using SCS type II design rainfall, with 6 inches total rainfall and 9 hours of storm duration, to convert observed flooding water level to flooding flow rate and vice versa.

After applying the method described to establish the relationship between SWMM 1D flow output and surface water levels for each node in the model, we were able to use citizen observations of surface water levels to validate our SWMM 1D model. Specifically, an isolated citizen observation reported during a flood event on July 24th, 2021 (hereafter: Event B) was utilized for model validation. As a bonus, this citizen science station also had a flood camera installed, allowing us to visually verify the citizen observation with a supporting image, as shown above in Figure 3.3c. In addition, the flood camera also captured a few data points on August 17th, 2022 (hereafter: Event C) (Table 3.2) (due to technical error the continuous image of the flood event was not

recorded) which was also used for the model validation. This methodology can also accommodate iterative calibration as more data is generated.

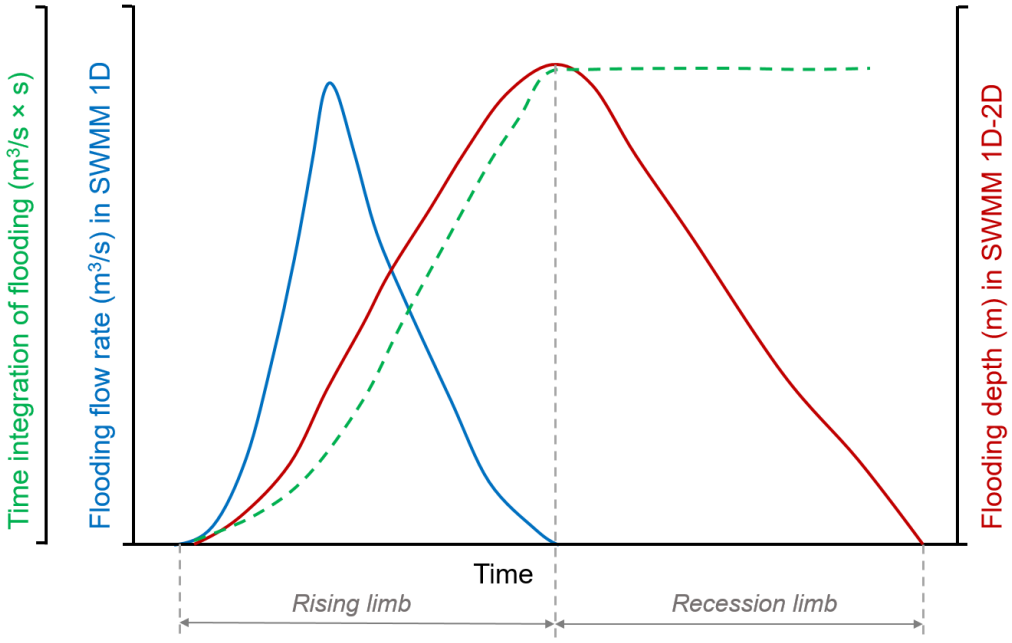

Figure 3.5. Schematic of Flooding (SWMM 1D) and Flooding Depth (SWMM 1D-2D) Occurring at the Same Location. Using Rising Limb, Time Integration of Flooding or the Area under the Curve of Flooding Flow Rate, and Flooding Depth Are Linearly Fit to Extract Surface Flooding Depth Using Flooding Flow Rate.

3.4 Results

3.4.1 Sensitivity Analysis and Parameter Grouping

The sensitivity analysis presented the 11 parameters as indicated by ranks of mean sensitivity gradient (Figure 3.6). Out of which 9 key parameters except conduits offsets (P10 and P11) were considered, since conduits offsets were known design parameters and it presented lowest sensitivity. These 9 key parameters correspond to relevant

characteristics of conduits (i.e., P5) and sub-catchments (i.e., P1, P2, P3, P4, P5, P6, P7, P8, P9). Calibrating each of these key parameters individually for each sub-catchment and conduit increases the parameters size significantly and, therefore, a reduction of the parameter space was undertaken, as described in the next section.

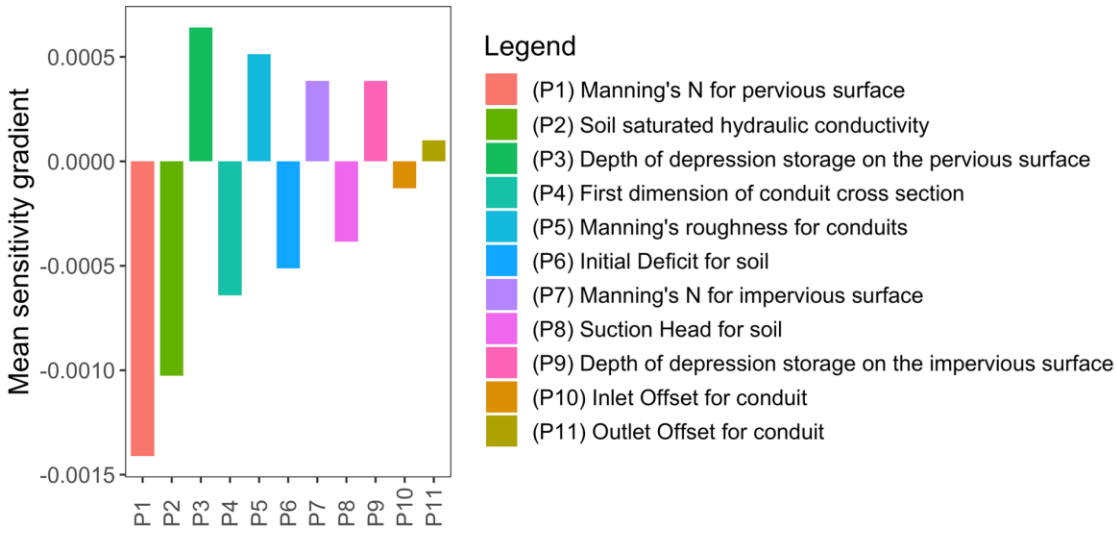

Figure 3.6. One-at-a-time Sensitivity Analysis Results

The identified key parameters for sub-catchments vary across soil (Figure 3.7a) and LULC types (Figure 3.7b). Thus, these two datasets were extracted as the new attributes to the discretized sub-catchments. Soil types and LULC are further categorized into four and three broad categories as the variation of Green-Ampt infiltration parameters are distributed across these broad categories (Table 3.3). With these combinations, 12 subgroups of sub-catchments were identified (Figure 3.7c). The age of stormwater infrastructure (through proxy building age) was categorized into newer (i.e., after 1990) or older (i.e., before 1990) conduits (Figure 3.7d). Material types (Figure 3.7e) were categorized into three major categories, as variations of Manning's roughness

assigned to smooth, concrete or rough conduits. In addition, conduits with missing roughness were added as an additional category to be calibrated (Table 3.4). With these combinations eight subgroups of conduits were identified (Figure 3.7f). Thus, 9 key parameters were distributed among these sub-groups of features and parameters, all with similar lower and upper bounds, and were combined further to create 28 sets of parameters for model calibration. The selected final set of parameters and its range for lower and upper bounds is summarized in Appendix E.

Table 3.3. Twelve Subgroups of Sub-catchments Identified

Soil type	**LULC (Intensity)**	**Category**
Stony clay loam	High	**1 – 12**
Cobbly clay loam	Medium-Low	
Lynx loam	Open space	
Sandy loam		

Table 3.4. Eight Subgroups of Conduits Identified

Material	**Age**	**Category**
Smooth (e.g., Steel, HDPE)	New	**1 – 8**
Concrete (e.g., RCP)	Old	
Rough (e.g., CM)		
Unknown (missing)		

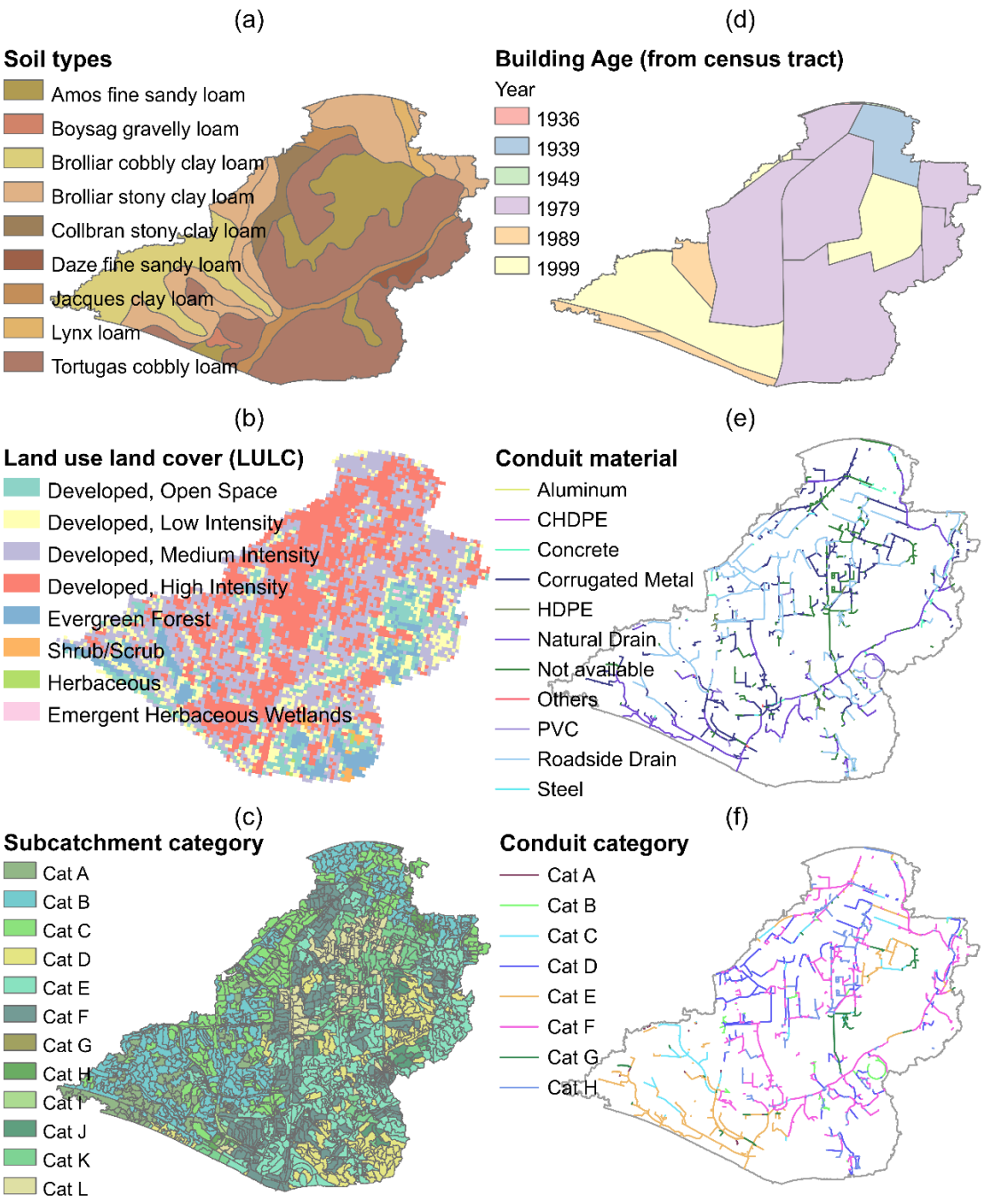

Figure 3.7. Layers of Surface Properties Data, Particularly (a) Soil Types and (b) LULC for Grouping Parameters Related to Sub-catchment, and (c) Built Material and (d) Building Age as a Proxy for As-built Stormwater Infrastructure Age for Grouping Parameters Related to Conduits.

3.4.2 Manual Validation of Model Inputs and Model Configuration

The uncalibrated stormwater model was tested for all three of the events where flooding was reported. The observations were used for manual testing to check if the model simulates the flooding at the observed locations. One of the locations during Event B failed to simulate flooding as there were a few disconnected sections in the model due to incomplete stormwater features in the database (Figure 3.8a). The model was manually corrected by adding the missing conduits and extracting their attribute-values from upstream and downstream features (Figure 3.8b). In this way, the model was able to simulate conveyance of water from upstream contributing area and subsequent flooding at the reported flooded location (Figure 3.8). In a stormwater model with a large number of features, such as our Flagstaff model (or larger), the novel data provides an efficient initial check to confirm that the current model input datasets are correctly selected and configured. Calibrating a model with incorrect model structure will obviously result in erroneous parameterization; this further supports the applicability of novel data sources: (1) as feedback from novel data supports detection of areas where infrastructure data may have errors or omissions prompting field visits or consultations with local experts, and (2) as novel data sources are distributed throughout urban catchment at a higher density (e.g. traffic cameras) harvesting data from such existing infrastructure sources is financially feasible.

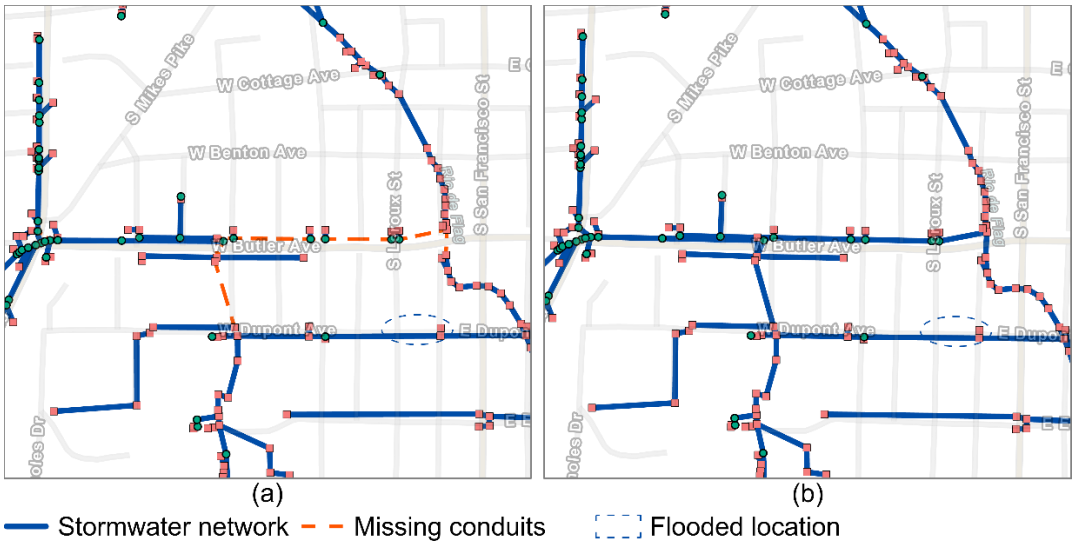

Figure 3.8. Stormwater Network Showing (a) Incomplete Disconnected Network with Missing Conduits Where Flooding Could Not Be Simulated and (b) Corrected Stormwater Network

3.4.3 Auto-Calibration using Genetic Algorithm

The results of auto-calibration of a SWMM model using a genetic algorithm (Holland, 1992) are shown in Figure 3.9 and Figure 3.10. Figure 3.9a shows the convergence of the solution, as measured by RSR value, from an initial value of 1.00 in the uncalibrated model, to a final global minimum of 0.55 over the course of 90 model generations, which is at acceptable range for good model fitness (D. N. Moriasi et al., 2007). This demonstrates the potential power of calibrating SWMM based models using genetic algorithms. The model was able to simulate the peak water depth (Figure 3.9a) and time to peak, although the model simulates the water level slightly earlier than the observation from novel data source. Two possible sources for this small discrepancy are

(a) the use of semi-distributed model instead of fully distributed model; and (b) uncertainty or inaccuracy in quantifying the observed water data.

Validation of the model using Event B (Figure 3.9c) and Event C (Figure 3.9d) was done using a linear regression fit between observed flood water level and time integration of flooding flow rate (see section 3.3.4.2). Although both of these events were observed at the same location, this linear fit of floodwater level (in the SWMM 1D-2D model) and time integrated flooding rate (in the SWMM 1D model) was done for the whole catchment. The resulting fitness is presented in Figure 3.10. Overall, the urban hydrologic-hydraulic model was well calibrated using the novel data.

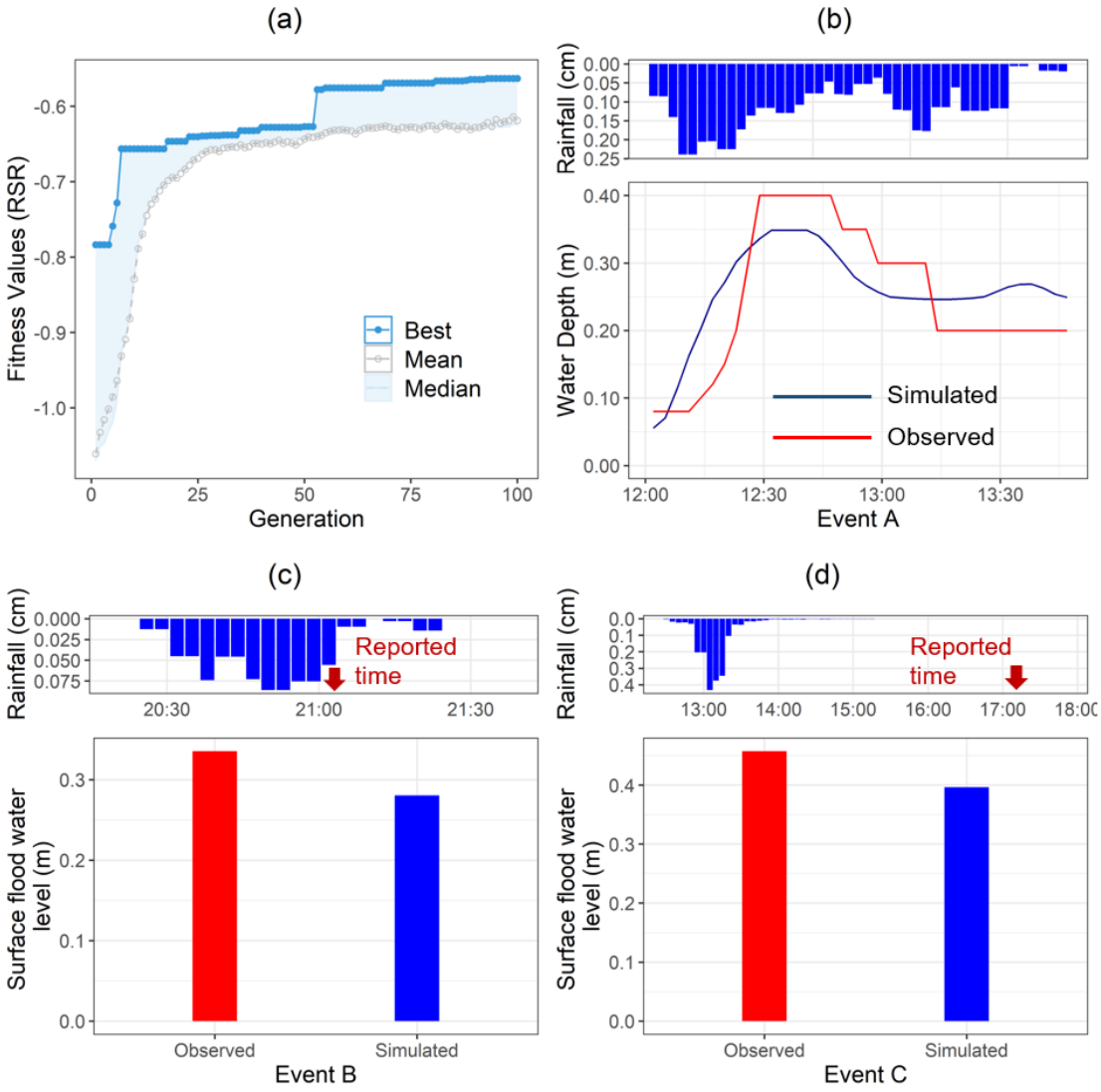

Figure 3.9. Calibration and Validation Results Showing (a) Fitness Using a Genetic Algorithm, (b) Simulated and Observed Flood Water Level Using Remotely Sensed Flood Camera Observations for Event A, and Validation Using Single Point Observations for (c) Event B and (d) Event C

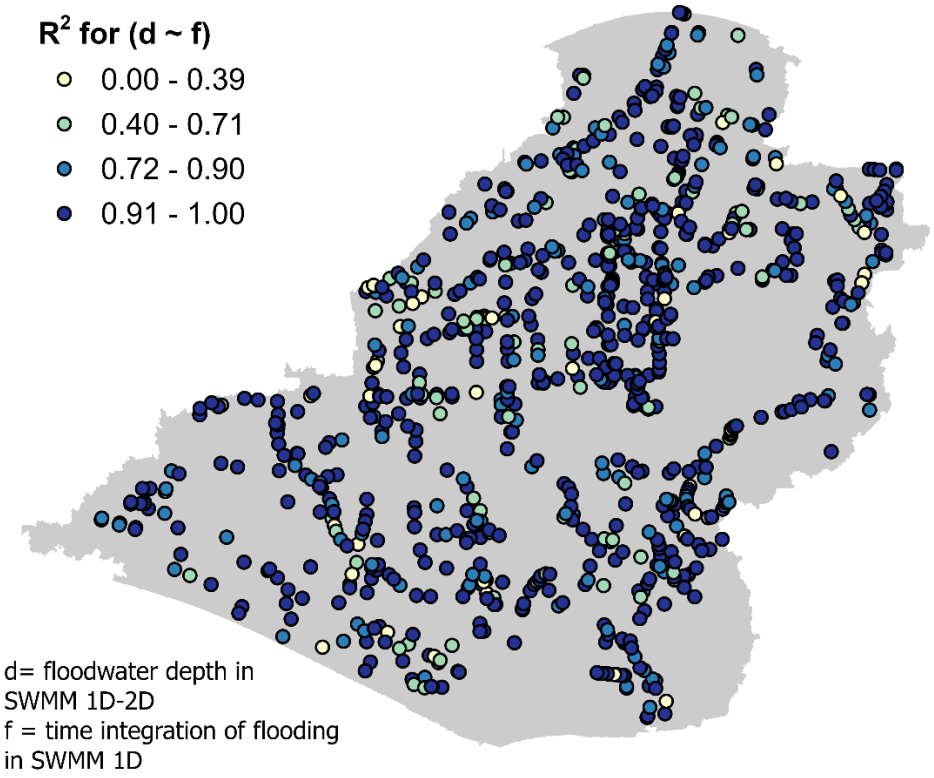

Figure 3.10. Coefficient of Determination (R^2) for Fitted Linear Relationship Between Floodwater Depth in SWMM 1D-2D Model Time Integration of Flooding Flow Rate in SWMM 1D at the given Location of Coupled 1D-2D Model

3.5 Discussion

3.5.1 Novel Data Supports Validation of Model Inputs and Configuration

Lack of long-term hydrological observation is the bottleneck to efficient urban flood model development and deployment. Despite of readily accessible computational resources and tools, lack of flood water level data prevent continual improvement of predictive accuracy of hydrologic-hydraulic model. Often collecting such measurements using the traditional sensors over the whole catchment require significant financial

resources to install and maintain new instruments. Therefore, alternate novel data sources made available by rapidly evolving networked infrastructure (e.g. traffic cameras, citizens, social networks) in many urban environments offer a potential solution to compensate the lack of hydrological observations in cities, by providing observations of water levels more or less continuously over time, and across very broad geographic areas. As demonstrated in this study, the pre-calibration of model to validate the input data, model configuration and model response using novel data was also able to highlight missing features or disconnected network elements, allowing focused repair and subsequent simulation of flooding conditions. For large modeled networks, it is easy to miss key details such as unusual attribute-values or gaps in infrastructure feature information and novel data, even in binary form (e.g. flood or no flood), was useful in identifying these potential sources of model error.

One key limitation of camera-based observations currently is attaining required image clarify and resolution during low light or low visibility (e.g. dust) conditions, which could result in missed or inaccurate observations. Improved techniques and image processing (e.g., using Infrared-reflective targets and imaging, currently in progress (ASU/NAU, 2021)) show strong promise for addressing this challenge. Similarly, citizen science observations are subject to inaccuracies due to measurement error or delayed submission of the observation by the human observer. Although novel data sources can also suffer from unreliability issues (e.g. camera failure, citizen science inaccuracy), our proof-of-concept analysis presented here shows that novel data can nonetheless be used to effectively calibrate a hydrological model. Moreover, improving technology (e.g.

improved image processing, higher-resolution cameras), better citizen science interfaces, and an increase in data volume as the number of data streams (i.e., sources such as flood camera, citizen science, or social media) and observations continues to grow should increase overall reliability of novel data sources and further improve calibration performance. For instance, in this study we used readings from a single experimental "flood camera" as a proxy for a municipal traffic camera; leveraging a full network of actual traffic cameras could achieve vastly higher spatial coverage and data volume, with a commensurate positive impact on the model development and testing process demonstrated here. As more novel data are collected both in density and volume, data uncertainty and errors can be identified and improved.

3.5.2 Novel Data Supports Calibration

In this study, we have explored the potential utility of novel data for hydrological model calibration, providing an encouraging proof-of-concept demonstration showing that useful calibration can be done even with the relatively sparse novel data we had available. Although the calibration experiment described here was done in single step auto-calibration fashion, novel data could eventually be used in continuous fashion for regular, automated (re)calibration of hydrologic-hydraulic models deployed for real time flood forecasting as new observation is available. By leveraging existing sensor (traffic cams, citizens with smart phones), novel data streams have the potential to cover large spatial areas continuously over time, and at relatively high measurement densities across relevant catchment areas. As surface level observations, novel data sources can also

capture and account for detailed spatial heterogeneities that occur within catchment areas, tracking any changes in these characteristics over time. This is particularly important in urbanized catchments where the physical surface properties tend to change rapidly: novel data streams can reflect changes in catchment response to physical changes in surface characteristics, while built stormwater infrastructure remains static; automated recalibration of the model to account for such surface level changes could be automatically triggered as observations and model predictions start to diverge.

In sum, the predictive accuracy of pluvial flood models has been hampered by the difficulty of reliably calibrating such models, due to the lack of hydrological observation data in urban areas. Automatically collected novel data can help fill this gap and, with integration of computing techniques such as evolutionary algorithms with powerful, scalable compute infrastructures provided by evolving cloud computing resources, sophisticated on-demand continuous auto-calibration is possible. The current hydrologic-hydraulic model selected here is a one-dimensional model for its faster computation. With evolving computational resources calibration of two-dimensional models can be viable from which not only more accurate surface flood depth can be simulated but also the flood extent. This sophisticated process, of course, depend on the capability and limitation of novel data sources to capture flooded extent through the network of cameras. The relative value of novel data is particularly high when nothing else exists, i.e., when there are no historical observations available or in the absence of traditional sensor instrumentation of the stormwater network at hand. These continuous observations from novel data sources could further improve the precision of model predictions, which

in turn could provide broader ranging benefits on some of the overlooked aspects of pluvial flood, such as proper estimate of pluvial flood hazard, risks and impacts in cities. One limitation of this study is that no data from a traditional sensor network was available (i.e., our targeted stormwater system was not instrumented), and we were therefore unable to compare and contrast the calibration efficiency of novel data versus traditional sensor data; this remains as an important focus for future work. Practically speaking, however, there is no reason that these two data sources – traditional sensor instrumentation and novel data sources – should not be fully complementary. Each of them has certain strengths and limitations and having both could both increase observational data density and provide for mutually reinforcing cross-checking between data types.

3.6 Conclusions

This study explored a novel method of calibrating a hydrologic-hydraulic model for an urban catchment in Flagstaff, Arizona, based on the use of experimental novel data collection infrastructure. Like most cities, consistent historical observations of hydrological variables such as flow or floodwater level in the urban catchment are not available in Flagstaff, making it impossible to effectively calibrate a traditional SWMM model of the stormwater system. This study provided a proof-of-concept demonstration of how novel data sources could be effectively leveraged to allow effective validation and calibration of a SWMM model of the targeted catchment basin; novel data was also shown to be useful in highlighting missing or misconfigured elements of the model,

improving model quality. The measurements of floodwater depths were collected and used to develop a calibration process based on coupling a SWMM model with a genetic algorithm to efficiently calibrate a large-scale model. Specifically, parameter grouping was used to identify key parameters necessary for parameterization. Parameter grouping was essential to calibrate a large catchment scale semi-distributed model given the computational resources available. Parameter grouping significantly reduced size of the parameter set and computational resource required while maintaining key spatial variation. Lastly, this study developed statistical relationships between surface level floodwater depth and flooding flow rate using two, 1D and 1D-2D, implementations of SWMM to leverage street level water depth observations.

In sum, this study provides a proof-of-concept for leveraging novel data sources for catchment scale urban hydrological modeling applications. The method is general and replicable to other catchments and could support single step auto-calibration or continuous auto-calibration as more data is generated over time, spanning multiple weather/flooding events. In particular, the findings of this study can be summarized as follows: (1) Novel data can provide continuous surface level hydrological observations with that can drive manual validation of the model inputs and model configuration, (2) novel data can be used in auto-calibration of hydrologic-hydraulic model, hence improving the model accuracy and reliability, (3) streamlining novel data sources for improving modeling of pluvial flooding (or any other form of flooding) will require reliable, automated networked data collection infrastructure that supports efficient

collection, transfer, storage, as well as automated high-performance modeling capabilities.

CHAPTER 4

EFFECTS OF PRECIPITATION UNCERTAINTY AND LAND USE CHANGE IN THE OPTIMAL CATCHMENT SCALE GREEN INFRASTRUCTURE CONFIGURATION

This chapter has been adapted from the working paper Shrestha, A., Garcia, M. (2022). Effects of precipitation uncertainty and land use change in the optimal catchment scale green infrastructure configuration.

Abstract: Adoption of green infrastructure (GI) as a sustainable stormwater infrastructure measure has gained momentum globally. GI can supplement the hydraulic capacity of the existing drainage network to reduce flood risk and maintain flood protection levels as conditions change. Modeling and analysis tools are available to guide design and planning. However, the impact of uncertainty in design precipitation estimates, change in precipitation and land use on the optimal configuration of GI has not yet been assessed. The uncertainty in design precipitation estimates influence the amount and cost of GI; and urban forms, space availability and existing drainage infrastructure influence the placement and ideal types of GI. Further, climate change and conversion of pervious surface to impervious create varied impact in cities. Here we investigate how such catchment scale optimal configuration of GI, defined as ideal selection of type, amount and spatial distribution of GI, vary (i) across uncertainty within standardized precipitation estimates from NOAA Atlas 14 and (ii) with increasing urban

imperviousness. We analyze this across two different cases of urban forms: (i) a catchment with mixed use buildings where green roofs and bio-retention are ideal, and (ii) a catchment with only residential buildings where only bio-retention is feasible. For this aim we utilize the U.S. Environmental Protection Agency's Storm Water Management Model (SWMM) to construct one-dimensional hydrologic-hydraulic models using stormwater networks of two separate locations in Phoenix, Arizona. We couple the SWMM model with non-dominated sorting genetic algorithm (NSGA-II) to develop a multi-objective optimal GI planning framework to determine amount, type and location for GI implementation. We found that varying the design precipitation across the lower to higher bound of the confidence interval for NOAA Atlas 14, resulted in significantly difference in the amount of GI required than the effect of land use change from 2001 to 2019. This highlights the important of accurate design storm estimates and the value of modular GI in adapting stormwater systems under uncertainty.

4.1 Introduction

Urban expansion results in increasing impervious cover and modifies hydrological processes by reducing runoff response time and increasing peak runoff. In addition, in some regions, increasingly frequent extreme events due to climate change (Kunkel et al., 2020) are overwhelming the stormwater infrastructure capacity causing functional failure before its design life (Mailhot & Duchesne, 2010; Swain et al., 2020). Consequently, rainfall induced urban (or pluvial) flooding has become a common phenomenon in many cities (Rahmati et al., 2020; University of Maryland & Texas A&M

University, 2018). Replacing and upgrading existing grey stormwater infrastructure (e.g., conduits or detention tanks), is financially and technically challenging due to spatial interdependencies (Chester & Allenby, 2019) with transportation and other infrastructure systems, resulting in lock-in (Gilrein et al., 2019). Networked infrastructure particularly transmission, distribution or conveyance systems are less adaptable because it cannot be changed or restructured easily. Furthermore, upgrading the capacity of underground drainage conduits to mitigate localized flooding requires the replacement of several sections of conduits both upstream and downstream. Eventually renewal and replacement of such infrastructure nearing the end of its design life is one of the present-day key issues facing stormwater management (Dolowitz, Bell, & Keeley, 2018). The inflexible properties of grey stormwater infrastructure motivate the need for alternate design choices, which are adaptable (Manocha & Babovic, 2017), flexible and sustainable. Green infrastructure (hereafter abbreviated as GI) fills this need while also providing a wide range of co-benefits (Alves, Gersonius, Sanchez, Vojinovic, & Kapelan, 2018; Bell et al., 2019; Choi, Berry, & Smith, 2021). However, the key challenges that remain are how the GI can be distributed across the catchment to achieve the optimum hydrological benefit at least cost, what design criteria shall be considered, and how robust design decisions are in a dynamic environment.

The use of GI in urban environments is recommended by the U.S. Environmental Protection Agency (USEPA, 2014), and the United Nations (WWAP, 2018); it is also widely accepted among scientific communities in hydrology, ecology, engineering and social science, for flood mitigation (Gaffin, Rosenzweig, & Kong, 2012; J. Sörensen &

Emilsson, 2019; Webber et al., 2020), ecological benefits (Benedict & McMahon, 2002; Tzoulas et al., 2007), heat mitigation, increases in property value (Manso, Teotónio, Silva, & Cruz, 2021), and improvements in wellbeing and public health (Nieuwenhuijsen, 2020). GI practices such as bio-retention, bio-swales and green roofs, most commonly known as Low Impact Development, are a subset of GI, engineered to function as a standalone unit or in concert with existing grey infrastructure to enhance hydrological functions of infiltration, storage, and pollutant removal via sedimentation and filtration. Bio-retention is engineered to promote infiltration (Golden & Hoghooghi, 2018), with soil filter media consisting of surface layer, soil layer and storage layer over native soil, planted with native vegetation; in arid climates for example, bunchgrass (e.g. Bluebunch wheat grass) and shrub (e.g. Apache plume) are recommended (Houdeshel, Pomeroy, & Hultine, 2012). Green roofs have shallow soil media with native vegetation. Unlike grey infrastructure, GI adds flexibility through modularity since it is customizable into numerous design forms (e.g. green roofs, detention basins, rain gardens), integrable into existing drainage network, and scalable as the need arises. Green infrastructure implemented in several U.S. cities (e.g., Philadelphia, Boston, Seattle) provides evidence that GI performance meets or exceeds design expectations (Hopkins et al., 2018; USEPA, 2014a; WEF, 2018). Despite growing evidence supporting success stories and performance efficiency, its adoption at catchment scale remains limited due to uncertainties affecting design and planning (Montalto, Behr, & Yu, 2011; O'Donnell, Lamond, & Thorne, 2017; Thorne, Lawson, Ozawa, Hamlin, & Smith, 2018; Zuniga-Teran et al., 2020). The flexible and modular property of GI allows it to be integrated as

grey-green infrastructure for capacity enhancement of stormwater system. Such integration requires tools to assess designs and plans at the catchment scale.

Urban drainage design standards typically define design precipitation according to the site-specific precipitation intensity, duration and frequency relationships, produced by federal government agencies such as National Oceanic and Atmospheric Administration (NOAA) Atlas 14 released in 2004 or older documents, the U.S. Weather Bureau Technical Paper 40 (TP40) released in 1961 and HYDRO 35 released in 1977 (V. Te Chow et al., 1998; Lopez-Cantu & Samaras, 2018). Historically TP40, which included precipitation estimates for durations from 30 min to 24 hours and return periods from 1 to 100 years, was adopted for infrastructure design, but was partially superseded by HYDRO 35 for its events ranging from 5 min to 60 min, which was more suitable for urban drainage design (V. Te Chow et al., 1998). Currently NOAA's Atlas 14 is the most comprehensive set of precipitation estimates which superseded TP40 and HYDRO 35 across most of the U.S. Atlas 14 quantifies the 90% confidence interval for precipitation intensity estimates for durations from 5 min to 60 days and return period of 1 to 1000 years. These confidence intervals were derived separately for each duration and represent the uncertainties arising from the distribution parameters and record lengths, and the authors caution users of likely scenarios using design based on these ranges (Perica et al., 2018). Lopez-Cantu & Samaras (2018) studied the variation in precipitation depth estimates between older and newer standardized precipitation analysis documents to identify regions and states across the U.S. that need to prioritize changing design standards. Markus et al (2007) studied variation in 100-year 24-h precipitation estimates

from station data, TP-40, Bulletin 70 and Atlas 14 for Northeastern Illinois and estimated modelled runoff peaks using HEC-HMS using different estimates, which suggested older design standards could underestimate precipitation depth. The effects of using different standardized precipitation sources or considering uncertainty within an estimate (e.g. Atlas 14 confidence interval), on the design of stormwater infrastructure such as GI has not been previously studied.

Stormwater design criteria such as precipitation intensity for a given frequency and catchment imperviousness do not remain static due to non-stationarity in climate and change in land use and land cover. Climate change will likely increase the number of wet extremes in 21st century compared to 20th century across North America, Eastern Africa and Western Europe (Stevenson et al., 2022). The effects on precipitation patterns differ by region, with varying changes in the magnitude and timing of precipitation (Carvalho, 2020), leading to increasing floods risk in some regions. In the U.S. the trend in extreme precipitation for 1 day event for the 1 to 20 annual recurrence interval indicate significant positive trends in most regions including the northeast, east north central, central, west north central, and southwest (Kunkel et al., 2020). Cannon & Innocenti (2018) suggest that the shorter duration precipitation intensities may become more intense in the future across North America. For example, the 1h duration precipitation in 10-year recurrence interval could increase from +29% (lower quartile) to +49% (upper quartile) by 2100 under the Representative Concentration Pathways (RCP) 8.5. Similar changes will likely occur globally; across European countries the intensity of the precipitation will increase across 1 to 100 year return period for all duration ranging from 30 min to 24 h, under

both RCP 4.5 and 8.5, causing the Intensity-Duration-Frequency curve to shift upward by 16% to 27% and steepen between 17% to 25% (Hosseinzadehtalaei, Tabari, & Willems, 2020). The developed land within and around cities has expanded significantly over the last century across the U.S. This is typified by urban sprawl (Barrington-Leigh & Millard-Ball, 2015; USGS, 2003) with largest horizontal urban growth observed in Sacramento, Phoenix, Houston, Atlanta, Providence and New York between 2000 and 2015. This typifies two pattern of urban surface change – the city core where urban imperviousness has already reached almost 100% in the last few decades (densification) and surrounding city areas which are expanding outwards (sprawl). In order to keep the stormwater infrastructure functional the existing infrastructure needs to be adapted to capture increased surface runoff and minimize pluvial flood risk (Arnbjerg-Nielsen et al., 2013). As identifying the optimal configuration of GI is an integral part of catchment scale GI planning, understanding how it varies under probable dynamics of such changes helps in GI decision making and planning.

The optimal configuration of GI is defined as ideal selection of GI types, optimal selection of the amount of GI and its spatial distribution over the catchment. For this study we used a fixed standard design specification and parameters for bio-retention and green roof as suggested by (Lewis A. Rossman & Huber, 2016). In this study, we aim to investigate the overarching research question of how the catchment scale optimal configuration of GI is influenced by uncertainty in design standards and changes in design conditions. Specifically, we break down this problem into three sub-questions: (1) How to optimally configure GI for ideal type, amount and spatial distribution for

catchment scale planning to mitigate urban flood while minimizing cost of implementation? (2) How does the uncertainty in precipitation (measured by the confidence interval in Atlas 14) affect the optimal design configuration of GI? (3) How the change in urban imperviousness affect the optimal GI configuration? To answer these questions, we utilize the U.S. Environmental Protection Agency's Storm Water Management Model (SWMM) to build a hydrologic-hydraulic model for two urban catchments in Phoenix, Arizona. These two catchments represent two distinct urban forms, where the urban blocks are already heavily urbanized consisting of commercial buildings (i.e., the urban core) and other has developed over the past 20 years and consists of residential buildings (i.e. sprawl). The physically based, semi-distributed one-dimensional SWMM model simulates the physical hydrologic and hydraulic process of runoff generation and routing in sub-catchments and underground conduits, and the interaction of implemented GI with the existing drainage network. The SWMM model is coupled with non-dominated sorting genetic algorithm (NSGA-II) to optimize GI for achieving pareto optimal solutions for maximum flood mitigation at least GI implementation cost.

4.2 Material and Methods

In the following sections we describe the selection process of two urban catchments in the city of Phoenix frequently affected by pluvial flooding, and the hydrologic-hydraulic model setup and data requirements in the two catchments. Finally,

we present the configuration of GI for the ideal type, optimal amount and spatial distribution of bio-retention and green roofs.

4.2.1 Catchments Selection

Urban expansion and horizontal growth occur at different spatial and temporal scales across cities. This results in changes in impervious surfaces over time. To compare this process in the 20 largest U.S. cities by population (U.S. Census Bureau, n.d.) (Table 4.1), using urban imperviousness data from National Land Cover Database, Multi-Resolution Land Characteristics Consortium available at a spatial resolution of 30 m, the sum of the percent changes in urban imperviousness between 2001 and 2019 was normalized by the total area within the city boundary (Eq. 1). The change in urban imperviousness (Δ_I) is defined as:

$$\Delta_I = \frac{\sum_{i=1}^{n}\sum_{j=1}^{m}\left(\mathrm{I}_{i,j}^{2019} - \mathrm{I}_{i,j}^{2001}\right) \times A_p}{A_c} \quad (1)$$

where, *I* is the percent imperviousness (for 2001 or 2019) and *n* and *m* are the rows and columns of the raster data, A_p is the area of a pixel and A_c is the area of the city. A_c is defined as the product of A_p and number of raster pixels within city boundary (N_c). Several of the 20 largest cities are expanding with new impervious surface being added. In general, higher values of Δ_I implies greater sprawl and low values implies minimal sprawl over the study period (2001-2019, Table 4.1). The city of Phoenix, Arizona, which is one of the largest metropolitan regions in the U.S. (Figure 4.1a) with a population over 1.6 million, represent cities experiencing sprawl where impervious area in city core peaked prior to 2001 and the peripheral area of the city has continued increasing

impervious cover (Figure 4.1b). Figure 4.1b shows the change in urban imperviousness in Phoenix at 30 m resolution in between 2001 and 2019.

Table 4.1. Change in Imperviousness from 2001 to 2019, and 90% Confidence Interval for NOAA Atlas 14 Precipitation Estimates in 20 Most Populated (U.S. Census Bureau, n.d.) U.S. Cities

City, State	**Sum of change in imperviousness in each cell** *(% × m^2)*	**Total area within city boundary** *(N_c × m^2)*	Δ_I *(%)*	**Latitude, Longitude for Atlas 14 Stations** *(°)*	**Atlas 14, 90% CI for 5-yr return period, 60-min storm** *(cm)*
Austin, TX	5,459,106,600	721,885,500	7.56	30.2676, -97.7430	4.72 - 8.10
San Antonio, TX	9,183,889,800	1,272,037,500	7.22	29.4246, -98.4946	4.55 - 7.80
Phoenix, AZ	7,769,770,200	1,343,764,800	5.78	33.4483, -112.0758	2.16 - 3.15
San Jose, CA	4,606,549,200	798,119,100	5.77	37.3387, -121.8854	1.07 - 1.49
Charlotte, NC	4,606,549,200	798,119,100	5.77	35.2229, -80.8380	4.65 - 5.46
Fort Worth, TX	1,277,393,400	261,274,500	4.89	32.7510, -97.3309	3.94 - 6.78
Columbus, OH	2,559,526,200	584,719,200	4.38	39.9620, -83.0027	3.71 - 4.55
Houston, TX	6,508,602,900	1,544,800,500	4.21	29.7608, -95.3695	5.23 - 8.99
Denver, CO	1,663,968,600	403,884,900	4.12	39.7400, -104.9920	2.07 - 3.33
Dallas, TX	3,394,937,700	993,075,300	3.42	32.7782, -96.7951	4.19 - 7.24
Jacksonville, FL	6,500,905,200	2,125,287,900	3.06	30.3315, -81.6562	5.41 - 7.75
Indianapolis, IN	3,114,387,000	1,043,739,000	2.98	39.7669, -86.1501	3.99 - 4.90
San Diego, CA	1,796,976,000	859,053,600	2.09	32.7157, -117.1617	1.57 - 2.27
Washington, DC	282,590,100	165,132,900	1.71	38.8904, -77.0320	4.19 - 5.11
Philadelphia, PN	448,420,500	368,908,200	1.22	39.9522, -75.1622	4.09 - 4.85
Chicago, IL	703,442,700	598,457,700	1.18	41.8843, -87.6324	3.96 - 5.03
New York, NY	887,688,000	766,017,000	1.16	40.7146, -74.0071	3.18 - 5.11
San Francisco, CA	111,637,800	121,137,300	0.92	37.7771, -122.4196	1.60 - 2.05
Los Angeles, CA	997,891,200	1,226,620,800	0.81	34.0536, -118.2454	1.74 - 2.53
Seattle, WA	114,475,500	225,593,100	0.51	47.6036, -122.3294	NA

The current uncertainty in the Atlas 14 estimates, as presented through 90% confidence interval, (Bonnin, Martin, Lin, Yekta, & Riley, 2006) informs the infrastructure designers and decision makers about the potential for over and under design. The uncertainty in short duration rainfall (e.g. 5 min) could be quite high for cities, including in Phoenix (NOAA/NWS, n.d.). Continued population growth and city expansion increases the demand for new stormwater infrastructure or upgrades to existing

infrastructure. In Phoenix, stormwater drainage for streets including catch basin spacing and conduits are required to manage the 2-year return period rainfall (City of Phoenix, 2013). However, flooding impacts prompt rethinking of this standard. Extending capacity of infrastructure at frequently flooded locations to handle the 5-year return period rainfall would mitigate flood impacts and increase infrastructure resilience. This pertinent design challenge makes Phoenix an appropriate choice for this study, and the conclusions drawn from this case have implications for other fast-growing cities. Furthermore, stormwater infrastructure data was comprehensively available for Phoenix. Thus, Phoenix was considered for this study.

Despite of the hot desert or arid climate (Köppen BWh) with extreme hot summers and mild short winters, that receives 204 mm of average yearly precipitation, several locations within Phoenix experience frequent urban flooding. Figure 4.1b shows that the city has expanded outward in the last two decades. The first catchment selected (Cat. 1) is situated in the Central City neighborhood in downtown Phoenix (DTP) is representative of areas that were fully urbanized in the previous decades; thus, we observe relatively no change in urban imperviousness between 2001 and 2019 (Figure 4.1b). The second catchment (Cat. 2), which is situated south of the Central City in the South Mountain Village Phoenix (SMP) is representative of an area of urban expansion and densification (Figure 4.1b). The details of the as built stormwater infrastructure features for Cat. 1 (DTP) (Figure 4.1c) and Cat. 2 (SMP) (Figure 4.1d) are implemented in the SWMM model, which is described in next section. Both the catchments are similar in size with areas of 1.6 km^2. The distribution of change in urban imperviousness (%) per

pixel value (of 30 m resolution) shows that the median urban imperviousness in Cat. 1 was 79% in 2001 and 81% in 2019 and the shape of distribution is left skewed (Figure 4.2a). While in Cat. 2 the median (and distribution shape) of urban imperviousness (%) has changed from 15% (right skewed) to 45% (symmetrical) from 2001 to 2019 (Figure 4.2b). These two hydrologically independent catchments face frequent flooding as shown in the Figure 4.3a-b.

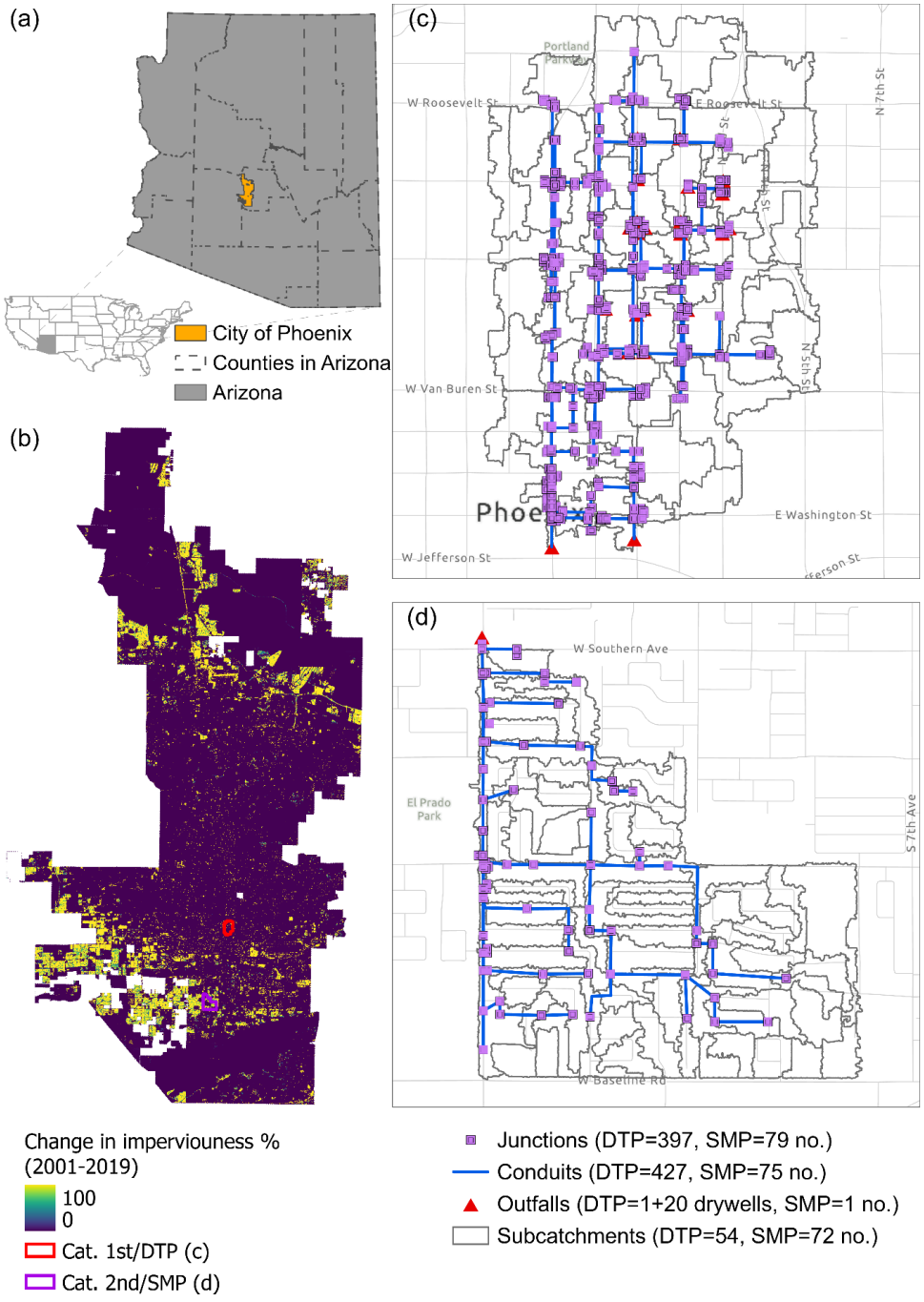

Figure 4.1. (a) Location of the City of Phoenix, (b) Change in Urban Imperviousness (%) from 2001 to 2019 and Locations of Two Catchments, Stormwater Components in (c) Study Cat. 1 or Downtown Phoenix (DTP) and (d) Study Cat. 2 or South Mountain Phoenix (SMP)

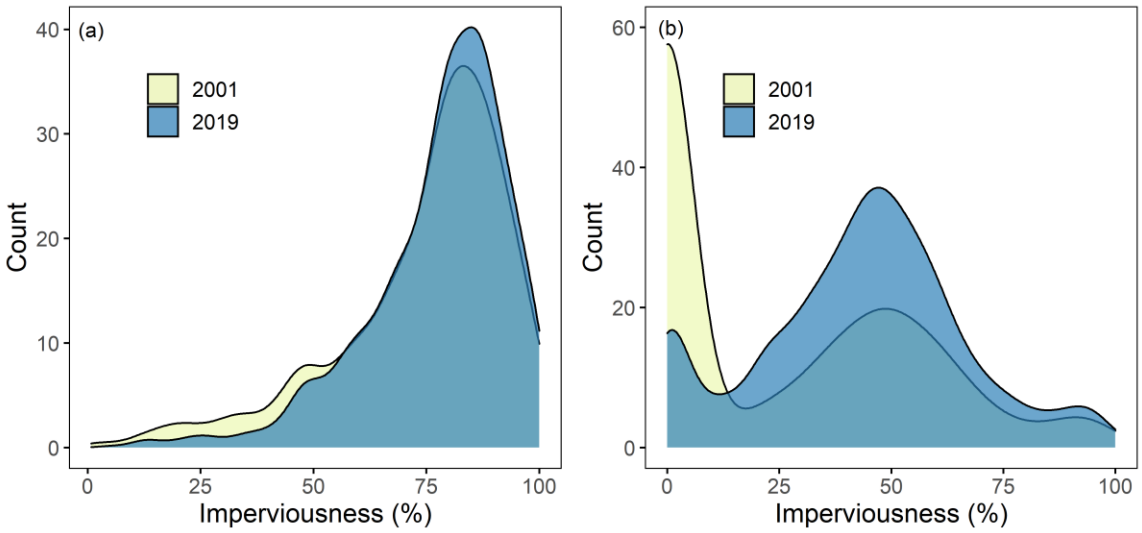

Figure 4.2. Change in Urban Imperviousness (%) from 2001 to 2019 Using Data from NLCD (MRLC, n.d.) in (a) Cat. 1 and (b) Cat. 2

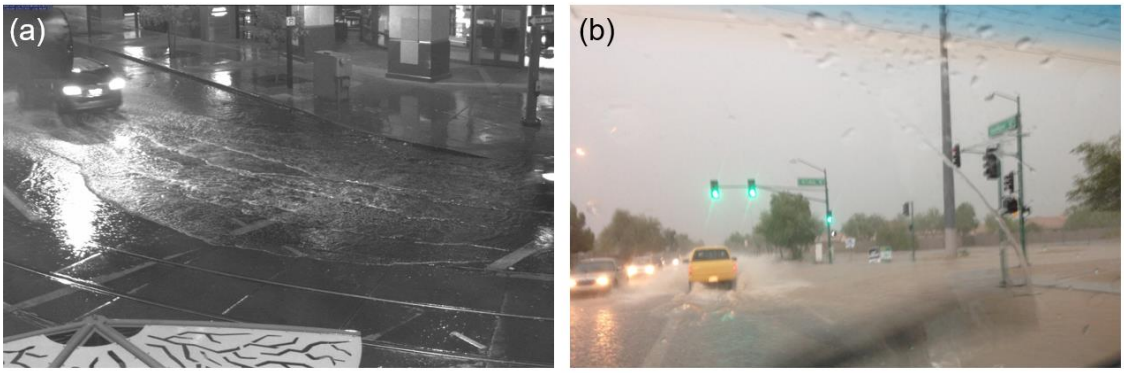

Figure 4.3. Example of Flooding (a) in Cat. 1, Occurred on September 23rd, 2019 and (b) in Cat. 2, Occurred on August 12th, 2014 (Source: *FloodAware* (ASU/NAU, 2021) and *Report a Flood, Flood Control District of Maricopa County* (FCDMC, n.d.))

4.2.2 Hydrologic-Hydraulic Model

U.S. EPA's SWMM 5 is a hydrologic-hydraulic model that computes the rainfall-runoff and routing processes and that has a Low Impact Development (LID) module. This

semi-distributed model accounts for time varying rainfall, evaporation from standing water, rainfall interception in depression storage, infiltration into unsaturated soil layers, non-linear reservoir routing of overland flow and stormwater capture by low impact development (W. James et al., 2010; Lewis A. Rossman, 2017). Dynamic wave routing is used to solve the complete one-dimensional Saint-Venant flow equations which account for channel storage, backwater effects, entrance/exit losses and pressurized flow (L.A. Rossman, 2006). The stormwater infrastructure data obtained from Phoenix Public Works Department and Flood Control District of Maricopa County consists of all the features (attributes) such as conduits (diameter, roughness, offset, depth), junctions (invert and rim elevation), outfalls (invert and rim elevation). Stormwater data in Cat. 1 is more comprehensive compared to Cat. 2, which has a few concrete conduits in some sub-catchments but is primarily drained via roadside drains. The 0.3-m resolution LiDAR point cloud data from Arizona State University (ASU) Geo Spatial hub database (ASU, 2018) was used to create Digital Elevation Model (DEM). The DEM was used to extract correct rim and invert elevations for junctions, delineate and discretize sub-catchments, and extract width and slope of the sub-catchments. For further details on model construction, see Shrestha, Mascaro, & Garcia (2022). The soil types data in two catchments were obtained from the U.S. Department of Agriculture – Natural Resources Conservation Service, Web Soil Survey database (USDA-NRCS, n.d.), and Green-Ampt infiltration parameters (e.g., suction head, saturated hydraulic conductivity) were obtained from the Arizona Department of Transportation (ADOT, 2014). The soil properties data and urban imperviousness data (MRLC, n.d.), were extracted into sub-

catchment by extracting overlaying polygons and taking average values of pixels contained within each sub-catchment, respectively. The rainfall design storm from Atlas 14 (NOAA/NWS, n.d.) for 5-year return period, 45-min duration was selected as a design standard. At both the locations the existing stormwater system is not able to accommodate runoff from short duration 5-year return period rainfall. The spatial distribution of flooded locations and functional condition of existing infrastructure is measured in terms of (1) the maximum flooding rate at each node which is defined as the peak flooding rate from an overflowing node (note that flooding in the system occurs when hydraulic grade line exceeds rim elevation of the catch basin or manhole for the underground conduits (or street curb height for roadside drains)) and, (2) peak runoff from each sub-catchment , and (3) duration of exceedance of conduits' capacity which occurs when a conduit's upstream end is full and hydraulic grade line is greater than conduit slope (W. James et al., 2010).

4.2.3 GI Optimization

4.2.3.1 GI Configuration

The two types of GI considered here, bio-retention and green roofs, were selected as they represent common ground surface and building based GI types. The availability of space and types of buildings in the two study catchments make these two types of GIs particularly viable. However, there are other types of GI, not considered in this study, which could also be viable such as the one based on the ground surface (e.g. infiltration trench, rain garden) and above ground surface (e.g. rain barrel). The size of a single unit

of both the bio-retention cell and intensive green roof is specified here as 10 m^2. The design specification and parameters for both types of GI are shown in Appendix F. The number of GI units for each variation of bio-retention and green roof in Cat. 1, and only bio-retention in Cat. 2 is optimized at the sub-catchment level. The sub-catchment layer in SWMM in divided into pervious and impervious segments. The sum of area occupied by streets, buildings and free space constitute the total area of each discretized sub-catchments, defined as:

$$Area\ of\ subcatchment = Free\ Space + Roof\ areas + Streets \quad (2)$$

Figure 4.4 shows the spatial distribution of available space and the built surfaces. The impervious segments are from buildings and streets. In the current GI implementation, bio-retention are placed only in the pervious segments, and green roofs are placed on buildings. By placing green roofs in the sub-catchment, the impervious percent of the sub-catchment decreases by equivalent area occupied by the green roofs as suggested by James et al. (2010).

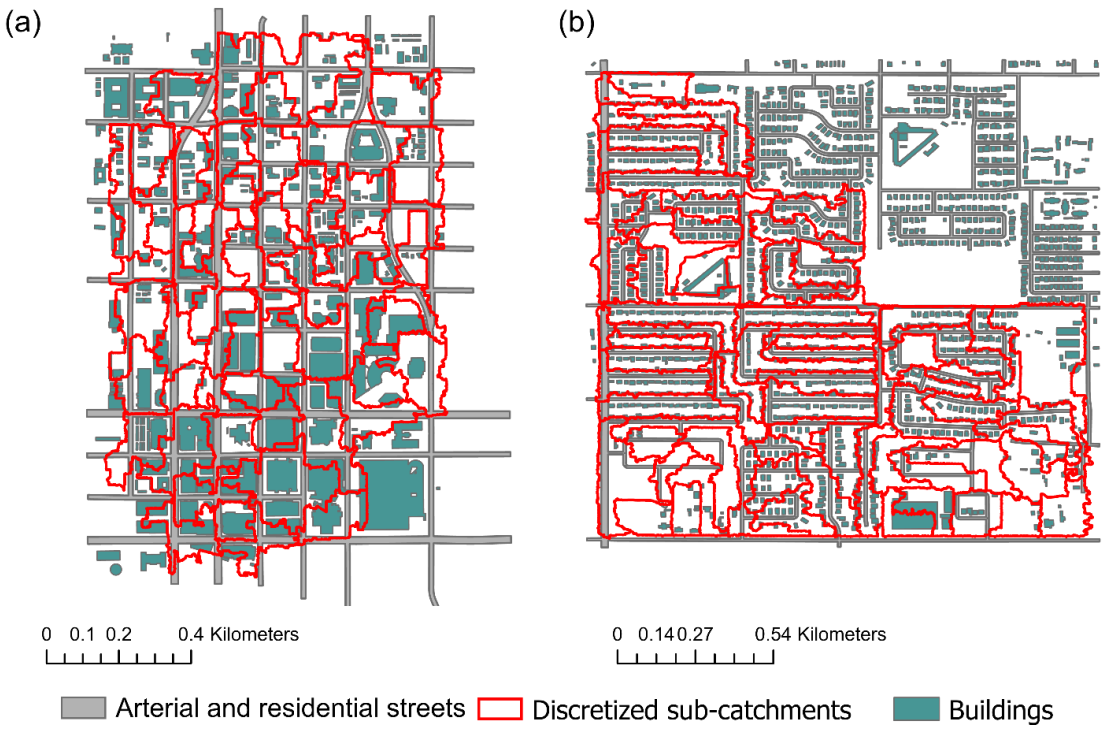

Figure 4.4. Available Space for GI in Each Discretized Sub-catchment Is Estimated by Extracting Area Occupied by Buildings and Streets For (a) Cat. 1 and (b) Cat. 2

4.2.3.2 Optimization Framework

The hydrologic-hydraulic models were coupled with the non-dominated sorting genetic algorithm that solves multiple optimization problems simultaneously (Blank, Deb, & Roy, 2019; Jain & Deb, 2014). The non-dominated sorting genetic algorithm-II (NSGA-II) is the pareto-based multi-objective evolutionary algorithm, and a subsequent version of NSGA, that uses a pareto dominance relation for searching entire Pareto front in a single run (Deb, Pratap, Agarwal, & Meyarivan, 2002; Reed, Hadka, Herman, Kasprzyk, & Kollat, 2013). Several studies have used non-dominated sorting genetic algorithm in water resources planning. Kumar et al. (2022) applied NSGA-II to minimize

urban runoff volume using optimal size and costs of LIDs. Mwiya et al. (2020) applied NSGA-III for identifying optimal irrigation scheduling to maximize water use efficiency and minimize risk. The implementation of NSGA-II with SWMM 5 model is done in R environment using R packages – *swmmr* (Leutnant et al., 2019) and *nsga2r* (Tsou, 2013).

The two objectives were considered in the optimization framework to minimize both the peak flooding (*Qpk*) resulting from 5-year return period storm and the cost of GI implementation. The first (f_1) and second (f_2) optimization objectives were defined as:

$$f_1 = min\left(\sum_{i=1}^{N} Qpk_i\right) \tag{3}$$

where, *Qpk* is the peak flooding at node i and N is the number of nodes in the model

$$f_2 = min\left(\sum_{S=1}^{N} Cost_s\right) \tag{4}$$

where, *Cost* refer to the capital cost for construction of GIs in sub-catchments (it does not reflect operation and maintenance, and life cycle cost) and N is the number of sub-catchments in the model. The optimization is constrained by the availability of space for GI implementation, which is defined as, $0 \leq AGI_S \leq AGI_M$ where, AGI_S is the area of assigned GI, and AGI_M is the maximum allowable area for GI which is maximum roof area for green roof installation and maximum free space for bio-retention installation in each sub-catchment.

Each parameter value $\{p_1, p_2, \ldots, p_n\}$ represents the number of GI to be implemented in each sub-catchment. The minimum and maximum value of these

parameters is defined as, $P_l = \{p_1, p_2, \dots, p_n\}$ and $P_u = \{p_1, p_2, \dots, p_n\}$ where, P_l is the set of lower bounds with $p_1, p_2, \dots, p_n$ = 1 and P_u is the set of upper bounds with $p_1, p_2, \dots, p_n$ determined by maximum space available, for parameter value for n = 108 (for Cat. 1) and n = 72 (for Cat. 2) corresponding to number of discretized sub-catchments and types of GI implemented. The assignment of a number of GI units for every sub-catchment within the fitness function is defined as:

$$NGI_S = round\left(min\left(\frac{AGI_M}{GI_U},\ p_{an}\right)\right)\ \forall S \in \{S_1, \dots, S_N\} \text{ sub-catchments} \tag{5}$$

where, $p_l \leq p_{an} \leq p_u$, GI_U is the unit area of GI. Here, the $min\left(\frac{AGI_M}{GI_U},\ p_{an}\right)$ function ensures that the space constraint is maintained. The total cost of green infrastructure is defined as:

$$Cost = \sum_{S=1}^{N} NGI_S \times GI_U \times cp\ \ \forall S \in \{S_1, \dots, S_N\} \tag{6}$$

where, the standard capital cost (*cp*) per unit square meter of GI installation \$430/m^2 for bio-retention and \$332/m^2 for green roof (Rutgers, n.d.; Terrascope, 2022) was used.

4.3 Results

For Cat. 1 in Central City, Phoenix the mean rainfall depth from Atlas 14 for 5-year return period for 1h duration is 2.59 cm, while the 90% confidence interval are 2.15 cm and 3.15 cm. For Cat. 2 in south mountain, Phoenix, the mean is 2.59 cm and 90% confidence interval are 2.16 cm and 3.17 cm. Using these rainfall depths as the design standards, shows that both the systems experience flooding at different locations before

GI is adopted (Figure 4.5a-i). The first row (Figure 4.5a-c) shows the model simulation result for Cat. 1; since there was slight change in urban imperviousness between 2001 to 2019, this result represents both the conditions. The second and third rows (Figure 4.5d-i) shows the model simulation for Cat. 2, for 2001 and 2019 conditions, respectively. The increasing impervious surface as shown in Figure 4.2b in Cat. 2 generate higher runoff and peak flood in 2019 as compared to 2001.

The maximum flooding rate from nodes and peak runoff from sub-catchments increases as the rainfall estimates change from lower, mean to upper bound of the Atlas 14 confidence intervals for both the catchments across time (Figure 4.5a-i). GI, sited within a sub-catchment, reduces the peak runoff from that sub-catchment, subsequently reducing pressure on downstream conduits. The optimization algorithm seeks a quantity and spatial distribution of GI across sub-catchments that minimizes the objectives.

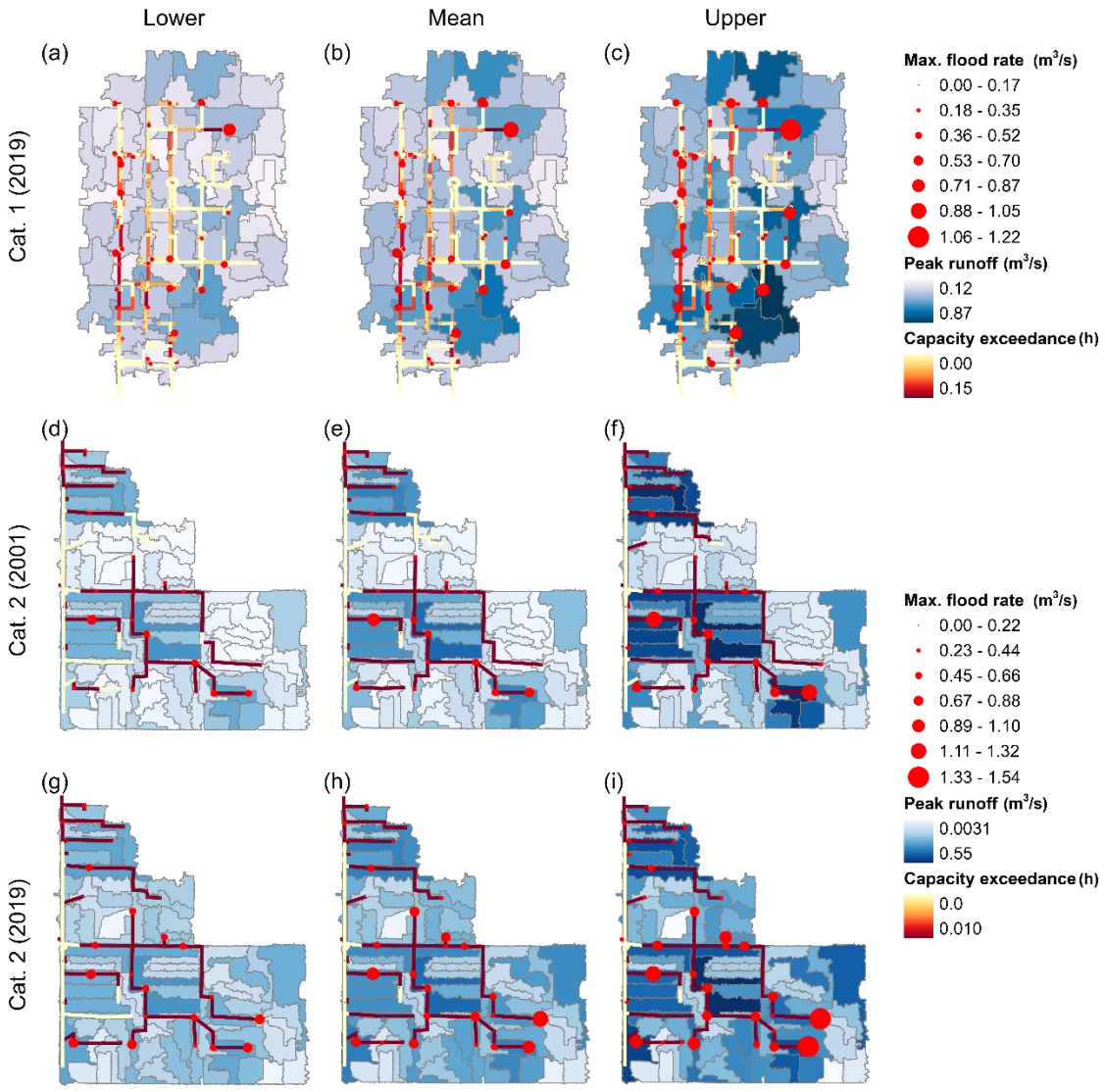

Figure 4.5. Pre-green Infrastructure Condition in Two Catchments as Simulated by SWMM Showing the Maximum Flood Rate from Flooded Junctions, Peak Runoff from Sub-catchments, and the Duration of Exceedance of Conduits' Capacity. The Year in Parentheses for Cat. 1 Refer to Imperviousness Conditions in 2019 (as well as for 2001) and for Cat. 2 Refer to 2001 or 2019.

4.3.1 Effects of Uncertainty in Design Precipitation Estimates

Figure 4.6a-i. illustrates the results of the multi-objective optimization and shows the Pareto optimal solutions. The black points are the non-dominated pareto optimal solution with 1st pareto front rank and grey points are the remaining dominated solutions. For Cat. 1, there is slight difference between imperviousness of 2001 and 2019, but for Cat. 2 there are significant difference (Figure 4.2a-b). Thus, result for the Cat. 1 include that of 2001 conditions (Figure 4.6a-c) (which represents 2019 condition too) and for Cat. 2 includes both the years (Figure 4.6d-i). The first column (Figure 4.6a,d,g) shows the results for the lower bound of the confidence interval of the design storm (referred to as lower estimate), the second column (Figure 4.6b,e,h) shows the result for mean value (referred to as mean estimate) and third column (Figure 4.6c,f,i) shows the result for upper bound of the confidence interval (referred to as upper estimate). For Cat. 1 (Figure 4.6a-c), the pareto front shifts upwards as we move from lower to upper bound of the Atlas 14 design rainfall estimates, indicating that achieving a given level of flood control comes at a higher cost. The cost of minimizing flooding using GI increases by 15% - 30% in from the lower to mean and mean to upper estimates. Figure 4.7 further illustrates this by showing the number of GI units required to mitigate flooding resulting from 5-year return period 45-min storm. The number of required bio-retentions (with unit area of 10 m^2) increases from 11,046 to 28,649 which is 0.11 km^2 to 0.28 km^2 while depending on the design standards from lower to upper bound of the Atlas 14 design rainfall estimates (Figure 4.7a-c). Similarly, the number of required green roofs (with unit area of 10 m^2) increases from 6,257 to 16,696 (in area: 0.06 km^2 to 0.16 km^2) (Figure 4.7d-f).

It should also be noted that the algorithm was able to prioritize the sub-catchments which are the likely source of flooding in Cat. 1 by adopting bio-retention or green roofs on those areas (Figure 4.5a-c and Figure 4.7a-f). Prioritizing these locations reduces the total cost and amount of GI required.

For Cat. 2, minimizing the peak flood is constrained by the availability of space, as only bio-retention was adopted due to only presence of residential building without flat roofs. This restriction resulted in higher residual flooding when mean and upper estimates were implemented (Figure 4.6e,f). When the lower end of the precipitation confidence interval is used, the flooding can be almost eliminated (Figure 4.6d). Here we see that within the confidence interval, different precipitation estimates could result in drastically different levels of flood risk and cost of flood mitigation. The pareto optimal solution showed drastically higher residual flooding for a given GI investment using lower to upper bound of the Atlas 14 design rainfall estimates (for both 2001 and 2019 conditions, Figure 4.6d-f and Figure 4.6g-i). Using the lower estimate, the same amount of least cost of GI investment, result in flood reduction to 2.2 m^3/s (Figure 4.6d) but using mean and upper estimates resulted in flood reduction potential only to 2.5 m^3/s (Figure 4.6e) and 7 m^3/s (Figure 4.6f). As using the lower, mean and upper estimates would require 6,377, 10,433 and 97,930 numbers (in area: 0.06 km^2, 0.1 km^2 and 0.90 km^2) of bio-retentions in 2001 condition. In 2019 condition it would require 50% - 100% more.

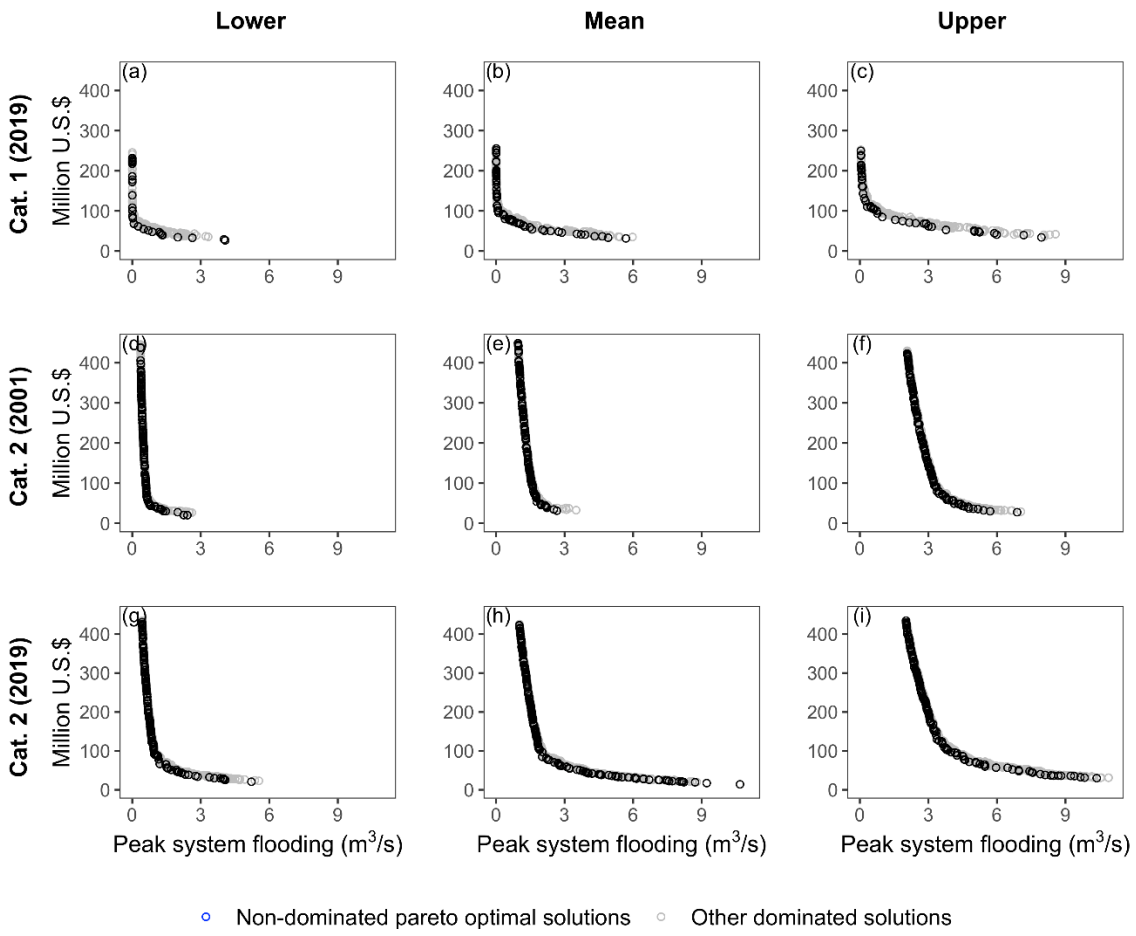

Figure 4.6. Pareto Optimal Solution for GI Installations to Reduce the Peak System Flooding in Two Catchments (at the Imperviousness Level of 2001 and 2019) Using Mean and Confidence Intervals (i.e. Lower and Upper Values) of the Atlas 14 Estimates. The Year in Parentheses for Cat. 1 Refer to Imperviousness Conditions in 2019 (as well as for 2001) and for Cat. 2 Refer to 2001 or 2019.

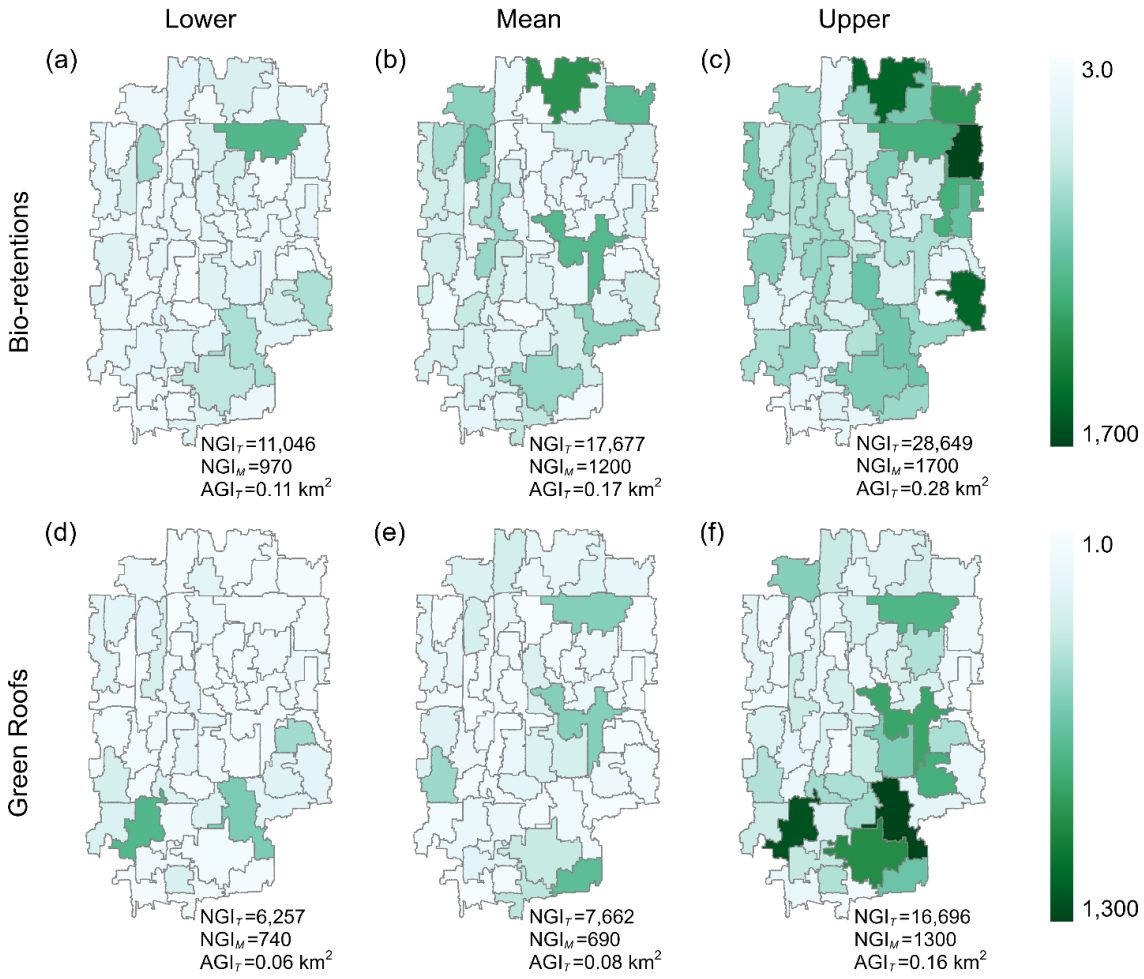

Figure 4.7. Optimal Configuration of GI (Bio-retentions and Green Roofs) at Least Possible Cost in Cat. 1 for Mitigating Peak Flooding. Panels Are Showing the Number of GI Required. NGI_T, NGI_M and AGI_T Refers to the Total Number, Maximum Number in Any of the Sub-catchments and Total Area of GI Required.

Similar, to Cat. 1, the optimization algorithm was able to target the sub-catchments that has the highest runoff or one which is at the proximity to the capacity constrained conduits and flooded nodes (Figure 4.5d-i and Figure 4.8a-f). The optimization algorithm allows bio-retention to be placed only in open space. Thus, in

absence of available space nearby sub-catchments are instead chosen for GI implementation. The cost of flood reduction in Cat. 2 is higher than in Cat. 1, primarily due to the lower amount of existing underground grey-infrastructure in Cat. 2 to convey stormwater and because the cost of bio-retention is 1.3 times that of green roofs. Most of the extended urban areas since 2001 or earlier around Cat. 2 in Phoenix do not have an extensive network of grey stormwater infrastructure, which presents another challenge in flood management. The analysis on optimal configuration due to change in imperviousness is presented next.

4.3.2 Effects of Changes in Urban Imperviousness

The increase in urban imperviousness results in two different patterns of catchment response in Cat. 2: an increase in the amount of flooding in previously flooded locations and flooding in the new locations as shown by the changes in the maximum flood rate and change in peak runoff in Figure 4.5d-i. The optimal GI configuration under these conditions as computed for two periods, shows that amount of investment required to mitigate the same amount of flooding in 2019 could be significantly higher than in 2001 (Figure 4.6d-i). For example, using the mean estimate for the design storm, the investment of $50 million could achieve the peak flood mitigation up-to 2 m^3/s (Figure 4.6e). However, under 2019 condition, the same investment could only achieve peak flood reduction to 4 m^3/s (Figure 4.6h). Figure 4.8 shows the number of GI installations (assuming a 10 m^2 area) required to reduce the flooding resulting from 5-year return period 45-min storm to 2 m^3/s. Note that under the given space constraint the full

mitigation of flooding is not possible here and result in residual flooding. The number of GI installations required to achieve the same level of flood reduction increases from 6,377 to 10,567 (using the lower estimate), 10,433 to 22,679 (using the mean estimate), and 97, 930 to 100,934 (using the upper estimate) from the 2001 to the 2019 land use (Figure 4.8). As the system receives more intense rainfall by moving from the lower to upper bound of rainfall estimates, the allowable capacity for GI reaches its limit and reducing flooding becomes more difficult even with higher GI investment. The effect of uncertainty from the confidence interval in 5-year return period rainfall estimate in optimal GI requirement is much larger compared to the effect of land use change that happened between 2001 and 2019.

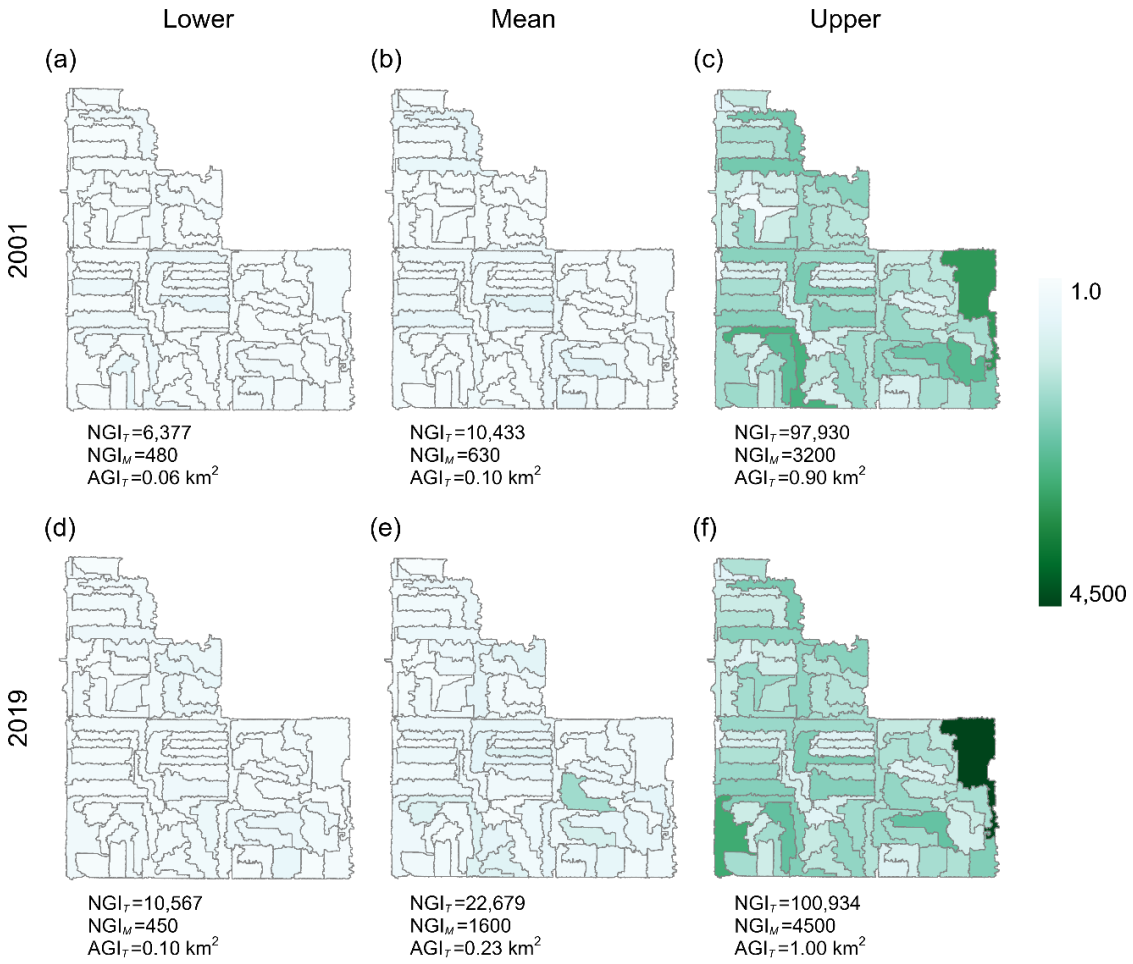

Figure 4.8. Optimal Configuration of GI (Bio-retentions) at Least Possible Cost in Cat. 1 for Reducing Peak Flooding to 2 m^3/s. Note: The Maximum Flood Reduction Possible is up-to 2 m^3/s given the Constraint and GI Configuration Options. Panels Are Showing the Number of GI Required. NGI_T, NGI_M and AGI_T Refers to the Total Number, Maximum Number in Any of the Sub-catchments and Total Area of GI Required.

4.3.3 Effects of Increasing Precipitation Estimates

As shown in section 4.3.1 the uncertainty in design precipitation estimate could result in significant variation in the amount of GI required, we further examined how the increase in precipitation depths by 5% to 50% will influence the GI configuration. The non-stationarities in climate could increase precipitation differently over the region. Although not specific to Phoenix, understanding how the relative increase in precipitation would require the different level of GI investment is necessary from planning perspective. Thus, the same model for Cat. 1 was utilized to examine how the optimal GI configuration change under the scenarios of rainfall depth increments by 5, 20, 25 and 50% from the mean value (of 5-year return period, 45 min storm) adopted thus far. Figure 4.9 shows the results of the optimization under four such rainfall scenarios. The current GI investment of little less than $100 million was required to mitigate the current Atlas 14 estimate of 5-year return period, 45 min storm (Figure 4.6b). With 5% increase in that rainfall estimate, up-to ~$110 million is required to fully mitigate the flooding (Figure 4.7a). With +10%, +25% and +50% increase in rainfall estimate, the required investment increases to $120, $150 and above $220 million (Figure 4.9b-d).

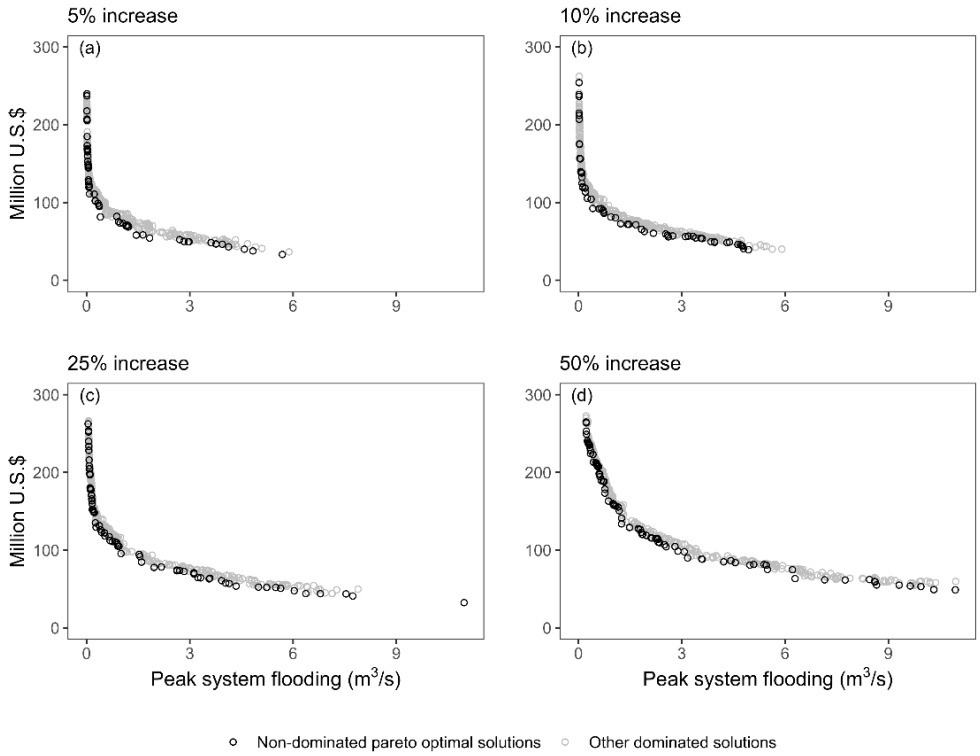

Figure 4.9. Pareto Optimal Solution for GI Installations to Reduce the Peak System Flooding under Four Stages of 5-year Return Period Rainfall Estimate Change (a) +5%, (b) +10%, (c) +25%, (d) +50%

4.4 Discussion

4.4.1 GI Design for Pluvial Flood Risk Management

The adaptable and modular nature of GI helps to mitigate pluvial flood risk that occur from frequent rainfall events, while also providing numerous co-benefits to the environment and society (Bell et al., 2019). Pluvial flood risks are higher in urban areas where benefits of GI are also high. The optimal benefits are sought by identifying GI configurations with optimal amount and spatial distribution within the catchment. The optimization algorithm in combination with a physically based hydrologic-hydraulic

model (e.g., SWMM) can search for global optimal solution that is optimally configured at least investment. Here, that search space is characterized by individual discretized sub-catchments. Consistent with recent work in arid catchments (Li & Burian, 2022), the results show that both increasing precipitation intensity and land change can worsen pluvial flooding. However, here we find that variation in design storm precipitation within the confidence interval for the 5-year, 45-min Atlas 14 storm has a greater impact than land use in a Phoenix catchment that experienced a median 30% increase in imperviousness. Note that Cat. 2 is located in one of the neighborhoods with the highest 2001-2019 increase in imperviousness (Figure 4.1) and that Phoenix is one of the large cities with the greatest increase in imperviousness in the U.S. over the same period (Table 4.1). This result highlights the importance of assessing the impact of precipitation uncertainty in stormwater design.

The approach presented here can be extended to larger catchments or to different category of spatial discretization such as the parcel or block. The objective of the optimization algorithm could also be revised to reflect alternate design or planning goals. The objective presented here is to minimize overall flooding in the system while controlling cost. Alternate objectives of enhancing infiltration or storage, removing runoff pollutants or prioritizing critical locations could warrant different configurations or new designs, which should be investigated further. Other uncertainties not studied here such as long-term performance variation and influence of micro-climatic variation on performance, could be an important future research which could inform different GI configuration or design choice. Future research should focus on the life-cycle cost,

benefit-cost ratio, net present value, and cost of delayed decision of implementing green infrastructure (Bernagros, Pankani, Struck, & Deerhake, 2021; DelGrosso, Hodges, & Dymond, 2019), if flexible planning approach is to be adopted (Eckart, Sieker, Vairavamoorthy, & Alsharif, 2012; Sieker, Helm, Krebs, Schlottmann, & Tränkner, 2008).

4.4.2 GI Adaptation Under Uncertainty

The current uncertainty in Atlas 14 estimates could result in a risk of over or under building stormwater capacity. If the mean estimate is chosen it could be over (under) building the system if the true 5-year event is indeed closer to the lower (upper) bound of the confidence interval. In terms of GI, this could result in 6,581 GI each of 10 m^2 or (0.08 km^2) being unnecessary if it is over built or facing functional failure if under built as shown for Cat. 1 in Figure 4.7. The risk of over and under building is comparatively higher for Cat. 2 as there is currently inadequate grey infrastructure (Figure 4.1b and Figure 4.8). This risk further augments when there is uncertainty of increase in urban imperviousness or land use change (Figure 4.8d-f).

However, the flexibility and modularity of GI reduces the risk of over or under design (Gilrein et al., 2019). Following the principles of flexible design, after initial GI is installed, additional modules may be added over time as warranted by changes in land use or by either changes in or mis-estimation of the design storm (De Neufville & Scholtes, 2011). As such these uncertainties are not barriers to GI adoption but an opportunity to identify the risk in design and construction and implement appropriate

adaptation strategies under uncertainty. Further, learning over time will reduce uncertainties with respect to design storm estimates and the impacts of climate change. For example, applying Bayesian learning to climate uncertainty over time can be used to inform planning strategies (Fletcher, Lickley, & Strzepek, 2019; Fletcher, Strzepek, Alsaati, & De Weck, 2019). A similar framework could be used to inform implementation of GI over time as part of a flexible planning approach.

The results (Figs 6-9) also illustrate that GI is not a panacea, particularly if high precipitation estimates are accurate or if short duration precipitation intensifies with climate change. The GI required to mitigate flooding for the high estimate of precipitation covers 0.44 km^2 or 27.5% of Cat. 1, and 0.9 km^2 or 56.3% of Cat. 2 with 2001 land use and 1.0 km^2 or 62.5% of Cat. 2 with 2019 land use. While technically feasible given the definition of free space used in the optimization routine (all land that is not street or building), this level of GI implementation is unrealistic practically due to other competing land uses. GI can be part of the solution; however, when the drainage system is significantly underbuilt, GI alone will often be insufficient. As presented in Figs. 6d-i the high cost of GI implementation in Cat. 2, GI is not a replacement for sufficient grey-infrastructure. Instead, the integration of grey-green infrastructure is needed, where GI can incrementally add capacity as needed.

4.4.3 Reflections to Other U.S. Cities

The confidence interval for Atlas 14 precipitation estimates, particularly for shorter storm duration relevant for stormwater infrastructure design, varies across cities.

Similarly, the change in imperviousness varies across and within cities. Understanding the historic city expansion and future probable direction for urban expansion, and uncertainty in design rainfall estimates helps the decision makers to understand risk of over or under building GI. Furthermore, future uncertainty due to climate change not incorporated in Atlas 14 estimates, will layer upon the uncertainty in current design rainfall estimates, further complicating the GI planning process. However, such effects will not be uniform across cities. We can conceptualize the dynamics brought into the urban context due to the combination of climate change and land use change into four typologies of change (Figure 4.10). The risk of drainage system functional failure is low in typology 1 and highest in typology 4. The two catchments presented here for Phoenix represent low and high change in urban imperviousness. Most of the other cities with higher Δ_I that are expanding outward experience both low (in the city core) and high (at satellite cities or suburbs) changes in imperviousness. Comparing between the variation in imperviousness (i.e., Typologies 1 vs. 3 or 2 vs. 4) the areas which experience high change in imperviousness (Typology 3 or 4) experience more complex challenge of optimal GI planning. This is particularly true for catchments that have highly permeable soils, the loss of which due to urban expansion, will result higher response to rainfall-runoff process. The majority of soils in Cat. 2 are Estrella loam and Antho sandy loam with moderate hydraulic conductivity in of 0.07 – 0.3 cm/hr (ADOT, 2014; USDA-NRCS, n.d.). A catchment with higher hydraulic conductivity would be expected to have a stronger response to changing imperviousness. The catchment topography, network geometry and capacity of the network will also play a role in shaping the response to both

precipitations change and land use change. This study also showed that higher variation in the precipitation estimate, which could be exacerbated by climate change, combined with relatively lower change in imperviousness (i.e., Typology 2) can have greater uncertainty compared to the catchment that experiences a higher change in imperviousness but a lower change in precipitation (i.e., Typology 3). Understanding where the catchment and cities are within the four typologies helps the planners and designers to understand the uncertainty and risk in planning.

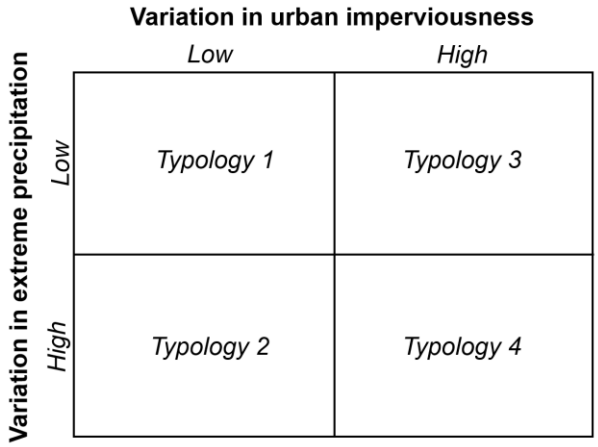

Figure 4.10. Dynamics of Change Occurring Across Cities That Will Potentially Influence GI Planning

4.5 Conclusions

This study investigated the impacts of precipitation uncertainty and land use change on the optimal configuration of GI by applying a coupled hydrologic-hydraulic model (SWMM) and an optimization algorithm (NSGA-II) in two study catchments in Phoenix, AZ. The GI configuration defined for this study select ideal type, optimize the

amount and spatial distribution of GI, where considered types include bio-retention and green roofs. Based on the results of this analysis, we present the following conclusions:

1. While both increasing precipitation intensity and land change can worsen pluvial flooding, variation in precipitation estimates within the confidence interval for the 5-year, 45-min storm Atlas 14 storm has a greater impact than land use in a Phoenix catchment that experienced a median 30% increase in imperviousness. This effect is sensitive to soil type, with catchments with higher soil hydraulic conductivity expected to display a stronger response to land use change. However, the results highlight the importance of considering precipitation uncertainty in stormwater design.
2. The uncertainty in design storm precipitation and the potential degree of near-term land use change (~20 years) collectively result in a wide range of optimal GI configurations. If designing a traditional grey-infrastructure system (i.e., stormwater conduits) this would present a significant risk of over or underbuilding. The risk highlights the benefit of the modular nature of GI, which can be incrementally deployed over time as land use conditions change or the best estimate of design storm precipitation is updated.
3. The results also show that GI is not a panacea and cannot mitigate all flooding impacts even within the Atlas 14 design storm confidence interval. This indicate that relying on GI to adapt to climate change driven increases in precipitation intensity may be beneficial but, alone, inadequate.

Limitations of this study point to the need for future research efforts. While this study placed the case of two Phoenix catchments in the context of land use trends and precipitation uncertainty in large U.S. cities broadly, further research should investigate the impact of local catchments characteristics on the effects found here. For example, soil properties, catchment topography, and urban form may all shape the nature and strength of the relationship between precipitation, land use change and pluvial flooding. Additionally, future efforts should evaluate life cycle costs and benefits, net present value, and cost of delayed action related to GI implementation. Lastly, the standard GI specification used in practice was used for this study. However, this should be compared against performance of GI practices in the field.

CHAPTER 5

CONCLUSION

5.1 Research Summary

This research is motivated by the challenges in urban flood management concerning both the scientific research and practical application. Limitations in data availability, gaps in data, and uncertainty in data are key precluding factors for reliable urban flood model construction, testing, deployment, knowledge generation, effective communication of flood risks, and adaptation decision making. Data limitations affect all sub-disciplines of hydrological studies, resulting in model structure, parameter and output uncertainty. As rainfall-runoff response time is shorter in urban catchments and flood impacts are localized, there is need to represent finer physical details and heterogeneity of catchment properties in physically based model, i.e., accurate estimation of flood response and hazard estimation, require higher resolution temporal (i.e., minutely precipitation) and spatial (i.e., 1-m terrain data such as DEM) data. This underscores the need to evaluate effects of stormwater infrastructure data completeness as a first step to develop methods for filling missing stormwater dataset. The nature of missing data exists in random order or distributed randomly across the catchment. Its effects in combination with resolution of model, on model accuracy or error, is less understood which motivated the chapter 2 of this dissertation.

Past efforts on flood management disproportionately focused fluvial and coastal flooding and less on pluvial flooding, in regard to flow or flood water level data collection efforts and flood assessments. Past flood damages in the pre-urbanized

watersheds are mainly concentrated in large rivers and floodplains. This historically resulted in data collection infrastructure primarily distributed along major river networks. Urbanization has increased the population at risk of pluvial flooding. However, the lack of hydrological data collection infrastructure in urban environment posed another major challenge for flood monitoring and model construction. There is an urgent need to streamline cost effective data collection infrastructure, utilizing the potential of novel data sources, into urban hydrological modeling. Although the concept of novel data application in hydrological application is not new, how such potential could be leveraged for large scale urban catchment, how it can be integrated into model development and testing process, and in general how to navigate its benefits for large urban catchment is less known. This challenge motivated chapter 3 of this dissertation.

Physically based hydrologic-hydraulic models are also useful infrastructure planning and adaptation tools. These models can be used to simulate hydrologic-hydraulic variables and compare system performance in a deterministic manner for various design parameters and to diagnose key drivers of differences in performance. The challenges mentioned above impede such application, and hence chapters 2 and 3 are precursor to advance stormwater modeling for adaptation decision making. In model-based stormwater infrastructure decision making, first, the accurate estimation of design rainfall is critical to ensure the design avoids critical functional failures. Second, the robustness of designed infrastructure (or adaptation strategies) is vital against external environmental change such as non-stationarities in precipitation or change in land use. The adaptation of existing stormwater infrastructure that need retrofit and replacement is

increasingly becoming costly, if not unfeasible. The motivation for selecting green infrastructure (GI) as the adaptation option is the current need of sustainable solutions in urban stormwater system. Despite of its flexible properties and multiple co-benefits, GI adoption is limited for catchment scale grey-green system integration. The current design precipitation estimates available for stormwater infrastructure design present range of uncertainties mainly for shorter duration precipitation. The designed system also endures consequences of changing land use. These challenges further motivate chapter 4.

In the following points the key findings and contributions of chapters 2-4 are summarized:

- In chapter 2, a two-part experiment was conducted to investigate the effects of missing attribute-values on model error, bias and accuracy in simulating flood duration and flooding flow rate, and the combined effect of missing stormwater features and model resolution on simulating accurate surface flood water level, extent and volume. The Monte Carlo sampling was applied to create realizations for randomness in amount and spatial distribution of missing attributes, done across three stormwater infrastructure related parameters. This experiment was extended to evaluate the effects of missing attribute-values at the upstream versus the downstream section of the network. The second experiment combines the missing features (i.e., 50% of ground truth data) or full ground truth data with high (i.e., 0.3-m DEM and 4.6-m mesh grid) or low (i.e., 9.7-m DEM and mesh grid) to investigate the effect on model's ability to simulate flood depth, extent and volume correctly. The selection of these DEM and mesh grid resolutions for

high- and low-resolution models is informed by the commonly and less commonly available DEM resolutions across the U.S. The study found the non-linear relationship between percent of missing data and model uncertainty and caution the modelers and practitioner to treat missing data differently for the attribute in question. In case where field survey is necessary prioritizing efforts and resources on downstream section of the network yield overall better model accuracy. Generally, the high-resolution model simulates higher flood depth (in this case close to real value) as oppose to low resolution model which simulates lower flood depth but higher flooded extent and volume. The model resolution and stormwater infrastructure feature data completeness further interact in simulating correct flooded location, extent and volume. The finding suggests that if the goal of urban flood modeling is to estimate correct flood depth which is essential for building flood protection structures then modelers should go for highest model resolution and also make sure the stormwater infrastructure is complete. For flood forecasting and communicating risks quickly, the lower resolution model should suffice. In the first part of the experiment the Monte Carlo sampling algorithm primarily developed to conduct random sampling experiment, can also be used for filling missing attribute-value data for large stormwater network. However, it depends on the parameter and its distribution.

- In chapter 3, a proof-of-concept for utilizing novel data to calibrate urban catchment scale hydrologic-hydraulic model was demonstrated. The observations using remotely sensed flood cameras generating image-based proxy flood water

level data and hydrograph; and citizen reported observed flood water level data were collected from experimental novel data collection infrastructure setup by *FloodAware* project. To improve the stormwater infrastructure data quality some of the missing conduits' attributes were filled using method developed in chapter 2. The construction of the model utilized the newest terrain properties data available to current date. Application of novel data might require additional novel approaches to integrate data into the modeling process. For the large-scale urban stormwater model, it is essential to identify key parameters to be calibrated but at the meantime capture the spatial heterogeneity of the parameters across the catchment. A statistical relationship between flooding flow rate simulated by SWMM 1D model and surface flood water depth simulated by SWMM 1D-2D model, was a novel approach implemented to convert the flooding flow rate into approximate surface water depth. The parameter grouping to reduce the size of parameter set was done before the auto-calibration using a genetic algorithm. Several key benefits of leveraging large scale novel data collection infrastructure was identified in this proof-of-concept study. The novel data sources have the potential to generate hydrological meaningful spatially distributed data in a cost-effective manner. This is a potential benefit of novel data sources over traditional in-situ sensor-based data collection system. The novel data was found to be useful in model construction as the pre-calibrated model was manually tested, and novel data observation guided identifying missing and misconfigured elements of the model. It informed a better understanding of the hydraulic processes in the

catchment. Novel data was useful in auto-calibration as it proved some improvement over pre-calibrated model. Some key features and limitation of other different novel data sources for urban flood monitoring and modeling is discussed in Table 5.1.

Table 5.1. Key Features and Limitations of Different Novel Data Sources in Urban Flood Model Development

Types of novel data sources	Type of observation possible	Value	Limitations
Traffic cameras	• Binary flood observation (wet or dry) • Water level • Possibility for flood area	• Provide continuous observation • Higher coverage over the catchment • Less data error and uncertainty	• Observations mostly limited to the street intersections • Field of view • Low light conditions
Surveillance camera	• Binary flood observation (wet or dry) • Water level • Possibility for flood area	• Provide continuous observation • Less data error and uncertainty	• Coverage and density depend on availability • Field of view • Low light conditions
Citizen science	• Binary flood observation (wet or dry) • Water level • Flow or velocity	• Mostly useful to report binary flood observation or water level • Do not require sophisticated data collection and processing	• Requires additional instruments for measurement for flow and velocity, instead of simple gauge • Special training might require • Single point data • Some data error and uncertainty on time stamp and magnitude of measurement
Social media mining	• Binary flood observation (wet or dry) • Water level (Image based)	• Estimation of flood damage	• Single point data • Data error and uncertainty on time stamp.

The two types of novel data sources, flood cameras and citizen science contribution, was tested in this proof-of-concept to measure flood water level on the overland surface and channels. The flood camera is the proxy to traffic cameras, while surveillance camera also requires the similar technology for data collection and processing. Citizen science and other forms of citizen-based observation such as social media (e.g. twitter) data mining are supplemental to camera-based observation due to limitation in data sparsity. Further study on how to maximize the potential uses of combination of such sources should be explored. A current version of the calibrated model (last updated on 15th March 2022) is now in use for real-time urban flood forecasting for the city of Flagstaff through FloodAware website (ASU/NAU, 2021). The method implemented in this chapter can be extended to re-calibrate the same model as more observations from novel data sources are collected. The chapter highlighted the need for the data collection infrastructure by leveraging existing data sources (e.g., traffic cameras) for efficient utilization in urban hydrological studies.

- In chapter 4, the effects on optimal configuration of green infrastructure for catchment scale flood management from uncertainty in design precipitation estimate and land use change was demonstrated. The multi-objective optimization approach coupled with a SWMM model identified the ideal location, amount and spatial distribution of green infrastructure. These optimal solutions varied significantly across the uncertainty or confidence interval of NOAA Atlas 14 rainfall estimates with cost of investment significantly increasing as rainfall

estimate was selected from lower to upper bound of the confidence interval. The increasing urban imperviousness demonstrated similar outcome. For a study catchment in Phoenix, effect of uncertainty in design rainfall estimate was found to be higher than the effect of change in urban imperviousness between 2001 and 2019. Such risks of over or under building could be same for any other type of stormwater infrastructure (e.g., grey infrastructure/stormwater conduits or detention tank). As the uncertainty in precipitation estimates exist across the U.S. and several of the most populated cities continue to develop land and expand horizontally, this chapter draws onto the challenge common across the cities. This chapter highlights the need for flexible planning process that embrace the uncertainty, as such green infrastructure are deployed over time as knowledge of best design estimate, or uncertainty in land use change or climate change is updated.

5.2 Future Research

This dissertation first addressed how the gaps in stormwater infrastructure data results in uncertainty in model outputs. Accurate and high precision urban stormwater models are of great uses for applications in flood assessment and adaptation planning. This study undertook a way to quantify and understand those uncertainty but also addressed how such infrastructure gaps can be filled particularly for large network with thousands of stormwater components. The study was limited to assessment of the gaps in attribute-values, but the future research should also investigate how the spatial

distribution of gaps in features (such as randomly missing section of conduits) create an uncertainty in model and importantly how to fill such missing gaps. An experimental analysis using an algorithm to randomly remove sections of network, then complete the missing gap (perhaps following the street layout which stormwater network closely follows) by creating polylines and object (that defines the conduits), supplemented by current algorithm to replace attribute-values would likely be a possible direction to extend this work. This has an added benefit of creating a stormwater network and model quickly in places where there is urgent need for urban flood assessment. An in-situ measurements for the amount of flow conveyed in the existing drainage network either through the measurement from sensor or novel data infrastructure could be an alternative way, as oppose to the ground truth created for Phoenix in this study due to this data limitation.

The proof-of-concept in leveraging novel data sources was found to be of great value in advancing urban flood modeling. It was demonstrated the benefits of novel data sources in constructing and testing model, as well as understanding the hydraulics in the catchment. For different urban catchments baseflow might be a contributing factor to urban flooding downstream, observation from novel data sources for extended period of time and rainfall-runoff relationship can further inform hydrological processes in different catchments. The current Flagstaff stormwater model was calibrated and validated with only a few observation points as demonstrated in chapter 3. Further validation of the model performance using the new observations and adding the capacity to periodically auto-(re)calibrate as new data are observed across the catchment would be

beneficial. Extending this work brings in a new set of important research questions: (1) How does using many spatially distributed flood observations (vs. a few observation) in model (re)calibration improves the predictive ability of the model? (2) How change in urban land surface over the years might result in different model parametrization? (3) How to address uncertainty in novel data accuracy that could arise from camera limitation (e.g., low light condition) or incorrect time stamp (e.g., delayed or incorrect reporting time by citizens)? The first question helps to guide the development of novel data infrastructure on how extensive the novel data observation network should be expanded both in coverage and density. The second question helps to frame the best management practice in model development as it will guide how often model should be re-calibrated, at the meantime investigate how flooding condition change with land use through observation. The third question is also an important one which investigate the effects of observed data uncertainty (particularly when the volume of novel data grows, and manual verification will be a tedious task) and develop a framework on how to mitigate it. The current novel data observation framework is based on the measurement of flood depth, future research should explore use of flooded extent. There is particularly an opportunity for this as future development in computational resources could allow faster runtime of two-dimensional models. These recommended future research direction helps to further advance the technology, framework and purposeful uses of novel data sources as the world is more connected than ever before, and infrastructure system are interconnected through “internet of things”. This certainly benefit in advancing pluvial

flood modeling, other types of flood modeling, and even different engineering and science disciplines where data availability is constrained.

This study demonstrated how the data uncertainty affects the modeling results and how it could affect the infrastructure planning. In the real world, at present and in future, stormwater managers and planners increasingly need to make decisions under uncertainty. The future research directions should be focused on: (1) understanding the uncertainties in long term performance efficiency of green infrastructure (GI) and (2) evaluate planning processes and frameworks that address uncertainties. The long-term efficiency of GI might vary across cities, urban forms and design. The role of micro-climate on GI efficiency, selection of vegetation, and clogging issues are important to be addressed. In-situ measurements of conductivity, infiltration, and change in porosity over time of the designed GI can further inform the optimal design, configuration, maintenance routine and operational cost. Future research protocol should also utilize the economic and engineering analysis tools for flexible infrastructure design (De Neufville & Scholtes, 2011), that can contribute to support GI planners.

REFERENCES

Abbott, M. B. (1999). The 3rd Danish Hydraulic Institute Software Conference within its sociotechnical context. *Journal of Hydroinformatics*, *1*(2), 139–141. https://doi.org/10.2166/hydro.1999.0012

Abebe, Y., Kabir, G., & Tesfamariam, S. (2018). Assessing urban areas vulnerability to pluvial flooding using GIS applications and Bayesian Belief Network model. *Journal of Cleaner Production*, *174*, 1629–1641. https://doi.org/10.1016/j.jclepro.2017.11.066

Acosta-Coll, M., Ballester-Merelo, F., Martinez-Peiró, M., & De la Hoz-Franco, E. (2018). Real-time early warning system design for pluvial flash floods—a review. *Sensors (Switzerland)*, *18*(7). https://doi.org/10.3390/s18072255

ACS. (n.d.). American Community Survey Data. Retrieved from https://www.census.gov/programs-surveys/acs/data.html

ADOT. (2014). *Highway Drainage Design Manual Volume 2 - Hydrology*. Arizona Department of Transportation 206 S. 17th Ave, Phoenix, AZ 85007.

Alves, A., Gersonius, B., Sanchez, A., Vojinovic, Z., & Kapelan, Z. (2018). Multi-criteria Approach for Selection of Green and Grey Infrastructure to Reduce Flood Risk and Increase CO-benefits. *Water Resources Management*, *32*(7), 2505–2522. https://doi.org/10.1007/s11269-018-1943-3

American Society of Civil Engineers. (1992). *Design and construction of urban stormwater management systems*. *American Society of Civil Engineers, Manuals and Reports on Engineering Practice*. https://doi.org/10.1061/9780872628557

Arnbjerg-Nielsen, K., Willems, P., Olsson, J., Beecham, S., Pathirana, A., Bülow Gregersen, I., … Nguyen, V. T. V. (2013). Impacts of climate change on rainfall extremes and urban drainage systems: A review. *Water Science and Technology*, *68*(1), 16–28. https://doi.org/10.2166/wst.2013.251

Arrighi, C., & Campo, L. (2019). Effects of digital terrain model uncertainties on high-resolution urban flood damage assessment. *Journal of Flood Risk Management*, *12*(December 2018), 1–12. https://doi.org/10.1111/jfr3.12530

ASFPM. (2020). *Urban Flood Hazards : Challenges and Opportunities*. Association of State Floodplain Managers, Stormwater Management Committee, 8301 Excelsior Dr., Madison, WI 53717 Phone:

Assumpção, T. H., Popescu, I., Jonoski, A., & Solomatine, D. P. (2018). Citizen observations contributing to flood modelling: Opportunities and challenges. *Hydrology and Earth System Sciences*, *22*(2), 1473–1489. https://doi.org/10.5194/hess-22-1473-2018

ASU/NAU. (2021). FloodAware. Retrieved from https://floodaware.net/

ASU. (2018). Metro Phoenix USGS LiDAR Data. Retrieved from https://asu.maps.arcgis.com/apps/webappviewer/index.html?id=0372792855514dd3bf9654c20bbe10e6

Balling, R. C., & Brazel, S. W. (1986). Diurnal Variations in Arizona Monsoon Precipitation Frequencies. *Monthly Weather Review*.

Barrington-Leigh, C., & Millard-Ball, A. (2015). A century of sprawl in the United States. *Proceedings of the National Academy of Sciences of the United States of America*, *112*(27), 8244–8249. https://doi.org/10.1073/pnas.1504033112

Bates, P. D., Marks, K. J., & Horritt, M. S. (2003). Optimal use of high-resolution topographic data in flood inundation models. *Hydrological Processes*, *17*(3), 537–557. https://doi.org/10.1002/hyp.1113

Bell, C. D., Spahr, K., Grubert, E., Stokes-Draut, J., Gallo, E., McCray, J. E., & Hogue, T. S. (2019). Decision Making on the Gray-Green Stormwater Infrastructure Continuum. *Journal of Sustainable Water in the Built Environment*, *5*(1), 04018016. https://doi.org/10.1061/jswbay.0000871

Benedict, M. A., & McMahon, E. T. (2002). Smart Conservation for the 21st Century. *Green Infrastructure*, *20*, 12–17. Retrieved from https://www.merseyforest.org.uk/files/documents/1365/2002+Green+Infrastructure+Smart+Conservation+for+the+21st+Century..pdf

Bermúdez, M., & Zischg, A. P. (2018). Sensitivity of flood loss estimates to building representation and flow depth attribution methods in micro-scale flood modelling. *Natural Hazards*, *92*(3), 1633–1648. https://doi.org/10.1007/s11069-018-3270-7

Bernagros, J. T., Pankani, D., Struck, S. D., & Deerhake, M. E. (2021). Estimating Regionalized Planning Costs of Green Infrastructure and Low-Impact Development Stormwater Management Practices: Updates to the US Environmental Protection Agency's National Stormwater Calculator. *Journal of Sustainable Water in the Built Environment*, *7*(2), 04020021. https://doi.org/10.1061/jswbay.0000934

Beven, K. (2019). How to make advances in hydrological modelling. *Hydrology Research*, *50*(6), 1481–1494. https://doi.org/10.2166/nh.2019.134

Bitew, M. M., & Gebremichael, M. (2011). Evaluation of satellite rainfall products through hydrologic simulation in a fully distributed hydrologic model. *Water Resources Research*, *47*(6), 1–11. https://doi.org/10.1029/2010WR009917

Blank, J., Deb, K., & Roy, P. C. (2019). Investigating the Normalization Procedure of NSGA-III. In K. Deb, E. Goodman, C. A. Coello Coello, K. Klamroth, K. Miettinen, S. Mostaghim, & P. Reed (Eds.), *Evolutionary Multi-Criterion Optimization* (pp. 229–240). Cham: Springer International Publishing.

Bonnin, G. M., Martin, D., Lin, B., Yekta, M., & Riley, D. (2006). *Precipitation-Frequency Atlas of the United States Volume I Version 4.0: Semiarid Southwest (Arizona, Southeast California, Nevada, New Mexico, Utah)* (Vol. 1). U.S. Department of Commerce National, National Oceanic and Atmospheric Administration, National Weather Service, Silver Spring, Maryland.

Boyle, D. P., Gupta, H. V., & Sorooshian, S. (2000). Toward improved calibration of hydrologic models: Combining the strengths of manual and automatic methods. *Water Resources Research*, *36*(12), 3663–3674. https://doi.org/10.1029/2000WR900207

Cannon, A., & Innocenti, S. (2018). Projected intensification of sub-daily and daily rainfall extremes in convection-permitting climate model simulations over North America: Implications for future Intensity–Duration–Frequency curves. *Natural Hazards and Earth System Sciences Discussions*, 1–29. https://doi.org/10.5194/nhess-2018-290

Cantone, J., & Schmidt, A. (2011). Improved understanding and prediction of the hydrologic response of highly urbanized catchments through development of the Illinois Urban Hydrologic Model. *Water Resources Research*, *47*(8), 1–16. https://doi.org/10.1029/2010WR009330

Carvalho, L. M. V. (2020). Assessing precipitation trends in the Americas with historical data: A review. *Wiley Interdisciplinary Reviews: Climate Change*, *11*(2), 1–21. https://doi.org/10.1002/wcc.627

Chang, T. J., Wang, C. H., & Chen, A. S. (2015). A novel approach to model dynamic flow interactions between storm sewer system and overland surface for different land covers in urban areas. *Journal of Hydrology*, *524*, 662–679. https://doi.org/10.1016/j.jhydrol.2015.03.014

Chester, M. V., & Allenby, B. (2019). Toward adaptive infrastructure: flexibility and agility in a non-stationarity age. *Sustainable and Resilient Infrastructure*, *4*(4), 173–191. https://doi.org/10.1080/23789689.2017.1416846

CHI. (n.d.). Sensitivity-based Radio Tuning Calibration (SRTC). Retrieved from https://support.chiwater.com/

Cho, J. H., & Seo, H. J. (2007). Parameter optimization of SWMM for runoff quantity and quality calculation in a eutrophic lake watershed using a genetic algorithm. *Water Supply*, *7*(5–6), 35–41. https://doi.org/10.2166/ws.2007.114

Choi, C., Berry, P., & Smith, A. (2021). The climate benefits, co-benefits, and trade-offs of green infrastructure: A systematic literature review. *Journal of Environmental Management*, *291*(January), 112583. https://doi.org/10.1016/j.jenvman.2021.112583

Chow, V. Te, Maidment, D. R., & Mays, L. W. (1998). *Applied Hydrology*.

Chow, V. T. (1959). Open channel hydraulics, McGraw-Hill, New York.

City of Flagstaff. (n.d.). City of Flagstaff GIS Open Data Portal. Retrieved from https://gis.flagstaffaz.gov/portal/apps/sites/#/opendata

City of Phoenix. (2013). *Storm Water Policies and Standards*.

D. N. Moriasi, J. G. Arnold, M. W. Van Liew, R. L. Bingner, R. D. Harmel, & T. L. Veith. (2007). Model Evaluation Guidelines for Systematic Quantification of Accuracy in Watershed Simulations. *Transactions of the ASABE*, *50*(3), 885–900. https://doi.org/10.13031/2013.23153

Davids, J. C., van de Giesen, N., & Rutten, M. (2017). Continuity vs. the Crowd—Tradeoffs Between Continuous and Intermittent Citizen Hydrology Streamflow Observations. *Environmental Management*, *60*(1), 12–29. https://doi.org/10.1007/s00267-017-0872-x

Dawson, R. J., Speight, L., Hall, J. W., Djordjevic, S., Savic, D., & Leandro, J. (2008). Attribution of flood risk in urban areas. *Journal of Hydroinformatics*, *10*(4), 275–288.

De Neufville, R., & Scholtes, S. (2011). *Flexibility in engineering design*. MIT Press.

Deb, K., Pratap, A., Agarwal, S., & Meyarivan, T. (2002). A fast and elitist multiobjective genetic algorithm: NSGA-II. *IEEE Transactions on Evolutionary Computation*, *6*(2), 182–197. https://doi.org/10.1109/4235.996017

DelGrosso, Z. L., Hodges, C. C., & Dymond, R. L. (2019). Identifying Key Factors for Implementation and Maintenance of Green Stormwater Infrastructure. *Journal of Sustainable Water in the Built Environment*, *5*(3), 05019002. https://doi.org/10.1061/jswbay.0000878

Dent, S., Hanna, R. B., & Wright, L. T. (2004). Automated Calibration using Optimization Techniques with SWMM RUNOFF. *Journal of Water Management Modeling*, *6062*. https://doi.org/10.14796/jwmm.r220-18

Dolowitz, D. P., Bell, S., & Keeley, M. (2018). Retrofitting urban drainage infrastructure: green or grey? *Urban Water Journal*, *15*(1), 83–91. https://doi.org/10.1080/1573062X.2017.1396352

Dottori, F., Di Baldassarre, G., & Todini, E. (2013). Detailed data is welcome, but with a pinch of salt: Accuracy, precision, and uncertainty in flood inundation modeling. *Water Resources Research*, *49*(9), 6079–6085. https://doi.org/10.1002/wrcr.20406

Eckart, J., Sieker, H., Vairavamoorthy, K., & Alsharif, K. (2012). Flexible design of urban drainage systems: Demand led research for Hamburg-Wilhelmsburg. *Reviews in Environmental Science and Biotechnology*, *11*(1), 5–10. https://doi.org/10.1007/s11157-011-9256-5

Elliott, A. H., Trowsdale, S. A., & Wadhwa, S. (2009). Effect of Aggregation of On-Site Storm-Water Control Devices in an Urban Catchment Model. *Journal of Hydrologic Engineering*, *14*(9), 975–983. https://doi.org/10.1061/(ASCE)HE.1943-5584.0000064

Endreny, T. A. (2005). *Land Use and Land Cover Effects on Runoff Processes: Urban and Suburban Development*. *Encyclopedia of Hydrological Sciences*. https://doi.org/10.1002/0470848944.hsa122

Etter, S., Strobl, B., van Meerveld, I., & Seibert, J. (2020). Quality and timing of crowd-based water level class observations. *Hydrological Processes*, *34*(22), 4365–4378. https://doi.org/10.1002/hyp.13864

Farris, S., Deidda, R., Viola, F., & Mascaro, G. (2021). On the Role of Serial Correlation and Field Significance in Detecting Changes in Extreme Precipitation Frequency. *Water Resources Research*, *57*(11). https://doi.org/10.1029/2021wr030172

FCDMC. (n.d.). Report a Flood. Retrieved from https://gis.maricopa.gov/reportaflood/map.html

Festing, H., Copp, C., Sprague, H., Wolf, D., Shorofsky, B., & Nichols, K. (2014). *The Prevalence and Cost of Urban Flooding: A Case Study of Cook County, IL*. Retrieved from http://www.cnt.org/news/2013/05/14/urban-flooding-is-chronic-and-costly-but-not-correlated-with-floodplains/

Fewtrell, T. J., Bates, P. ., Horritt, M., & Hunter, N. M. (2008). Evaluating the effect of scale in flood inundation modelling in urban environments. *Hydrol. Process*, *22*(November 2008), 5107–5118. https://doi.org/10.1002/hyp

Fewtrell, Timothy J., Duncan, A., Sampson, C. C., Neal, J. C., & Bates, P. D. (2011). Benchmarking urban flood models of varying complexity and scale using high resolution terrestrial LiDAR data. *Physics and Chemistry of the Earth*, *36*(7–8), 281–291. https://doi.org/10.1016/j.pce.2010.12.011

Finney, K, James, R., & Perera, N. (2012). Benchmarking SWMM5/PCSWMM 2D Model Performance. In *International Conference on Water Management Modeling*. ON.

Finney, Karen, & Gharabaghi, B. (2011). Using the PCSWMM 2010 SRTC Tool to Design a Compost Biofilter for Highway Stormwater Runoff Treatment. *Journal of Water Management Modeling*, *6062*, 157–166. https://doi.org/10.14796/jwmm.r241-09

First Street Foundation. (2020). The First National Flood Risk Assessment. Defining America's Growing Risk, 1–163. Retrieved from https://assets.firststreet.org/uploads/2020/06/first_street_foundation__first_national_flood_risk_assessment.pdf

Fletcher, S., Lickley, M., & Strzepek, K. (2019). Learning about climate change uncertainty enables flexible water infrastructure planning. *Nature Communications*, *10*(1), 1–11. https://doi.org/10.1038/s41467-019-09677-x

Fletcher, S., Strzepek, K., Alsaati, A., & De Weck, O. (2019). Learning and flexibility for water supply infrastructure planning under groundwater resource uncertainty. *Environmental Research Letters*, *14*(11), 114022. https://doi.org/10.1088/1748-9326/ab4664

Fox, C., Levitin, A., & Redman, T. (1994). The notion of data and its quality dimensions. *Information Processing and Management*, *30*(1), 9–19. https://doi.org/10.1016/0306-4573(94)90020-5

Gaffin, S. R., Rosenzweig, C., & Kong, A. Y. Y. (2012). Adapting to climate change through urban green infrastructure. *Nature Climate Change*, *2*(10), 704–704. https://doi.org/10.1038/nclimate1685

Gallegos, H. A., Schubert, J. E., & Sanders, B. F. (2009). Two-dimensional, high-resolution modeling of urban dam-break flooding: A case study of Baldwin Hills, California. *Advances in Water Resources*, *32*(8), 1323–1335. https://doi.org/10.1016/j.advwatres.2009.05.008

Gao, X., Yang, Z., Han, D., Huang, G., & Zhu, Q. (2020). A Framework for Automatic Calibration of SWMM Considering Input Uncertainty, (August), 1–25.

Gilrein, E. J., Carvalhaes, T. M., Markolf, S. A., Chester, M. V, Allenby, B. R., & Garcia, M. (2019). Concepts and practices for transforming infrastructure from rigid to adaptable. *Sustainable and Resilient Infrastructure*, *0*(0), 1–22. https://doi.org/10.1080/23789689.2019.1599608

Golden, H. E., & Hoghooghi, N. (2018). Green infrastructure and its catchment-scale effects: an emerging science. *WIREs Water*, *5*(1), 1–14. https://doi.org/10.1002/wat2.1254

Guo, K., Guan, M., & Yu, D. (2020). Urban surface water flood modelling – a comprehensive review of current models and future challenges. *Hydrology and Earth System Sciences Discussions*, (December), 1–27. https://doi.org/10.5194/hess-2020-655

Guo, Y. (2001). Hydrologic design of urban flood control detention ponds. *Journal of Hydrologic Engineering*, *6*(6), 472–479.

Guptill, S. C., & Morrison, J. L. (1995). Elements of spatial data quality. *Elements of Spatial Data Quality*. https://doi.org/10.1016/s0098-3004(97)87525-5

Hall, J. W., Sayers, P. B., & Dawson, R. J. (2005). National-scale assessment of current and future flood risk in England and Wales. *Natural Hazards*, *36*(1–2), 147–164. https://doi.org/10.1007/s11069-004-4546-7

Harvey, R., de Lange, M., McBean, E., Trenouth, W., Singh, A., & James, P. (2017). Asset condition assessment of municipal drinking water, wastewater and stormwater systems–Challenges and directions forward. *Canadian Water Resources Journal*, *42*(2), 138–148. https://doi.org/10.1080/07011784.2016.1224684

Helmrich, A. M., Ruddell, B. L., Bessem, K., Chester, M. V., Chohan, N., Doerry, E., … Zahura, F. T. (2021). Opportunities for crowdsourcing in urban flood monitoring. *Environmental Modelling and Software*, *143*, 105124. https://doi.org/10.1016/j.envsoft.2021.105124

Henonin, J., Russo, B., Mark, O., & Gourbesville, P. (2013). Real-time urban flood forecasting and modelling - A state of the art. *Journal of Hydroinformatics*, *15*(3), 717–736. https://doi.org/10.2166/hydro.2013.132

Hereford, R. (2015). Climate Variation at Flagstaff , Arizona--1950 to 2007 Prepared in Cooperation with Effects of Climate Variability and Land Use on Dynamics Program Climate Variation at Flagstaff , Arizona — 1950 to 2007 By Richard Hereford, (September).

Hjelmstad, A., Shrestha, A., Garcia, M., & Mascaro, G. (2021). Propagation of radar rainfall uncertainties into urban pluvial flood modeling during the North American monsoon. *Hydrological Sciences Journal*, null-null. https://doi.org/10.1080/02626667.2021.1980216

Holland, J. H. (1992). *Adaptation in natural and artificial systems: an introductory analysis with applications to biology, control, and artificial intelligence*. MIT press.

Horritt, M. S. (2006). A methodology for the validation of uncertain flood inundation models. *Journal of Hydrology*, *326*(1–4), 153–165. https://doi.org/10.1016/j.jhydrol.2005.10.027

Hossain Anni, A., Cohen, S., & Praskievicz, S. (2020). Sensitivity of urban flood simulations to stormwater infrastructure and soil infiltration. *Journal of Hydrology*, *588*(May). https://doi.org/10.1016/j.jhydrol.2020.125028

Hosseinzadehtalaei, P., Tabari, H., & Willems, P. (2020). Climate change impact on short-duration extreme precipitation and intensity–duration–frequency curves over Europe. *Journal of Hydrology*, *590*(March), 125249. https://doi.org/10.1016/j.jhydrol.2020.125249

Houdeshel, C. D., Pomeroy, C. A., & Hultine, K. R. (2012). Bioretention Design for Xeric Climates Based on Ecological Principles. *Journal of the American Water Resources Association*, *48*(6), 1178–1190. https://doi.org/10.1111/j.1752-1688.2012.00678.x

Jain, H., & Deb, K. (2014). An evolutionary many-objective optimization algorithm using reference-point based nondominated sorting approach, Part II: Handling constraints and extending to an adaptive approach. *IEEE Transactions on Evolutionary Computation*, *18*(4), 602–622. https://doi.org/10.1109/TEVC.2013.2281534

James, R., Finney, K., Perera, N., James, B., & Peyron, N. (2013). SWMM5/PCSWMM Integrated 1D-2D Modeling. In U. E. (retired); M. B. J. A.S. Donigian, AQUA TERRA Consultants; Richard Field (Ed.), *Fifty Years Of Watershed Modeling - Past, Present And Future*. ECI Symposium Series. http://dc.engconfintl.org/watershed/12. Retrieved from http://dc.engconfintl.org/watershed/12

James, W. (2003). Rules for responsible modeling. CHI Guelph, Ontario.

James, W., Rossman, L. A., & James, W. R. C. (2010). *User's guide to SWMM5 13th Edition*.

Jha, A. K., Bloch, R., & Lamond, J. (2012). *Cities and Flooding A Guide to Integrated Urban Flood Risk Management for the 21st Century*. *The World Bank* (Vol. 8). The World Bank, 1818 H Street NW, Washington, DC 20433, USA: The World Bank. https://doi.org/10.1596/978-0-8213-8866-2

Jiang, Y., Zevenbergen, C., & Ma, Y. (2018). Urban pluvial flooding and stormwater management: A contemporary review of China's challenges and "sponge cities" strategy. *Environmental Science and Policy*, *80*(September 2017), 132–143. https://doi.org/10.1016/j.envsci.2017.11.016

Jung, I. W., Chang, H., & Moradkhani, H. (2011). Quantifying uncertainty in urban flooding analysis considering hydro-climatic projection and urban development effects. *Hydrology and Earth System Sciences*, *15*(2), 617–633. https://doi.org/10.5194/hess-15-617-2011

Kabisch, N., Korn, H., Stadler, J., & Bonn, A. (2017). *Nature-based solutions to climate change adaptation in urban areas: Linkages between science, policy and practice*. Springer Nature.

Kişi, O., Ali Baba, A. P., & Shiri, J. (2012). Generalized Neurofuzzy Models for Estimating Daily Pan Evaporation Values from Weather Data. *Journal of Irrigation and Drainage Engineering*, *138*(4), 349–362. https://doi.org/10.1061/(asce)ir.1943-4774.0000403

Krebs, G., Kokkonen, T., Valtanen, M., Koivusalo, H., & Setälä, H. (2013). A high resolution application of a stormwater management model (SWMM) using genetic parameter optimization. *Urban Water Journal*, *10*(6), 394–410. https://doi.org/10.1080/1573062X.2012.739631

Krebs, G., Kokkonen, T., Valtanen, M., Setälä, H., & Koivusalo, H. (2014). Spatial resolution considerations for urban hydrological modelling. *Journal of Hydrology*, *512*, 482–497. https://doi.org/10.1016/j.jhydrol.2014.03.013

Kumar, S., Guntu, R. K., Agarwal, A., Villuri, V. G. K., Pasupuleti, S., Kaushal, D. R., … Bronstert, A. (2022). Multi-objective optimization for stormwater management by green-roofs and infiltration trenches to reduce urban flooding in central Delhi. *Journal of Hydrology*, *606*(May 2021), 127455. https://doi.org/10.1016/j.jhydrol.2022.127455

Kunkel, K. E., Karl, T. R., Squires, M. F., Yin, X., Stegall, S. T., & Easterling, D. R. (2020). Precipitation extremes: Trends and relationships with average precipitation and precipitable water in the contiguous United States. *Journal of Applied Meteorology and Climatology*, *59*(1), 125–142. https://doi.org/10.1175/JAMC-D-19-0185.1

Kuriqi, A., & Hysa, A. (2021). Multidimensional Aspects of Floods: Nature-Based Mitigation Measures from Basin to River Reach Scale (pp. 1–23). Berlin, Heidelberg: Springer Berlin Heidelberg. https://doi.org/10.1007/698_2021_773

Le Coz, J., Patalano, A., Collins, D., Guillén, N. F., García, C. M., Smart, G. M., … Braud, I. (2016). Crowdsourced data for flood hydrology: Feedback from recent citizen science projects in Argentina, France and New Zealand. *Journal of Hydrology*, *541*, 766–777. https://doi.org/10.1016/j.jhydrol.2016.07.036

Leandro, J., Djordjević, S., Chen, A. S., Savić, D. A., & Stanić, M. (2011). Calibration of a 1D/1D urban flood model using 1D/2D model results in the absence of field data. *Water Science and Technology, 64*(5), 1016–1024. https://doi.org/10.2166/wst.2011.467

Leandro, Jorge, Chen, A. S., Djordjević, S., & Savić, D. A. (2009). Comparison of 1D/1D and 1D/2D coupled (sewer/surface) hydraulic models for urban flood simulation. *Journal of Hydraulic Engineering*, *135*(6), 495–504. https://doi.org/10.1061/(ASCE)HY.1943-7900.0000037

Leandro, Jorge, & Martins, R. (2016). A methodology for linking 2D overland flow models with the sewer network model SWMM 5.1 based on dynamic link libraries. *Water Science and Technology*, *73*(12), 3017–3026. https://doi.org/10.2166/wst.2016.171

Leitão, J. P., Boonya-aroonnet, S., Prodanović, D., & Maksimović, Č. (2009). The influence of digital elevation model resolution on overland flow networks for modelling urban pluvial flooding. *Water Science and Technology*, *60*(12), 3137–3149. https://doi.org/10.2166/wst.2009.754

Leitão, J. P., & de Sousa, L. M. (2018). Towards the optimal fusion of high-resolution Digital Elevation Models for detailed urban flood assessment. *Journal of Hydrology*, *561*(December 2017), 651–661. https://doi.org/10.1016/j.jhydrol.2018.04.043

Leitão, João P., Peña-Haro, S., Lüthi, B., Scheidegger, A., & Moy de Vitry, M. (2018). Urban overland runoff velocity measurement with consumer-grade surveillance cameras and surface structure image velocimetry. *Journal of Hydrology*, *565*(September), 791–804. https://doi.org/10.1016/j.jhydrol.2018.09.001

Leitão, Joo P., Moy De Vitry, M., Scheidegger, A., & Rieckermann, J. (2016). Assessing the quality of digital elevation models obtained from mini unmanned aerial vehicles for overland flow modelling in urban areas. *Hydrology and Earth System Sciences*, *20*(4), 1637–1653. https://doi.org/10.5194/hess-20-1637-2016

Leitold, R., Garschagen, M., Tran, V., & Revilla Diez, J. (2021). Flood risk reduction and climate change adaptation of manufacturing firms: Global knowledge gaps and lessons from Ho Chi Minh City. *International Journal of Disaster Risk Reduction*, *61*(May), 102351. https://doi.org/10.1016/j.ijdrr.2021.102351

Leutnant, D., Döring, A., & Uhl, M. (2019). swmmr - an R package to interface SWMM. *Urban Water Journal*, *16*(1), 68–76. https://doi.org/10.1080/1573062X.2019.1611889

Li, J., & Burian, S. J. (2022). Effects of Nonstationarity in Urban Land Cover and Rainfall on Historical Flooding Intensity in a Semiarid Catchment. *Journal of Sustainable Water in the Built Environment*, *8*(2), 1–12. https://doi.org/10.1061/jswbay.0000978

Lopez-Cantu, T., & Samaras, C. (2018). Temporal and spatial evaluation of stormwater engineering standards reveals risks and priorities across the United States. *Environmental Research Letters*, *13*(7). https://doi.org/10.1088/1748-9326/aac696

Lowry, C. S., Fienen, M. N., Hall, D. M., & Stepenuck, K. F. (2019). Growing pains of crowdsourced stream stage monitoring using mobile phones: The development of crowdhydrology. *Frontiers in Earth Science*, *7*(May), 1–10. https://doi.org/10.3389/feart.2019.00128

Lyu, H., Ni, G., Cao, X., Ma, Y., & Tian, F. (2018). Effect of temporal resolution of rainfall on simulation of urban flood processes. *Water (Switzerland)*, *10*(7). https://doi.org/10.3390/w10070880

Mailhot, A., & Duchesne, S. (2010). Design Criteria of Urban Drainage Infrastructures under Climate Change. *Journal of Water Resources Planning and Management*, *136*(2), 201–208. https://doi.org/10.1061/(asce)wr.1943-5452.0000023

Manocha, N., & Babovic, V. (2017). Development and valuation of adaptation pathways for storm water management infrastructure. *Environmental Science and Policy*, *77*(1), 86–97. https://doi.org/10.1016/j.envsci.2017.08.001

Manso, M., Teotónio, I., Silva, C. M., & Cruz, C. O. (2021). Green roof and green wall benefits and costs: A review of the quantitative evidence. *Renewable and Sustainable Energy Reviews*, *135*(November 2019). https://doi.org/10.1016/j.rser.2020.110111

Mark, O., Weesakul, S., Apirumanekul, C., Aroonnet, S. B., & Djordjević, S. (2004). Potential and limitations of 1D modelling of urban flooding. *Journal of Hydrology*, *299*(3–4), 284–299. https://doi.org/10.1016/j.jhydrol.2004.08.014

Markus, M., Angel, J. R., Yang, L., & Hejazi, M. I. (2007). Changing estimates of design precipitation in Northeastern Illinois: Comparison between different sources and sensitivity analysis. *Journal of Hydrology*, *347*(1–2), 211–222. https://doi.org/10.1016/j.jhydrol.2007.09.024

Martínez-Solano, F. J., Iglesias-Rey, P. L., Saldarriaga, J. G., & Vallejo, D. (2016). Creation of an SWMM toolkit for its application in urban drainage networks optimization. *Water (Switzerland)*, *8*(6), 1–16. https://doi.org/10.3390/w8060259

Martínez, C., Sanchez, A., Toloh, B., & Vojinovic, Z. (2018). Multi-objective Evaluation of Urban Drainage Networks Using a 1D/2D Flood Inundation Model. *Water*

Resources Management, *32*(13), 4329–4343. https://doi.org/10.1007/s11269-018-2054-x

Mascaro, G. (2017). Multiscale spatial and temporal statistical properties of rainfall in central Arizona. *Journal of Hydrometeorology*, *18*(1), 227–245. https://doi.org/10.1175/JHM-D-16-0167.1

Mascaro, G. (2018). On the distributions of annual and seasonal daily rainfall extremes in central Arizona and their spatial variability. *Journal of Hydrology*, *559*, 266–281. https://doi.org/10.1016/j.jhydrol.2018.02.011

Mascaro, G. (2020). Comparison of Local, Regional, and Scaling Models for Rainfall Intensity–Duration–Frequency Analysis. *Journal of Applied Meteorology and Climatology*, *59*(9), 1519–1536. https://doi.org/10.1175/JAMC-D-20-0094.1

Miguez, M. G., & Veról, A. P. (2017). A catchment scale Integrated Flood Resilience Index to support decision making in urban flood control design. *Environment and Planning B: Urban Analytics and City Science*, *44*(5), 925–946. https://doi.org/10.1177/0265813516655799

Mike, D. H. I. (2009). Flow Model: Hydrodynamic Module Scientific Documentation. *MIKE by DHI*.

Mikelonis, A., Boe, T., Calfee, W., & Don Lee, S. (2018). Urban fate and transport modeling of contaminants: The unique needs of emergency response and the potential for adapting existing models. *Journal of Water Management Modeling*, *2018*, 1–7. https://doi.org/10.14796/JWMM.C447

Moftakhari, H. R., AghaKouchak, A., Sanders, B. F., Allaire, M., & Matthew, R. A. (2018). What Is Nuisance Flooding? Defining and Monitoring an Emerging Challenge. *Water Resources Research*, *54*(7), 4218–4227. https://doi.org/10.1029/2018WR022828

Moftakhari, H. R., AghaKouchak, A., Sanders, B. F., Feldman, D. L., Sweet, W., Matthew, R. A., & Luke, A. (2015). Increased nuisance flooding due to sea-level rise: past and future. *Geophysical Research Letters*, *42*, 9846–9852. https://doi.org/10.1002/2015GL066072

Montalto, F. A., Behr, C. T., & Yu, Z. (2011). Accounting for uncertainty in determining green infrastructure cost-effectiveness. *Economic Incentives for Stormwater Control*, *246*.

Moy De Vitry, M., Dicht, S., & Leitão, J. P. (2017). FloodX: Urban flash flood experiments monitored with conventional and alternative sensors. *Earth System Science Data*, *9*(2), 657–666. https://doi.org/10.5194/essd-9-657-2017

Moy de Vitry, M., & Leitão, J. P. (2020). The potential of proxy water level measurements for calibrating urban pluvial flood models. *Water Research*, *175*. https://doi.org/10.1016/j.watres.2020.115669

MRLC. (n.d.). Urban Imperviousness. Retrieved from https://www.mrlc.gov/data

Mwiya, R. M., Zhang, Z., Zheng, C., & Wang, C. (2020). Comparison of approaches for irrigation scheduling using AquaCrop and NSGA-III models under climate uncertainty. *Sustainability (Switzerland)*, *12*(18). https://doi.org/10.3390/su12187694

Nanía, L. S., León, A. S., & García, M. H. (2015). Hydrologic-Hydraulic Model for Simulating Dual Drainage and Flooding in Urban Areas: Application to a Catchment in the Metropolitan Area of Chicago. *Journal of Hydrologic Engineering*, *20*(5), 04014071. https://doi.org/10.1061/(asce)he.1943-5584.0001080

Nardi, F., Cudennec, C., Abrate, T., Allouch, C., Annis, A., Assumpção, T., … Grimaldi, S. (2021). Citizens AND HYdrology (CANDHY): conceptualizing a transdisciplinary framework for citizen science addressing hydrological challenges. *Hydrological Sciences Journal*, *00*(00), 1–18. https://doi.org/10.1080/02626667.2020.1849707

Nicklin, H., Leicher, A. M., Dieperink, C., & Van Leeuwen, K. (2019). Understanding the costs of inaction-An assessment of pluvial flood damages in two European cities. *Water (Switzerland)*, *11*(4), 1–18. https://doi.org/10.3390/w11040801

Nieuwenhuijsen, M. J. (2020). Green Infrastructure and Health. *Annual Review of Public Health*, *42*, 317–328. https://doi.org/10.1146/annurev-publhealth-090419-102511

Nithila Devi, N., Sridharan, B., & Kuiry, S. N. (2019). Impact of urban sprawl on future flooding in Chennai city, India. *Journal of Hydrology*, *574*(April), 486–496. https://doi.org/10.1016/j.jhydrol.2019.04.041

NOAA/NWS. (n.d.). NOAA Atlas 14 Point Precipitation Frequency Estimates: KS. Retrieved from https://hdsc.nws.noaa.gov/hdsc/pfds/pfds_map_cont.html

Noh, S. J., Lee, J. H., Lee, S., Kawaike, K., & Seo, D. J. (2018). Hyper-resolution 1D-2D urban flood modelling using LiDAR data and hybrid parallelization. *Environmental Modelling and Software*, *103*, 131–145. https://doi.org/10.1016/j.envsoft.2018.02.008

NSSL. (n.d.). Multi-Radar/Multi-Sensor System (MRMS). Retrieved from https://www.nssl.noaa.gov/projects/mrms/

NWS. (n.d.-a). Northern Arizona Event Summaries. Retrieved from https://www.weather.gov/fgz/EventSummaries

NWS. (n.d.-b). Turn Around Don't Drown. Retrieved from https://www.weather.gov/tsa/hydro_tadd

NWS. (2014). Record rainfall & widespread flooding across Phoenix Metro Area. Retrieved from https://www.wrh.noaa.gov/psr/pns/2014/September/Sep8Flooding.php

O'Donnell, E. C., Lamond, J. E., & Thorne, C. R. (2017). Recognising barriers to implementation of Blue-Green Infrastructure: a Newcastle case study. *Urban Water Journal*, *14*(9), 964–971. https://doi.org/10.1080/1573062X.2017.1279190

Ogidan, O., & Giacomoni, M. (2016). Multiobjective Genetic Optimization Approach to Identify Pipe Segment Replacements and Inline Storages to Reduce Sanitary Sewer Overflows. *Water Resources Management*, *30*(11), 3707–3722. https://doi.org/10.1007/s11269-016-1373-z

Ozdemir, H., Sampson, C. C., De Almeida, G. A. M., & Bates, P. D. (2013). Evaluating scale and roughness effects in urban flood modelling using terrestrial LIDAR data. *Hydrology and Earth System Sciences*, *17*(10), 4015–4030. https://doi.org/10.5194/hess-17-4015-2013

Pathak, C. S., Teegavarapu, R. S. V., Olson, C., Singh, A., Lal, A. M. W., Polatel, C., … Senarath, S. U. S. (2015). Uncertainty Analyses in Hydrologic/Hydraulic Modeling: Challenges and Proposed Resolutions. *Journal of Hydrologic Engineering*, *20*(10), 02515003. https://doi.org/10.1061/(asce)he.1943-5584.0001231

Perica, S., Pavlovic, S., Laurent, M. S., Trypaluk, C., Unruh, D., & Wilhite, O. (2018). *NOAA Atlas 14 Volume 11 Version 2, Precipitation-Frequency Atlas of the United States* (Vol. 11). NOAA, National Weather Service, Silver Spring, MD.

Price, R. K., & Vojinovic, Z. (2008). Urban food disaster management. *Urban Water Journal*, *5*(3), 259–276. https://doi.org/10.1080/15730620802099721

Prokić, M., Savić, S., & Pavić, D. (2019). Pluvial flooding in Urban Areas Across the European Continent. *Geographica Pannonica*, *23*(4), 216–232. https://doi.org/10.5937/gp23-23508

Rahmati, O., Darabi, H., Panahi, M., Kalantari, Z., & Naghibi, S. A. (2020). Development of novel hybridized models for urban flood susceptibility mapping. *Scientific Reports*, 1–19. https://doi.org/10.1038/s41598-020-69703-7

Ramos, H. M., Pérez-Sánchez, M., Franco, A. B., & López-Jiménez, P. A. (2017). Urban floods adaptation and sustainable drainage measures. *Fluids*, *2*(4), 1–18. https://doi.org/10.3390/fluids2040061

Reed, P. M., Hadka, D., Herman, J. D., Kasprzyk, J. R., & Kollat, J. B. (2013). Evolutionary multiobjective optimization in water resources: The past, present, and future. *Advances in Water Resources*, *51*, 438–456. https://doi.org/10.1016/j.advwatres.2012.01.005

Rosenzweig, B. R., Herreros Cantis, P., Kim, Y., Cohn, A., Grove, K., Brock, J., … Chang, H. (2021). The Value of Urban Flood Modeling. *Earth's Future*, *9*(1). https://doi.org/10.1029/2020ef001739

Rosenzweig, Bernice R., McPhillips, L., Chang, H., Cheng, C., Welty, C., Matsler, M., … Davidson, C. I. (2018). Pluvial flood risk and opportunities for resilience. *Wiley Interdisciplinary Reviews: Water*, *5*(6), 1–18. https://doi.org/10.1002/wat2.1302

Rossman, L.A. (2006). *Storm Water Management Model Quality assurance report: Dynamic Wave Flow Routing*. United States Environmental Protection Agency, Cincinnati, OH.

Rossman, Lewis A. (2017). *Storm Water Management Model Reference Manual Volume II – Hydraulics* (Vol. II). Office of Research and Development, U.S. Environmental Protection Agency, Cincinnati, OH. https://doi.org/10.1056/NEJMra0804615

Rossman, Lewis A., & Huber, W. C. (2016). *Storm Water Management Model Reference Manual Volume III – Water Quality*. National Risk Management Laboratory Office of Research and Development U.S. Environmental Protection Agency 26 Martin Luther King Drive Cincinnati, OH 45268.

Rossman, Lewis A., Huber, W. C., States, U., & Protection, E. (2016). Storm Water Management Model Reference Manual Volume I – Hydrology. *U.S. Environmental Protection Agency*, *I*(January), 231. https://doi.org/10.1016/S0021-9290(00)00018-X

Rutgers. (n.d.). Maintenance and Costs of Green Infrastructure. Retrieved from chrome-extension://efaidnbmnnnibpcajpcglclefindmkaj/viewer.html?pdfurl=https%3A%2F%2Fwater.rutgers.edu%2FPresentations-FixingFlooding%2FPM_TractA_MaintenanceConstructionCosts.pdf&clen=2078073&chunk=true

Saksena, S., & Merwade, V. (2015). Incorporating the effect of DEM resolution and accuracy for improved flood inundation mapping. *Journal of Hydrology*, *530*, 180–194. https://doi.org/10.1016/j.jhydrol.2015.09.069

Sampson, C. C., Fewtrell, T. J., Duncan, A., Shaad, K., Horritt, M. S., & Bates, P. D. (2012). Use of terrestrial laser scanning data to drive decimetric resolution urban inundation models. *Advances in Water Resources*, *41*, 1–17. https://doi.org/10.1016/j.advwatres.2012.02.010

Schmitt, T. G., & Scheid, C. (2020). Evaluation and communication of pluvial flood risks in urban areas. *WIREs Water*, *7*(1), 1–14. https://doi.org/10.1002/wat2.1401

Scrucca, L. (2021). Package 'GA.' Retrieved from https://luca-scr.github.io/GA/

Seyoum, S. D., Vojinovic, Z., Price, R. K., & Weesakul, S. (2012). Coupled 1D and Noninertia 2D Flood Inundation Model for Simulation of Urban Flooding. *Journal of Hydraulic Engineering*, *138*(1), 23–34. https://doi.org/10.1061/(asce)hy.1943-7900.0000485

Shahed Behrouz, M., Zhu, Z., Matott, L. S., & Rabideau, A. J. (2020). A new tool for automatic calibration of the Storm Water Management Model (SWMM). *Journal of Hydrology*, *581*(December 2019), 124436. https://doi.org/10.1016/j.jhydrol.2019.124436

Sharif, H. O., Ogden, F. L., Krajewski, W. F., & Xue, M. (2002). Numerical simulations of radar rainfall error propagation. *Water Resources Research*, *38*(8), 15-1-15–14. https://doi.org/10.1029/2001wr000525

Sheppard, P. R., Comrie, A. C., Packin, G. D., Angersbach, K., & Hughes, M. K. (2002). <Sheppard et al 2002 Climate Research.pdf>. *Climate Research*, *21*, 219–238.

Shinma, T. A., & Reis, L. F. R. (2011). Multiobjective automatic calibration of the storm water management model (SWMM) using non-dominated sorting genetic algorithm II (NSGA-II). In *World Environmental and Water Resources Congress 2011: Bearing Knowledge for Sustainability* (pp. 598–607).

Shrestha, A., Mascaro, G., & Garcia, M. (2022). Effects of stormwater infrastructure data completeness and model resolution on urban flood modeling. *Journal of Hydrology*, *607*(July 2021), 127498. https://doi.org/10.1016/j.jhydrol.2022.127498

Sieker, H., Helm, B., Krebs, P., Schlottmann, P., & Tränkner, J. (2008). Flexibility - a planning criterion for stormwater management. In *11th International Conference on Urban Drainage, Edinburgh, Scotland, UK*.

Sikorska, A. E., Scheidegger, A., Banasik, K., & Rieckermann, J. (2012). Bayesian uncertainty assessment of flood predictions in ungauged urban basins for conceptual rainfall-runoff models. *Hydrology and Earth System Sciences*, *16*(4), 1221–1236. https://doi.org/10.5194/hess-16-1221-2012

Soininen, A. (2004). TerraScan user's guide. *Terrasolid: Helsinki, Finland*.

Sörensen, J., & Emilsson, T. (2019). Evaluating Flood Risk Reduction by Urban Blue-Green Infrastructure Using Insurance Data. *Journal of Water Resources Planning and Management*, *145*(2), 04018099. https://doi.org/10.1061/(ASCE)WR.1943-5452.0001037

Sörensen, Johanna, & Mobini, S. (2017). Pluvial, urban flood mechanisms and characteristics – Assessment based on insurance claims. *Journal of Hydrology*, *555*, 51–67. https://doi.org/10.1016/j.jhydrol.2017.09.039

Spekkers, M. H., Veldhuis, J. A. E., & Clemens, F. H. L. R. (2011). Collecting data for quantitative research on pluvial flooding. *12th International Conference on Urban Drainage*, (September), 11–16.

Starkey, E., Parkin, G., Birkinshaw, S., Large, A., Quinn, P., & Gibson, C. (2017). Demonstrating the value of community-based (‘ citizen science ’) observations for catchment modelling and characterisation. *Journal of Hydrology*, *548*, 801–817. https://doi.org/10.1016/j.jhydrol.2017.03.019

Stevenson, S., Coats, S., Touma, D., Cole, J., Lehner, F., Fasullo, J., & Otto-Bliesner, B. (2022). Twenty-first century hydroclimate: A continually changing baseline, with more frequent extremes. *Proceedings of the National Academy of Sciences*, *119*(12), 1–9. https://doi.org/10.1073/pnas.2108124119/-/DCSupplemental.Published

Swain, D. L., Wing, O. E. J., Bates, P. D., Done, J. M., Johnson, K. A., & Cameron, D. R. (2020). Increased Flood Exposure Due to Climate Change and Population Growth in the United States. *Earth’s Future*, *8*(11). https://doi.org/10.1029/2020EF001778

Tanaka, T., Kiyohara, K., & Tachikawa, Y. (2020). Comparison of fluvial and pluvial flood risk curves in urban cities derived from a large ensemble climate simulation dataset: A case study in Nagoya, Japan. *Journal of Hydrology*, *584*(February), 124706. https://doi.org/10.1016/j.jhydrol.2020.124706

Terrascope. (2022). Implementation and Costs. Retrieved from https://terrascope2024.mit.edu/

The National Academy Press. (2019). *Framing the challenge of urban flooding in the United States*. Washington DC.

Thorne, C. R., Lawson, E. C., Ozawa, C., Hamlin, S. L., & Smith, L. A. (2018). Overcoming uncertainty and barriers to adoption of Blue-Green Infrastructure for urban flood risk management. *Journal of Flood Risk Management*, *11*(S2), 1–13. https://doi.org/10.1111/jfr3.12218

Tscheikner-Gratl, F., Zeisl, P., Kinzel, C., Leimgruber, J., Ertl, T., Rauch, W., & Kleidorfer, M. (2016). Lost in calibration: why people still do not calibrate their models, and why they still should – a case study from urban drainage modelling. *Water Science and Technology*, *74*(10), 2337–2348. https://doi.org/10.2166/wst.2016.395

Tsou, C. S. (2013). nsga2R: Elitist Non-Dominated Sorting Genetic Algorithm Based on R. *R Package Version*, *1*.

Tzoulas, K., Korpela, K., Venn, S., Yli-Pelkonen, V., Kaźmierczak, A., Niemela, J., & James, P. (2007). Promoting ecosystem and human health in urban areas using Green Infrastructure: A literature review. *Landscape and Urban Planning*, *81*(3), 167–178. https://doi.org/10.1016/j.landurbplan.2007.02.001

U.S. Census Bureau. (n.d.). U.S. and World Population Clock. Retrieved from https://www.census.gov/popclock/

University of Maryland, & Texas A&M University. (2018). The Growing Threat of Urban Flooding: A National Challenge 2018.

USACE. (1975). *Flood plain information Rio de Flag and Sinclair Wash - Vicinity of Flagstaff, Coconico County, Arizona*. Los Angeles District, California. Retrieved from https://www.weather.gov/fgz/EventSummaries

USDA-NRCS. (n.d.). Web Soil Survey. Retrieved from https://websoilsurvey.sc.egov.usda.gov/App/WebSoilSurvey.aspx

USEPA. (2014). *Getting to Green: Paying for Green Infrastructure: Financing Options and Resources for Local Decision-Makers*. *United States Environment Protection Agency*. Retrieved from http://www.epa.gov/sites/production/files/2015-02/documents/gi_financing_options_12-2014_4.pdf

USGS. (n.d.). 3D Elevation Program (3DEP). Retrieved from https://www.usgs.gov/core-science-systems/ngp/3dep/about-3dep-products-services?qt-science_support_page_related_con=0#qt-science_support_page_related_con

USGS. (2003). *Effects of Urban Development on Floods*. *USGS Fact Sheet FS-076-03*. U.S. Department of the Interior, U.S. Geological Survey. https://doi.org/USGS Fact Sheet FS-076-03

Veregin, H. (1999). Data quality parameters. In *Geographical information systems* (Vol. 1, pp. 177–189). Retrieved from https://pdfs.semanticscholar.org/127e/02e885c4b6aabfc49b2f0d0b816d31e54dd8.pdf

Vojinovic, Z., & Tutulic, D. (2009). On the use of 1D and coupled 1D-2D modelling approaches for assessment of flood damage in urban areas. *Urban Water Journal*, *6*(3), 183–199. https://doi.org/10.1080/15730620802566877

Walsh, C. J., Fletcher, T. D., & Burns, M. J. (2012). Urban Stormwater Runoff: A New Class of Environmental Flow Problem. *PLoS ONE*, *7*(9). https://doi.org/10.1371/journal.pone.0045814

Wang, Q. J. (1991). The Genetic Algorithm and Its Application to Calibrating Conceptual Rainfall-Runoff Models. *Water Resources Research*, *27*(9), 2467–2471. https://doi.org/10.1029/91WR01305

Webber, J. L., Fletcher, T. D., Cunningham, L., Fu, G., Butler, D., & Burns, M. J. (2020). Is green infrastructure a viable strategy for managing urban surface water flooding? *Urban Water Journal*, *17*(7), 598–608. https://doi.org/10.1080/1573062X.2019.1700286

Wehner, M. F., Arnold, J. R., Knutson, T., Kunkel, K. E., & LeGrande, A. N. (2017). *Ch. 8: Droughts, Floods, and Wildfires. Climate Science Special Report: Fourth National Climate Assessment, Volume I. Climate Science Special Report: Fourth National Climate Assessment, Volume I* (Vol. I). Washington, DC. https://doi.org/10.7930/J0CJ8BNN

Wickham, H. (2009). *ggplot2*. *Applied Spatial Data Analysis with R*. New York, NY: Springer New York. https://doi.org/10.1007/978-0-387-98141-3

WRCC. (n.d.). Evaporation stations. Retrieved from https://wrcc.dri.edu/Climate/comp_table_show.php?stype=pan_evap_avg

Wu, X., Wang, Z., Guo, S., Lai, C., & Chen, X. (2018). A simplified approach for flood modeling in urban environments. *Hydrology Research*, *49*(6), 1804–1816. https://doi.org/10.2166/nh.2018.149

WWAP. (2018). *The United Nations World Water Development Report 2018: Nature-Based Solutions for Water*. *UN Water Report 2018*. World Water Assessment Programme (United Nations). https://doi.org/https://unesdoc.unesco.org/ark:/48223/pf0000261424

Yang, X.-S. (2014). Chapter 5 - Genetic Algorithms. In X.-S. Yang (Ed.), *Nature-Inspired Optimization Algorithms* (pp. 77–87). Oxford: Elsevier. https://doi.org/https://doi.org/10.1016/B978-0-12-416743-8.00005-1

Yazdi, J., Yoo, D. G., & Kim, J. H. (2017). Comparative study of multi-objective evolutionary algorithms for hydraulic rehabilitation of urban drainage networks. *Urban Water Journal*, *14*(5), 483–492. https://doi.org/10.1080/1573062X.2016.1223319

Zhang, K., & Cui, Z. (2007). ALDPAT 1.0. Airborne LIDAR data processing and analysis tools. *National Center for Airborne Laser Mapping. Florida International University*.

Zhang, W., Villarini, G., Vecchi, G. A., & Smith, J. A. (2018). Urbanization exacerbated the rainfall and flooding caused by hurricane Harvey in Houston. *Nature*, *563*(7731), 384–388. https://doi.org/10.1038/s41586-018-0676-z

Zhou, Q., Lai, Z., & Blohm, A. (2019). Optimising the combination strategies for pipe and infiltration-based low impact development measures using a multiobjective evolution approach. *Journal of Flood Risk Management*, *12*(2), 1–14. https://doi.org/10.1111/jfr3.12457

Zoppou, C. (2001). Review of urban storm water models. *Environmental Modelling and Software*, *16*(3), 195–231. https://doi.org/10.1016/S1364-8152(00)00084-0

Zuniga-Teran, A. A., Staddon, C., de Vito, L., Gerlak, A. K., Ward, S., Schoeman, Y., … Booth, G. (2020). Challenges of mainstreaming green infrastructure in built environment professions. *Journal of Environmental Planning and Management*, *63*(4), 710–732. https://doi.org/10.1080/09640568.2019.1605890

APPENDIX A

GROUND TRUTH MODEL PARAMETERS

Table A1. Parameters for Green Ampt Infiltration Model (ADOT, 2014; USDA-NRCS, n.d.) In Ground Truth Model

Soil types	**Percent of basin area**	**Suction head (cm)**	**Conductivity (cm/hr)**	**Initial Deficit**
Avondale clay loam	1.24	38.53	0.15	0.21
Estrella loam	0.27	38.02	0.43	0.14
Gilman loam 1 to 3 percent slope	15.23	43.03	0.30	0.15
Glenbar clay loam	40.15	53.87	0.15	0.19
Laveen loam, 0 to 1 percent slope	34.41	36.50	0.61	0.11
Mohall clay loam	8.68	42.24	0.18	0.19

Table A2. Imperviousness of Sub-catchments (MRLC, n.d.) In Ground Truth Model

Imperviousness of sub-catchments (%)	**Area (%)**
0 - 10	0.012
11 – 20	0.408
21 – 30	0.520
31 – 40	1.315
41 – 50	5.500
51 – 60	10.034
61 - 70	19.600
71 – 80	35.084
81 – 90	24.040
91 - 100	3.476

Table A3. Parameters of Stormwater Systems in Ground Truth Model

Stormwater component	**Model component**	**Parameter**	**Source / Value**
Junctions	1D	Invert elevation	Design database
	1D	Rim elevation	Derived from DEM
	1D	Depth	Design database
	1D	Surcharge depth (Manholes)	0.4 m
Conduits	1D	Roughness	Design database
	1D	Diameter	Design database
	1D	Length	Design database
	1D	Shape	Design database
Outfalls	1D	Invert elevation	Design database
	1D	Rim elevation	Design database
2D Mesh grids	2D	Elevation	Derived from DEM
2D Nodes	2D	Invert elevation	Derived from DEM
2D surface channels	2D	Roughness	Concrete – 0.014
	2D	Length	Mesh grid resolution (~ 4.57 m)

APPENDIX B

SENSITIVITY ANALYSIS FOR PARAMETER SELECTION

The sensitivity analysis consists of one varying model coefficient or parameter one at a time, with the amount variation consistent with the uncertainty in the parameter being analyzed. The resulting normalized change in computed response is then divided by the normalized parameter estimation and the resulting modulus of the sensitivity gradients is ranked from highest to zero. The mathematical expression for relative sensitivity computed in SWMM5 as given by (W. James, 2003) is:

$$Relative\ sensitivity\ gradient = \frac{\frac{\partial COF}{COF}}{\frac{\partial p}{p}}$$

where, *COF* is computed objective function and *p* is input parameter. SWMM5 runs utilizing low to high values of the specified sensitivity range to generate sensitivity gradients for each parameter. Six infrastructure related parameters initial depth, conduits' roughness, depth of conduits, inlet offset, outlet offset, and conduits' diameter were selected and uncertainty range for all the parameters were assigned 50%. Using eight sensitivity points for 5 parameters, 40 model runs was completed using the same rainfall event of 50-year return period. The selection of eight sensitivity points, including lower and higher parameter values, captures non-linearity or piecewise linearity of *COF* with varying model *p*. The lower and higher parameter values are as suggested by (CHI, n.d.) is determined as:

$$Lower\ parameter\ value = p_{current} \times \left(\frac{1}{1 + \frac{U}{100}}\right)$$

$$Higher\ parameter\ value = p_{current} \times \left(1 + \frac{U}{100}\right)$$

where, $p_{current}$ is best estimated current parameter value and U is uncertainty. The *COF* was selected as total flooding and mean normalized sensitivity was estimated. Mean normalized sensitivity is calculated by dividing the difference between maximum and minimum objective function by the objective function value associated with current parameter value (CHI, n.d.).

APPENDIX C

INCOMPLETE INFRASTRUCTURE DATA

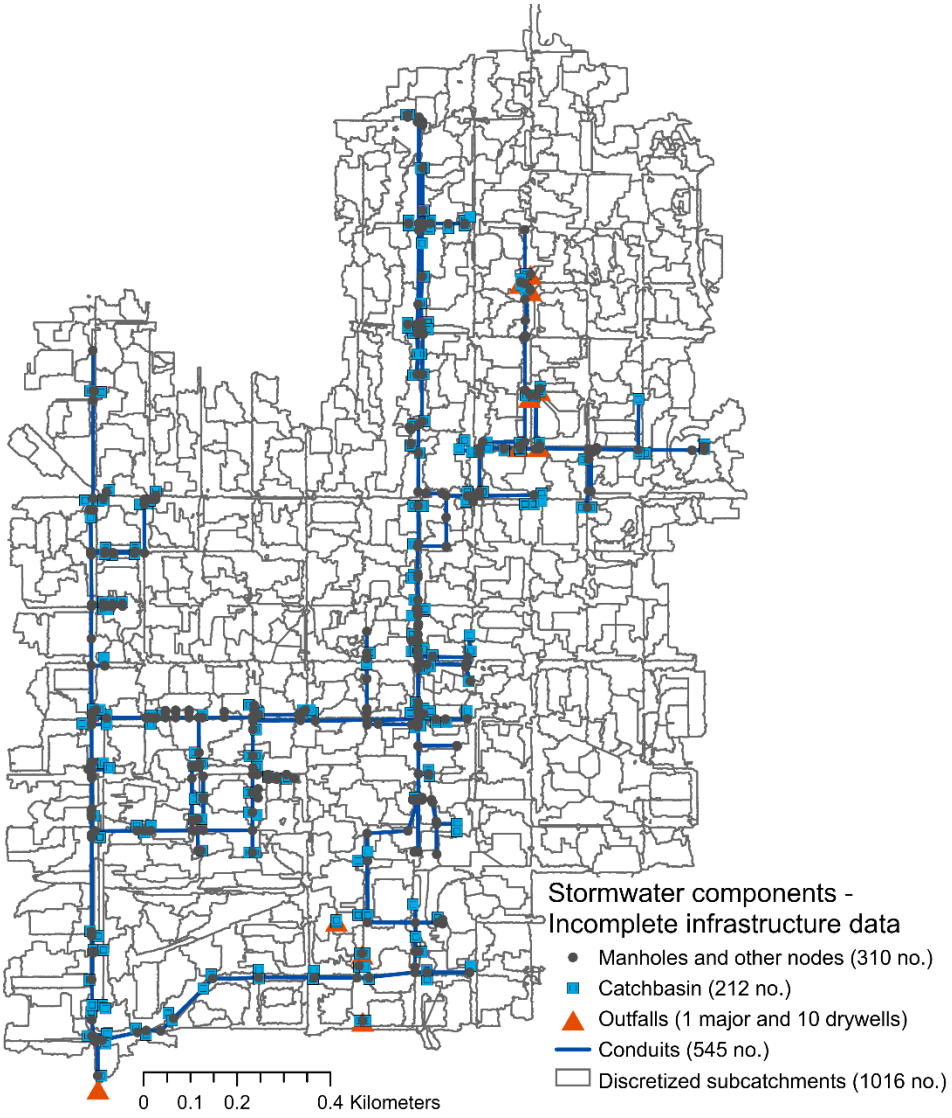

Figure C1. Incomplete Stormwater Infrastructure Data Used to Setup LDHM and LDLM Models

APPENDIX D

HYPOTHETICAL CONDUIT DISTRIBUTION FOR SAMPLING ROUGHNESS

The histograms showing roughness distributions corresponding to current distribution of material types in ground truth model and hypothetical distribution of conduits are shown in Figure D1. In ground truth model the majority of conduits' material are concrete with roughness of 0.015 sec/$m^{1/3}$ and few are corrugated metal pipe, ductile iron pipe, high density polyethylene (HDPE), polyvinyl chloride (PVC) and vitrifies clay pipes. The hypothetical distribution of conduits is an alternate material selection that is valid within the conditions below as per the drainage design standards (City of Phoenix, 2013):

1. All the conduits with length less than 10.9 m (~36 ft) are assigned as corrugated metal pipes (CMP). CMP has a typical roughness of 0.027 sec/$m^{1/3}$ (V. T. Chow, 1959; Lewis A. Rossman, 2017). The width of major streets in Phoenix is around 10.9 m, and CMP are generally used for shorter pipes and culverts.
2. All the conduits with length greater than 10.9 m whose diameter are greater than 0.6 m (~2 ft) is assigned concrete pipes with roughness 0.015 sec/$m^{1/3}$.
3. All other remaining conduits are assigned smooth pipe material of high-density polyethylene or polyvinyl chloride 0.009 sec/$m^{1/3}$.

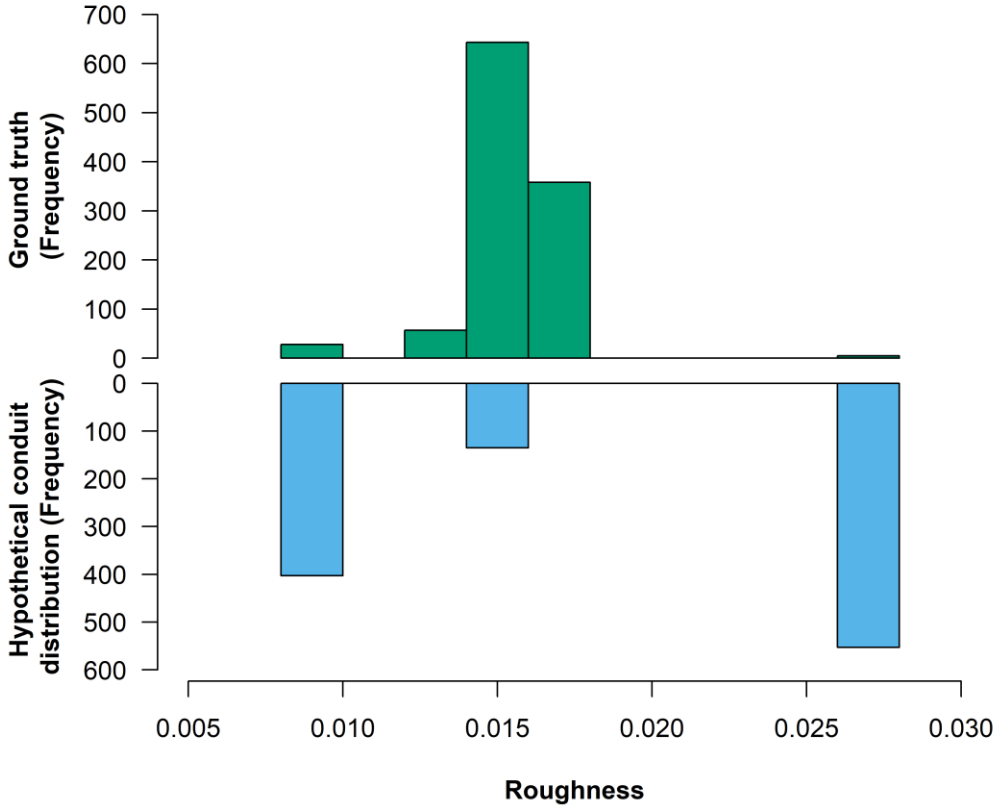

Figure D1. Histogram Showing Empirical Distribution of Conduits' Roughness (sec/$m^{1/3}$) in Current Ground Truth and Hypothetical Conduit Distribution. Hypothetical Conduit Distribution Consists of Mainly Corrugated Metal Pipes, HDPE/PVC and Reinforced Concrete Pipes

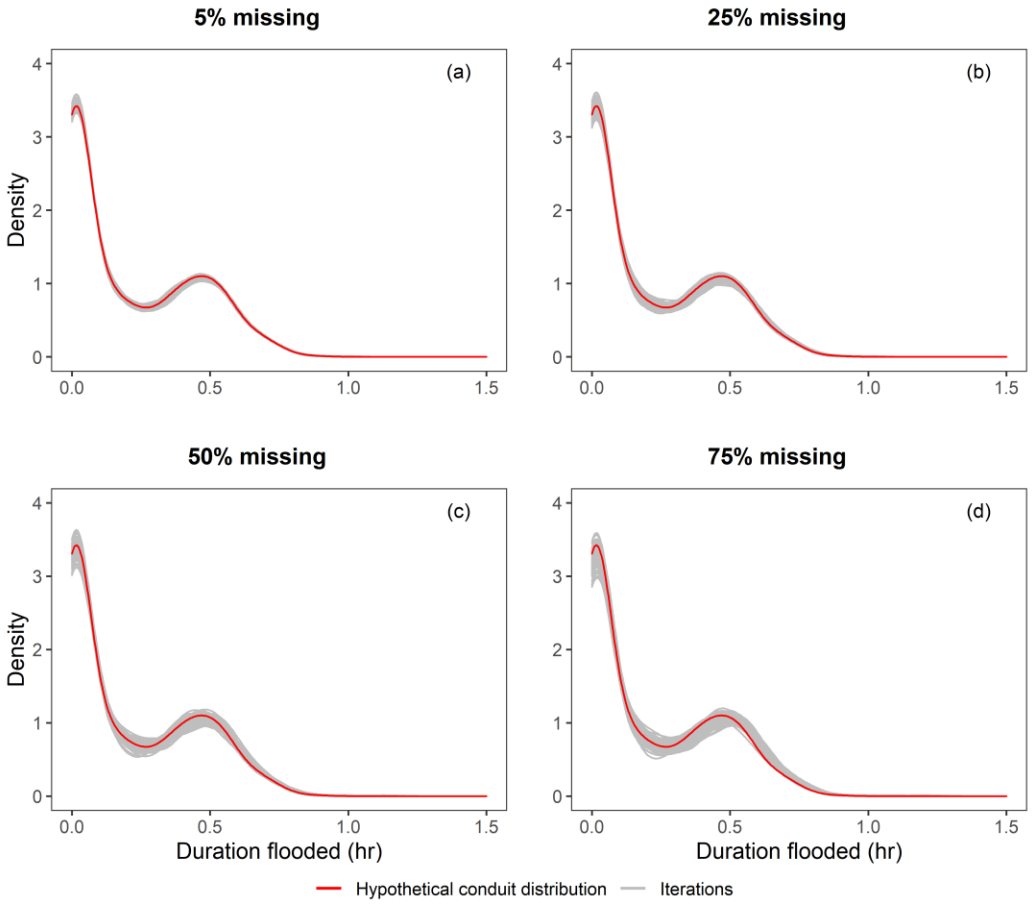

Figure D2. Monte Carlo Sampling Results Showing Distribution of Flood Duration at All Nodes with Observed Flooding While Sampling Roughness at Different Levels of Missing Attribute-values When There Is Hypothetical Conduit Distribution with Different Conduits Materials. One Hundred Iterations (Grey) Are Compared with the Hypothetical Conduit Distribution (Red). Note: Density Plots (Wickham, 2009) Are Smoothed Version of Frequency Polygon Based on Kernel Smoothers Useful to Compare Shape of the Distributions; Here, Default Bandwidth Adjustment of 1 and Gaussian Kernel Was Selected

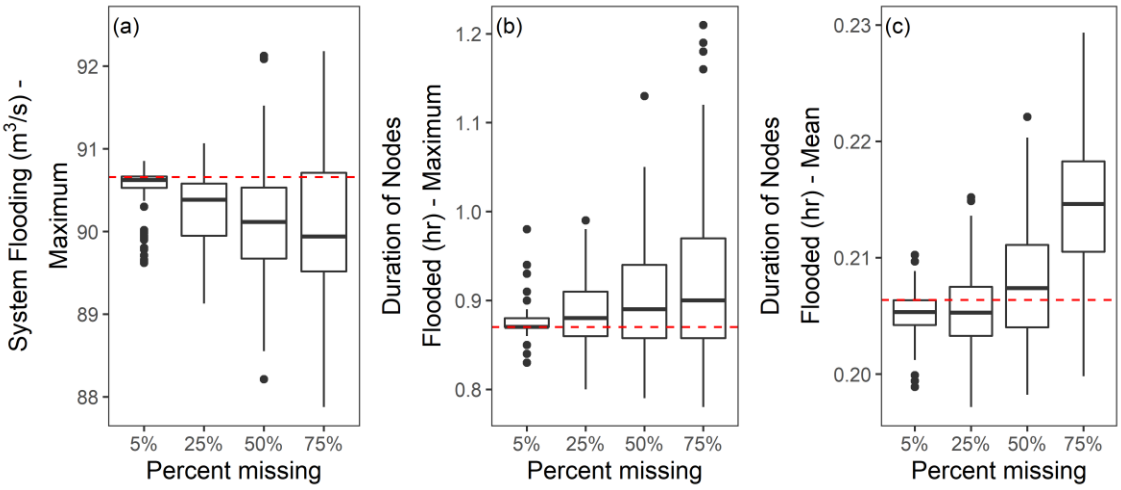

Figure D3. Monte Carlo Sampling Results Showing (a) Maximum System Flooding, (b) Maximum Duration of Nodes Flooding, and (c) Average Duration of Nodes Flooding with Different Percentages of Missing Roughness in Hypothetical Conduit Distribution

Table D1. System Flooding Metrics of Average of MAE and PBIAS (from Ensemble Simulations Vs. Hypothetical Conduit Distribution) and RIQR of Peak System Flooding; And Flood Duration Metrics of MAE and PBIAS (from the Maximum and Mean Duration of Flooding in Ensemble Simulations Vs. Hypothetical Conduit Distribution) and RIQR of Maximum and Mean Duration of Nodes Flooded for Random Sampling with Different Percentages of Missing Roughness in Hypothetical Conduit Distribution

Sampling		**System flooding**			**Flood duration (Maximum)**			**Flood duration (Mean)**		
Attri-bute	**PMD (%)**	**MAE (m^3/s)**	**PBIAS (%)**	**RIQR (%)**	**MAE (hr)**	**PBIAS (%)**	**RIQR (%)**	**MAE (hr)**	**PBIAS (%)**	**RIQR (%)**
Rough-ness	5	2.48	-0.00	0.15	0.01	0.70	1.15	0.00	-0.40	1.03
	25	5.84	-0.17	0.70	0.03	1.60	5.68	0.00	-0.50	2.05
	50	10.40	-0.32	0.95	0.05	3.20	9.27	0.00	0.60	3.42
	75	14.14	0.56	1.33	0.08	6.10	12.50	0.01	3.80	3.61

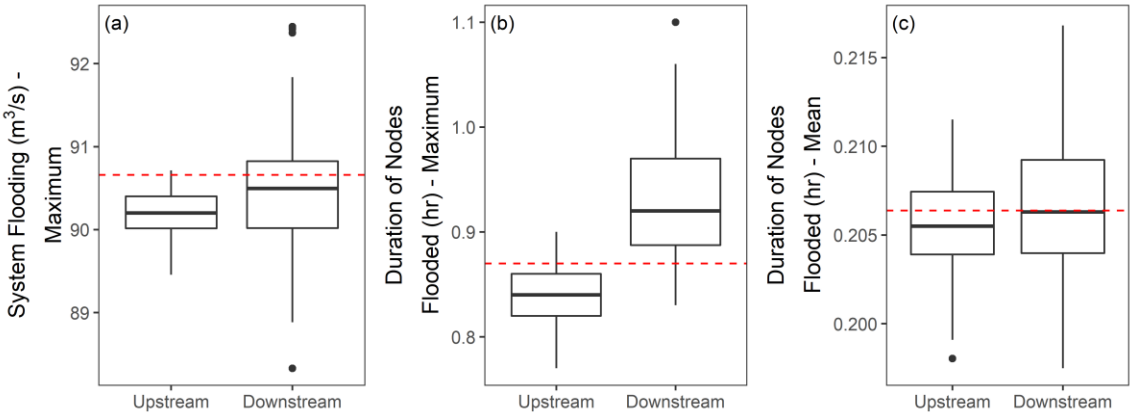

Figure D4. Monte Carlo Sampling Results Showing, (a) Maximum System Flooding, (b) Maximum Duration of Nodes Flooding, and (c) Average Duration of Nodes Flooding While Sampling Roughness at 50% PMD from Upstream Versus Downstream Locations in Hypothetical Conduit Distribution

Table D2. System Flooding Metrics of the Average MAE and PBIAS (from Ensemble Simulations Vs. Hypothetical Conduit Distribution) and RIQR of Peak System Flooding; And Flood Duration Metrics of MAE and PBIAS (from the Mean and Maximum Durations of Flooding in Ensemble Simulations Vs. Hypothetical Conduit Distribution) and RIQR of Mean and Maximum Durations of Nodes Flooded for Random Sampling of Missing Locations of Roughness in Hypothetical Conduit Distribution

Sampling		**System flooding**			**Flood duration (Maximum)**			**Flood duration (Mean)**		
Attri-bute	**Location of missing data**	**MAE (m^3/s)**	**PBIAS (%)**	**RIQR (%)**	**MAE (hr)**	**PBIAS (%)**	**RIQR (%)**	**MAE (hr)**	**PBIAS (%)**	**RIQR (%)**
Rough-ness	Upstream	5.74	-0.5	0.43	0.03	-3.3	4.76	0.002	-0.4	1.72
	Downstream	9.31	0.0	0.89	0.06	6.8	8.97	0.003	0.2	2.55

APPENDIX E

FLAGSTAFF MODEL PARAMETERS

The one-at-a-time sensitivity analysis and parameter grouping identified parameters as described in Table E1 – E8. The lower and upper values for SWMM parameters were based on several sources (Endreny, 2005; W. James, 2003; W. James et al., 2010; Lewis A. Rossman, Huber, States, & Protection, 2016).

Table E1. Calibrated Parameters for Conduits' Roughness (sec/$m^{1/3}$)

Parameter Number	Material Group	Age Group	Conduit category	Lower Value	Upper Value	Calibrated Value
1	Smooth	New	A	0.009	0.014	0.0140
2	Smooth	Old	B	0.009	0.017	0.0170
3	Concrete	New	C	0.011	0.015	0.0145
4	Concrete	Old	D	0.011	0.017	0.0161
5	Rough	New	E	0.019	0.021	0.0207
6	Rough	Old	F	0.019	0.033	0.0255
7	Unknown	New	G	0.011	0.08	0.0781
8	Unknown	Old	H	0.011	0.08	0.0790

Table E2. Calibrated Parameters for Sub-catchments' Manning n (sec/$m^{1/3}$) for Pervious (Parameter #9) and Impervious (Parameter #10) Surface

Parameter Number	Soil type	LULC	Sub-catchments Category	Lower Value	Upper Value	Calibrated Value
9	All	All	A-L	0.01	0.25	0.1560
10	All	All	A-L	0.01	0.04	0.0400

Table E3. Calibrated Parameters for Sub-catchments' Conductivity (in/hr)

Parameter Number	Soil type	LULC	Sub-catchments Category	Lower Value	Upper Value	Calibrated Value
11	Stony clay loam	High	A	0.06	0.07	0.0628
	Stony clay loam	Medium-low	B	0.06	0.07	
	Stony clay loam	Open space	C	0.06	0.07	
12	Cobbly clay loam	High	D	0.05	0.34	0.1935
	Cobbly clay loam	Medium-low	E	0.05	0.34	
	Cobbly clay loam	Open space	F	0.05	0.34	
13	Lynx loam	High	G	0.1	0.3	0.2182
	Lynx loam	Medium-low	H	0.1	0.3	
	Lynx loam	Open space	I	0.1	0.3	
14	Sandy loam	High	J	0.4	0.46	0.4349
	Sandy loam	Medium-low	K	0.4	0.46	
	Sandy loam	Open space	L	0.4	0.46	

Table E4. Calibrated Parameters for Sub-catchments' Initial Deficit

Parameter Number	Soil type	LULC	Sub-catchments Category	Lower Value	Upper Value	Calibrated Value
15	Stony clay loam	High	1	0.27	0.35	0.3436
	Stony clay loam	Medium-low	2	0.27	0.35	
	Stony clay loam	Open space	3	0.27	0.35	
16	Cobbly clay loam	High	4	0.24	0.34	0.2656
	Cobbly clay loam	Medium-low	5	0.24	0.34	
	Cobbly clay loam	Open space	6	0.24	0.34	
17	Lynx loam	High	7	0.25	0.347	0.3124
	Lynx loam	Medium-low	8	0.25	0.347	
	Lynx loam	Open space	9	0.25	0.347	
18	Sandy loam	High	10	0.19	0.368	0.2492
	Sandy loam	Medium-low	11	0.19	0.368	
	Sandy loam	Open space	12	0.19	0.368	

Table E5. Calibrated Parameters for Sub-catchments' Depression Storage (in) for Pervious Surface

Parameter Number	Soil type	LULC	Sub-catchments Category	Lower Value	Upper Value	Calibrated Value
19	Stony clay loam	High	A	0.05	0.55	0.3385
	Stony clay loam	Medium-low	B	0.05	0.55	
20	Stony clay loam	Open space	C	0.1	0.6	0.3875
19	Cobbly clay loam	High	D	0.05	0.55	0.3385
	Cobbly clay loam	Medium-low	E	0.05	0.55	
20	Cobbly clay loam	Open space	F	0.1	0.6	0.3875
19	Lynx loam	High	G	0.05	0.55	0.3385
	Lynx loam	Medium-low	H	0.05	0.55	
20	Lynx loam	Open space	I	0.1	0.6	0.3875
19	Sandy loam	High	J	0.05	0.55	0.3385
	Sandy loam	Medium-low	K	0.05	0.55	
20	Sandy loam	Open space	L	0.1	0.6	0.3875

Table E6. Calibrated Parameters for Sub-catchments' Depression Storage (in) for Impervious Surface

Parameter Number	Soil type	LULC	Sub-catchments Category	Lower Value	Upper Value	Calibrated Value
21	Stony clay loam	High	A	0.05	0.55	0.5474
	Stony clay loam	Medium-low	B	0.05	0.55	
22	Stony clay loam	Open space	C	0.1	0.6	0.3923
21	Cobbly clay loam	High	D	0.05	0.55	0.5474
	Cobbly clay loam	Medium-low	E	0.05	0.55	
22	Cobbly clay loam	Open space	F	0.1	0.6	0.3923
21	Lynx loam	High	G	0.05	0.55	0.5474
	Lynx loam	Medium-low	H	0.05	0.55	
22	Lynx loam	Open space	I	0.1	0.6	0.3923
21	Sandy loam	High	J	0.05	0.55	0.5474
	Sandy loam	Medium-low	K	0.05	0.55	
22	Sandy loam	Open space	L	0.1	0.6	0.3923

Table E7. Calibrated Parameters for Sub-catchments' Suction Head (in)

Parameter Number	Soil type	LULC	Sub-catchments Category	Lower Value	Upper Value	Calibrated Value
23	Stony clay loam	High	A	8.27	14.2	12.8663
	Stony clay loam	Medium-low	B	8.27	14.2	
	Stony clay loam	Open space	C	8.27	14.2	
24	Cobbly clay loam	High	D	8.27	11	9.7539
	Cobbly clay loam	Medium-low	E	8.27	11	
	Cobbly clay loam	Open space	F	8.27	11	
25	Lynx loam	High	G	7	14	10.6713
	Lynx loam	Medium-low	H	7	14	
	Lynx loam	Open space	I	7	14	
26	Sandy loam	High	J	3	5	4.1064
	Sandy loam	Medium-low	K	3	5	
	Sandy loam	Open space	L	3	5	

Table E8. Calibrated Parameters for Conduit Geometry (Geom 1 (ft)) for Unknown Material

Parameter Number	Material Group	Age Group	Conduit category	Lower Value	Upper Value	Calibrated Value
27	Unknown	ALL	G-H	1	5	2.9582
28	Unknown	ALL	G-H	1	5	1.0966

APPENDIX F

GREEN INFRASTRUCTURE DESIGN CONSIDERATION

Table F1. GI Parameters for Bio-retention and Green Roof Considered for This Study.

Layer	Parameters	Unit	Bio-retention	Green roof	References
Surface	Berm height	cm	15.24	12.7	(W. James et al., 2010)
	Vegetation volume	fraction	0.1	0.15	
	Surface roughness	$sec/m^{1/3}$	0	0	
	Surface slope	%	0	0	
Soil	Thickness	cm	90	50	
	Porosity	fraction	0.45	0.45	(ADOT, 2014; USDA-NRCS, n.d.)
	Field capacity	fraction	0.19	0.19	
	Wilting point	fraction	0.085	0.085	
	Conductivity	cm/hr	1	1	
	Conductivity slope	-	7.5	7.5	
	Suction head	cm	11	11	
Storage	Thickness	cm	45.72	-	(W. James et al., 2010)
	Void ratio	voids/solids	0.75	-	
	Seepage rate	cm/hr	1.27	-	
	Clogging factor	-	0	-	
	Drain coefficient	-	0	-	
Drainage mat	Thickness	cm	-	5.08	
	Void fraction	fraction	-	0.4	
	Roughness	$sec/m^{1/3}$	-	0.02	

APPENDIX G

R-CODES

The essential R-scripts for filing missing attribute-values, sampling algorithm as described in Chapter 2; calibration approach for SWMM model using genetic algorithm as described in Chapter 3, is available at the GitHub link: https://github.com/ashish-shrs.